REVIEWS OF MODERN PHYSICS VOLUME 18, NUMBER 2 APRIL, 1946

A Report on the Wilson Cloud Chamber and Its Applications in Physics

N. N. DAS GUPTA* AND S. K. GHOSH
Palit Laboratory in Physics, Calcutta University, Calcutta, India

TABLE OF CONTENTS

INTRODUCTION

THE Wilson cloud chamber has played a very important role in the development of modern physics. Rutherford has described the cloud chamber as "the most original and wonderful instrument in scientific history." It has also been called "the final court of appeal in physics" where many conflicting theories have been put to test and decisions made. Where many indirect evidences fail to convince, a single cloud-chamber picture is often sufficient and carries conviction.

The history of discovery of this wonderful instrument may be briefly stated as follows. The earliest researches of Coulier (1875), Kiessling (1884), and specially of Aitken (1880–1916) drew attention to the rather puzzling role played by dust particles in the condensation of water vapor into cloud drops. Trying to reproduce in the laboratory the conditions for cloud formation,

* At present, research associate, Stanford University, California.

they found that the clouds resulting from small adiabatic expansion of moist, dusty air disappear completely if the air is first made dust-free. Moreover, the drops of cloud that are formed in dusty air, are always found to collect round the particles of dust; the water drops are thus able to start with a finite radius—that of the dust particle—and so need not pass through a stage when their radii are of molecular dimensions, when, as Lord Kelvin has shown, the effect of surface tension would lead to such intense evaporation as to cause disappearance of the drops (see Chapter I, Section 2).

The discovery of the necessity of having dust particles for condensation of water vapor produced for sometime a feeling that the formation of clouds is to be ascribed in all cases to dust alone. It was at this stage that C. T. R. Wilson (1897) showed by direct experiments that under certain conditions, charged ions can also play a part in the formation of clouds. Wilson filled an expansion chamber with dusty, moist air and found that a very slight expansion produced a dense fog. That this preliminary fog is caused by condensation on dust particles is proved by the fact that when the expansion is repeated several times and all dust is carried down by the cloud, the air inside the chamber is dust-free and no fogs are then produced as a result of small expansion. If now the successive expansion ratios, i.e., the ratios of the final to the initial volume, are gradually increased, no clouds are produced in the dust-free air until the expansion ratio reaches the value of 1.25. When the expansion ratio exceeds the value of 1.25 and is between 1.25 and 1.37, a few rain drops are found. Beyond 1.37 again a much denser cloud of smaller particles is formed, the density of the cloud increasing with expansion ratio. Thus it was shown that even in the absence of dust particles, cloudy condensations could be produced if expansion ratios exceeded certain limits. The problem was to identify the nuclei on which cloudy condensation took place in the absence of dust.

Wilson soon found (1899) that when an x-ray tube or some uranium or other radioactive body is brought close to the chamber, the few drops that are always produced with expansion ratios between 1.25–1.37 are replaced by a dense cloud. But no matter how strong the source of radiation, no cloud is produced for expansions less than 1.25. The intensity of the source only affects the number of drops but leaves unchanged the limit at which drops begin to appear.

J. J. Thomson (1898) showed that the cloudy condensation that took place in the presence of an x-ray beam with expansion ratios between 1.25–1.37 have ions as nuclei. He introduced two parallel plates into the chamber containing dust-free air. By applying a strong field between the plates, he was able to show that the dense cloud that was previously produced when the chamber was traversed by x-rays, disappeared in the presence of the electric field. In some later experiments (1904) Wilson was able to show that the few drops that were formed with expansions between 1.25 and 1.38 in gases not exposed to any radiations, were also diminished in number when the expansions were made in the presence of strong electric fields. From all these observations it was clear that the nuclei responsible for condensation in dust-free air with expansion between 1.25–1.38 are charged ions produced in the gas by the action of the radiations.

C. T. R. Wilson (1911 and 1912) took advantage of these phenomena in the development of his cloud-chamber technique for photographing the tracks of α-rays, fast electrons, x-rays, and γ-rays. His method was to expand suddenly a definite volume of air saturated with water vapor. The result is that the air now at the lower temperature contains more vapor than it can hold in suspension in the saturated state. The excess amount of water vapor condenses on ions as nuclei and an instantaneous photograph of the drops makes the path of the charged particle visible. One also gets a picture of complicated processes that take place by the interaction of one particle with another.

The beauty and ingenuity of the method can hardly be exaggerated. Previous to the discovery of the Wilson chamber, it was possible only to observe the behavior of matter in bulk. The Wilson chamber enables us to study the behavior of individual atoms, to visualize and photograph the actual paths of atoms and electrons through gases and to study at leisure the complicated interactions taking place between individual atoms, nuclei, and charged particles.

The immense possibilities of the Wilson chamber were soon realized, and during the years that followed, there were rapid modifications and developments of the design of the Wilson chamber to suit different investigations. Some of these have been described briefly in Chapter II. A great deal of research has been carried out in recent years with a view to understand and improve the technique of operation of the Wilson chamber. Chapter III contains a summary of these works. But although the Wilson chamber has been developed to such a great extent during the 34 years since its inception, the fundamental processes of its operation, *viz.*, the formation and rapid growth of drops in supersaturated vapor, are not yet fully understood. In Chapter I are given some of the experimental results regarding the formation of drops and optimum liquid mixtures for cloud-chamber operation.

The last two chapters are devoted to a brief description of the application of Wilson chamber technique to different branches of modern physics and an enumeration of the important results obtained with its help. So varied and numerous have been the applications of Wilson chamber technique in physics that it has hardly been possible to do full justice to the work of all contributors in this field.

CHAPTER I. PHYSICS OF DROP FORMATION

1. Supersaturation

The general ideas of cloud formation are well known to all students of physics. When an air mass saturated with water vapor is borne upwards by convection currents, it expands adiabatically, temperature falls. The excess amount of water vapor separates out in the form of liquid drops which appear as cloud or fog. The Wilson cloud chamber operates on a similar principle. In this instrument a definite volume of noncondensible gas saturated with a vapor (or a mixture of vapors) is suddenly expanded. The result is that the gas, now at the lower temperature, contains more vapor than it can hold in the saturated state, i.e., it is *supersaturated.* The excess amount of vapor condenses on ions as nuclei, making the path of the charged particle visible.

Condensation on ions requires previous existence of a state of supersaturation. Supersaturation at any time may be defined as the ratio of the density of vapor at that time to the saturation density at the same temperature. The amount of supersaturation produced as a result of expansion in a cloud chamber depends on various factors, *viz.*, the nature of the noncondensible gas and vapor used, the initial pressure, temperature of the gaseous mixture, and the expansion ratio. When a mixture of two liquids (e.g., water and alcohol) is used as a source of the condensible vapor, supersaturation also varies with the composition of the liquid mixture. It is necessary to consider the effect of these various factors on the resultant supersaturation before one can discuss the critical supersaturation on which depends the efficiency of cloud chamber work.

For simplicity, we first assume that in a cloud chamber just before expansion, we have a noncondensible gas at a pressure P_g and a vapor at a pressure P_1 contained in a volume V_1 at temperature θ_1. We then have

$$P_1V_1=(M_1/M)R\theta_1, \tag{1.01}$$

where M_1 is the total mass of vapor present in the volume V_1 and M the g molecular weight of the vapor.

Now suppose a sudden expansion is produced changing the volume of the gas from V_1 to V_2. Because of the expansion, the temperature of the gaseous mixture falls from θ_1 to θ_2', where θ_2' is given by the adiabatic relation

$$\theta_1/\theta_2'=(V_2/V_1)^{\gamma-1}, \tag{1.02}$$

where γ is the ratio of the specific heats of the gaseous mixture present within the chamber.

Immediately after expansion but just before condensation, the original mass of vapor M_1 is distributed over the volume V_2. The pressure P_2' is then given by

$$P_2'V_2=(M_1/M)R\theta_2'. \tag{1.03}$$

However this is an unstable state since at the lower temperature θ_2' the amount of vapor that may be held in suspension is less than that at the higher temperature θ_1 and therefore condensation takes place reducing the mass from M_1 to M_2. When the excess amount has condensed, the

equilibrium is again attained and the vapor pressure falls to the P_2 saturation pressure at the lower temperature θ_2. The equilibrium temperature θ_2 after expansion and condensation is slightly higher than θ_2', the temperature immediately after expansion, as some heat is liberated by condensation of vapor.

For the vapor at the lower temperature θ_2, we have

$$P_2V_2=(M_2/M)R\theta_2, \qquad (1.04)$$

where M_2 is the mass of vapor present in the volume V_2 after condensation.

The vapor density ρ_2' immediately after expansion but before condensation when the original mass of vapor M_1 is still distributed over volume V_2 is given by $\rho_2'=M_1/V_2$ and the mass of vapor per unit volume after condensation is $\rho_2=M_2/V_2$. *Supersaturation* produced as a result of expansion is the ratio of the density of vapor immediately after expansion but before condensation to the saturation density at the lower temperature θ_2. Hence the supersaturation produced as a result of expansion is given by

$$S=\rho_2'/\rho_2=M_1/M_2=P_1V_1\theta_2/P_2V_2\theta_1. \qquad (1.05)$$

Also from Eqs. (1.03) and (1.04) we have

$$S=(P_2'/\theta_2')/(P_2/\theta_2). \qquad (1.06)$$

If the slight difference between θ_2 and θ_2' is neglected and we put $\theta_2=\theta_2'$, θ_2/θ_1 may be eliminated from Eqs. (1.05) with the help of Eq. (1.02) and we have

$$S=\frac{P_1}{P_2}\left(\frac{V_1}{V_2}\right)^{\gamma}=\frac{P_1}{P_2}\left(\frac{1}{1+\epsilon}\right)^{\gamma}, \qquad (1.07)$$

where $1+\epsilon$ is the expansion ratio; P_1, P_2 the saturation pressures at the initial and final temperatures; and γ the ratio of specific heats of the complex gaseous mixture present inside the chamber.

Because of the slight difference in θ_2 and θ_2' the amount of supersaturation as given by (1.07) is slightly less than the exact amount defined by the Eqs. (1.05) and (1.06).

In Eqs. (1.02) and (1.07) γ refers to the ratio of the specific heats of the gaseous mixture present within the Wilson chamber. If P_g and P_v be the partial pressures of the gas and vapor

TABLE I-1. Nature of gas and supersaturation produced.

Gas	Vapor	γ	θ_2	P_2 in mm Hg	S
A	H_2O	1.66	252.8	0.77	15.6
Air	H_2O	1.40	267.2	2.97	4.2
CO_2	H_2O	1.31	273.4	4.68	2.8
Air	C_2H_5OH	1.37	269.8	9.45	3.41

with the corresponding γ's, γ_g, and γ_v, γ for the composite mixture is given by the following formula due to Richarz (1906)

$$\frac{1}{\gamma-1}=\frac{1}{\gamma_g-1}\cdot\frac{P_g}{\pi}+\frac{1}{\gamma_v-1}\cdot\frac{P_v}{\pi}, \qquad (1.08)$$

where π is the total pressure equal to P_g+P_v. Where more than one vapor is used together with one non-condensible gas we have

$$\frac{1}{\gamma-1}=\frac{1}{\gamma_g-1}\cdot\frac{P_g}{\pi}+\frac{1}{\gamma_v'-1}\cdot\frac{P_v'}{\pi}+\frac{1}{\gamma_v''-1}\cdot\frac{P_v''}{\pi}. \qquad (1.08a)^*$$

Equation (1.08) shows how γ for the gaseous mixture changes with P_v, P_g, γ_v, and γ_g, etc. Since these depend on the initial temperature, pressure, and the nature of the gas and vapor, γ of the gas mixture, and hence supersaturation produced as a result of a fixed expansion, vary with these factors. In the following sections we have considered these variations in detail.

(a) *Variation of Supersaturation with the Nature of the Non-Condensible Gas and of Vapor*

Table I-1 shows how the nature of the gas modifies supersaturation produced with the same expansion ratio of 1.25. The first three rows show the effect of using argon, air, and carbon dioxide as the non-condensible gas and water vapor as the condensant. The initial temperature $T_1=20°C$, so that $P_1=1.75$ cm of Hg, $\gamma_{H_2O}=1.30$, the total initial pressure is taken to be $1\frac{1}{2}$ atmospheres in each case. The γ of the gas vapor mixture calculated from Eq. (1.08) is given in

* This follows from the fact that the work done by the mixture of gas and vapor while expanding adiabatically is given by $R(\theta_1-\theta_2')/(1-\gamma)$, where θ_1 and θ_2' are the initial and final temperatures. When the vapors and the gas are considered separately, the work done will be given by $R(\theta_1-\theta_2')P_g/(1-\gamma_g)\pi+R(\theta_1-\theta_2')P_v'/(1-\gamma_v')\pi+\cdots$ from which Eq. (1.08a) follows.

TABLE I-2. Variation of γ and S with total pressure π.

		Total pressure π in cm Hg							
		1140	380	114	76	38	20	10	6
Air and water vapor	γ	1.400	1.399	1.398	1.396	1.392	1.385	1.372	1.354
	S	3.018	3.017	3.016	3.016	3.014	2.889	2.772	2.572
Air and ethyl alcohol	γ	1.396	1.387	1.361	1.345	1.302	1.241	1.180	1.125
	S	2.703	2.648	2.439	2.38	2.049	1.706	1.422	1.206

column III. The lower temperature θ_2 produced as a result of the expansion and the vapor pressure at the lower temperature are included in columns IV and V.

The effect of using pure vapor C_2H_5OH in place of water is shown in the last row of Table I-1. It is easy to see, since the vapor pressure of alcohol is higher than that of water at the same temperature, as also $\gamma_{C_2H_5OH}=1.13$ and is less than γ_{H_2O}, the γ for air-water mixture is greater than γ for air-alcohol mixture. To produce the same degree of supersaturation higher expansions will be needed for air-alcohol mixtures than for air-water mixtures.

The table also illustrates that if we use a monatomic gas like A or He in place of air, supersaturation is very much greater. In fact, an expansion of 1.10 with A produces the same value of S as 1.25 with air. A smaller expansion obviates many mechanical difficulties, hence monatomic gases are used in many cloud chambers.

(b) *Variation of Supersaturation with Gas Pressure*

It is seen from Eq. (1.08) that when the total pressure π is decreased by diminishing the gas pressure P_g, P_v/π increases while P_g/π remains practically the same for $P_g \gg P_v$; as a result the value of γ decreases. For a given expansion ratio the fall of temperature is therefore less [see Eq. (1.02)] and supersaturation produced is smaller. To attain the same supersaturation, the expansion ratio should therefore be increased. An increase in π will require on the other hand smaller expansion ratios to attain the same supersaturation.

In Table I-2 the variation of γ and S with π has been calculated for air+H_2O, air+C_2H_5OH. The initial temperature is assumed to be 25°C in every case and the expansion ratio is 1.2. We assume $\gamma_{air}=1.4$, $\gamma_{H_2O}=1.3$ and $\gamma_{C_2H_5OH}=1.13$.

Table I-2 at once shows the utility of operating the cloud chamber with a non-condensible gas at high pressure. The γ of the gas is higher than that of the vapor, and because of the higher pressure, γ of the system is greater than it would have been at lower total pressure. As a result it is possible to work at a smaller expansion ratio, thus the turbulence is minimized. The higher density of the vapor also prevents the diffusion of water from the walls after the expansion. Also the track of a charged particle will in this case be more prominent as the number of ions produced per cm of its path will be larger when the pressure is large, thus easing to a large extent the problem of illumination of the tracks to be photographed.

(c) *The Effect of Variation of the Initial Temperature on Supersaturation*

If the initial temperature be increased while the initial volume V_1 and the total pressure π are kept constant, the increase in P_v/π will be more than in P_g/π; as a result γ will decrease and to reach the same lowering of temperature higher expansion ratios will be needed. This is shown in Table I-3 for air-C_2H_5OH mixture at $\pi=114$ cm of Hg and $\pi=38$ cm of Hg, when the initial temperature varies between 40°–10°C. The expansion ratio is taken to be 1.2 and γ_{air}, $\gamma_{alcohol}$ have the same values as in Table I-2.

TABLE I-3. Variation of γ and S with initial temperature.

π		Temperature 40°C	30°C	25°C	20°C	10°C
114 cm Hg	γ	1.322	1.35	1.361	1.370	1.383
	S	2.084	2.345	2.439	2.523	2.654
38 cm Hg	γ	1.232	1.280	1.302	1.322	1.356
	S	1.592	1.912	2.049	2.156	2.355

(d) *Variation of Supersaturation with Expansion Ratio*

The variation of supersaturation with expansion ratio may be calculated with the help of Eqs. (1.02) and (1.05). The calculated values for air-water and air-alcohol mixtures are shown in

TABLE I-4. Values of supersaturation at different expansion ratios.

	Expansion ratio								
	1.00	1.05	1.10	1.15	1.20	1.25	1.30	1.35	1.40
Air+water	1.00	1.28	1.78	2.36	2.96	4.00	5.52	7.16	9.14
Air+alcohol	1.00	1.29	1.62	1.84	2.55	3.25	4.15	5.32	6.94

Table I-4. In this calculation we have assumed $\gamma=1.4$ for air-water and $\gamma=1.37$ for air-alcohol; initial temperature is 20°C so that the partial pressures are 17.54 mm of Hg for water and 44 mm for ethyl alcohol vapor.

It will be found from Table I-4 that the supersaturation produced at an expansion of 1.25 is about 4 with air-water vapor mixture. In order to produce the same supersaturation with air-alcohol vapor mixture an expansion of 1.29 is required.

(e) *Variation of γ and Supersaturation S with Concentration of the Mixture*

When the condensant is a mixture of vapors, the partial vapor pressures P_v', P_v'', etc., depend on the composition of the liquid mixture. It has been shown by Duhem and Margules (1900) that in an enclosure containing a mixture of two liquids the partial vapor pressures satisfy the relation

$$\frac{d\log P_v'}{d\log P_v''}=-\frac{1-x}{x}, \tag{1.09}$$

where x and $(1-x)$ are the mole fractions of the liquids used and P_v' and P_v'' their corresponding partial pressures. Following the method of Lewis and Murphee (1924), Eq. (1.09) can be solved for P_v' and P_v'' provided that we know the total vapor pressures for the given compositions.

The variations in the partial pressures P_v' and P_v'' at 20°C and 40°C for different compositions of the water-ethyl alcohol mixture have been given (Table VI-2) in Appendix from Landolt and Börnstein's *Physical Chemistry Tables*. With the help of Table VI-2 and Eq. (1.08a), the variation in γ for different composition of the ethyl alcohol water mixture can be calculated. The calculated values are given in Table I-5 for $T_1=20$°C.

In Table I-5 the volume percent of C_2H_5OH has been calculated according to the relation,

volume per cent of

$$C_2H_5OH=(V_{\text{alcohol}}\times 100)/(V_{\text{alcohol}}+V_{\text{water}})$$

where V_{alcohol} and V_{water} are the true volumes by which they are mixed.

With the help of the calculated values of γ given in Table I-4 and Eq. (1.02), the lower temperature θ_2 produced as a result of any fixed expansion may be obtained and its variation with the composition of the liquid mixture studied. In order to obtain the supersaturations corresponding to the different liquid mixtures, the total pressure of the vapor mixture at the lowered temperature must be known [Eq. (1.05)]. However, there seem to be no experimental data for the total vapor pressure of alcohol-water mixtures at very low temperatures as are required in the present experiment. Hence the actual supersaturation produced as a result of expansion cannot be calculated.

2. Theories of Drop Formation

Let us now consider the present views regarding drop formation. The fundamental contribution is attributed to Lord Kelvin who showed in 1870, that owing to surface tension, the saturation vapor pressure (s.v.p.) over a drop of radius r is greater than over a plane sheet of liquid. The relation is

$$\log\frac{p_r}{p_\infty}=\frac{2T}{r}\frac{M}{R\theta\rho}, \tag{1.10}$$

where T=surface tension, ρ=density of liquid, R=gas constant, θ=temperature (absolute), and p_r, p_∞ are s.v.p. over drop and plane sheet.

TABLE I-5. Values of γ of different water-ethyl alcohol mixtures.

C_2H_5OH by wt percent	C_2H_5OH by volume percent	C_2H_5OH by mole percent	γ
0	0.00	0.00	1.398
10	12.31	4.167	1.393
20	24.00	8.913	1.389
30	35.12	14.35	1.386
40	45.71	20.69	1.384
50	55.80	28.12	1.382
60	65.46	36.99	1.381
70	74.66	47.62	1.379
80	83.47	61.02	1.377
90	91.91	77.87	1.374
100	100.00	100.00	1.370

For water vapor at $\theta = 291°A$, the equation becomes

$$p_r/p_\infty = \exp\,(1.09\times10^{-7}/r). \qquad (1.11)$$

p_r is therefore always $>p_\infty$, but unless r is $\leqslant 10^{-7}$ cm, the difference is not much.

If, therefore, a drop of this size is suspended in a space where relative humidity is 100 percent, the drop will evaporate. To prevent the drop from evaporating relative humidity should be 100 p_r/p_∞, i.e., the space must be supersaturated in the proportion p_r/p_∞.

The calculated values of p_r/p_∞ for different values of r are given in Table I-6. The results are also shown in the dotted curve of Fig. I-1.

From the dotted curve Fig. I-1 we find that the supersaturation required for the formation of a drop of radius r increases rapidly as r decreases. For the formation of a drop of radius 2×10^{-8} cm the supersaturation needed is about 235. Such small drops will therefore evaporate away at once even if formed.

The air usually contains dust particles whose sizes may vary from 10^{-4} to 10^{-6} cm. These present large surfaces of condensation, and very little supersaturation, 1.001 to 1.12, is all that is needed in order to condense on such nuclei. This explains the phenomenon observed by Aitken and also by Wilson that when dusty air fills the expansion chamber very slight expansion fills the chamber with dense fog; but if the air is first freed from dust, no such fogs are formed at small expansion.

The dotted curve of Fig. I-1 also shows that as the drop radius increases, lower supersaturations are needed to hold the drops in equilibrium. This is an unstable state. The larger the drops grow, the more rapidly they are formed until the supersaturation falls to unity. The important thing is the presence of nuclei on which water may first condense. Once it has condensed, the drops will grow rapidly to the visible size, the final size being determined by the amount of water available and the number of drops formed per cc.

TABLE I-6. Values of p_r/p_∞ for drops of water.

r in cm	p_r/p_∞	r in cm	p_r/p_∞	r in cm	p_r/p_∞
1.0×10^{-4}	1.001	7.8×10^{-8}	4.00	3.9×10^{-8}	16.5
1.0×10^{-5}	1.01	6.8	5.00	2.0	235.0
1.0×10^{-6}	1.12	6.1	6.00		
2.3×10^{-7}	1.60	5.6	7.00		
1.9×10^{-7}	1.78	5.2	8.00		
1.6×10^{-7}	2.00	5.0	9.00		
1.0×10^{-7}	3.00	4.7	10.00		

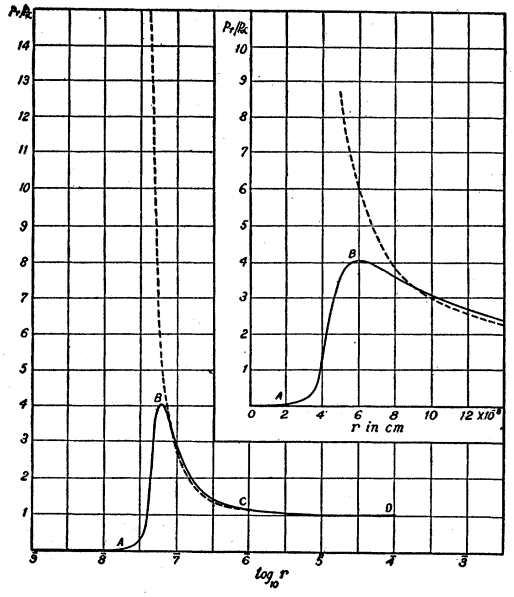

FIG. I-1. Variation of the saturated vapor pressure over a drop with the radius of the drop.

We next pass on to the explanation of the phenomenon first noticed by C. T. R. Wilson that when the expansion ratio is between 1.25 and 1.37 with dust free air and water vapor mixture, condensation can still take place around ions as centers. In this case the drops formed are charged. If we assume that a drop is formed on a single ion, that is, it carries an elementary charge e, Eq. (1.10) is according to Thomson* modified to

$$\log\frac{p_r}{p_\infty} = \frac{M}{R\theta\rho}\left(\frac{2T}{r} - \frac{e^2}{8\pi kr^4}\right). \qquad (1.12)$$

The left-hand side of Eq. (1.12) indicates the excess pressure at the surface of the drop over the saturation pressure p_∞. The two terms on the right-hand side signify the pressures due to the surface tension and electric field. The two are in opposite sense, for while the potential energy due to the surface tension ($4\pi r^2 T$) decreases with the decreasing radius r, that due to electrification $[\frac{1}{2}(e^2/kr)]$ decreases on increasing the drop radius. The former tends to decrease the radius

* General reference 8, p. 165.

of the drop thereby increasing the vapor pressure, while the latter tends to increase the radius of the drop and decrease its vapor pressure. A charged drop will therefore always have less vapor pressure than an uncharged one.

We see from Eq. (1.12) that for

$$r=c=(e^2/16\pi kT)^{\frac{1}{2}}, \quad p_r=p_\infty,$$
$$r>c, \quad p_r>p_\infty,$$
$$r<c, \quad p_r<p_\infty.$$

c is the critical radius determining the size of the charged drops when the space is just saturated, i.e., $p_r=p_\infty$. Each gaseous ion in saturated vapor will be surrounded by a drop of radius c.

If we assume that the drop is formed on a single ion, i.e., $e=4.8\times10^{-10}$ and that the surface tension of the drop is 76 dynes/cm which is true for thick water films, then $c=3.9\times10^{-8}$ cm.

Table I-7 gives the calculated values of p_r/p_∞ for charged drops of radius r. The variation of supersaturation p_r/p_∞ with drop radius r for a charged drop is shown by the solid curve of Fig. I-1. For the drop radius $r>10^{-7}$ cm the effect of charge is negligible and the supersaturation required is the same for charged and uncharged drops. But for smaller radii there are significant differences. Whereas for uncharged drops the equilibrium supersaturation increases rapidly with decrease of r, with charged drops supersaturation reaches a maximum value of 4.1 at $r=6.5\times10^{-8}$ cm and for still smaller drops supersaturation required is less. Thus while no uncharged drops can be formed in space for which supersaturation is less than 1, charged drops may be formed in space which is just saturated or even undersaturated ($S<1$).

Table I-7 shows that the radius of the drops formed around ions diminishes very slowly as the quantity of water vapor in air diminishes. Thus

TABLE I-7. Values of p_r/p_∞ for singly charged drops.

r in cm	p_r/p_∞	r in cm	p_r/p_∞
1.95×10^{-8}	10^{-18}	6.45×10^{-8}	4.0
3.55	0.37	7.80	3.71
3.90	1.00	8.80	3.36
4.25	2.00	11.70	2.62
4.65	3.00	15.6	2.09
5.80	4.00	19.5	1.81
5.85	4.08	23.4	1.64

if the quantity of water in air be diminished to 10^{-18} of that required to saturate it—a state of almost absolute dryness—the size of the drops is reduced by only half; it falls from 3.9×10^{-8} cm to 1.95×10^{-8} cm. Since there are always present in air some ions and some water vapor, such fine drops are also always present. But these drops cannot grow to visible size because it can be seen from the solid curve of Fig. I-1 that for the ascending part AB, the saturation vapor pressure must also increase as the drop radius increases. This is not possible physically.

Once the drop has crossed the point B, the saturation vapor pressure decreases as the drop gets bigger, so that water vapor will condense on the drops and the drops increase in size. But the bigger a drop gets, the smaller the saturation pressure and the faster it grows. In fact the region between B and C is unstable and when once the drop has passed the stage B, the drop soon becomes visible. Hence in the presence of ions if the supersaturation increases to 4.1 which corresponds to $V_2/V_1=1.25$ for air and water vapor (see Table I-4) drops will grow on ions as nuclei.

3. Cloud-Like Condensation

Wilson noticed that when the expansion ratio was increased beyond 1.37 with air-water vapor mixture, a dense cloud appeared throughout the chamber even in the absence of any ionizing source. This cloud took a minute or more to settle down and was attended with color phenomena. Below 1.37, the drops are too large for colors and too few for fog, but above 1.44, they are too small to produce colors. The density of the cloud increases rapidly with expansion ratio in this range. The limiting expansion ratio of 1.37 at which a dense cloud appears throughout the chamber is known as the *cloud limit*. At this expansion ratio, supersaturation produced in air-water vapor mixture is of the order of 8 as can be seen from Table I-4.

What are the nuclei on which condensation takes place at eightfold supersaturation? According to J. J. Thomson minute drops of water continuously form in saturated vapor, by the coalescence of vapor molecules, and then instantaneously evaporate away. Some of these may be caught during sudden expansions and

act as condensation centers. These minute droplets of water probably have different sizes with a fairly definite upper limit of 5×10^{-8} cm. When the supersaturation reaches a value of eight, but not before that, only the larger drops ($r=5.2\times10^{-8}$ cm) become effective as condensation centers, but when the expansion ratio exceeds this limit, smaller drops also take part in the condensation, explaining the rapid increase in the density of the cloud with increasing expansion ratio.

In support of his ideas Thomson points out that in the derivation of Eqs. (1.10) and (1.12) the surface tension of a drop has been assumed to be independent of the radius, which may not be true for such small drops. If we take into account the variation of surface tension with the drop radius, Eq. (1.12) is modified into

$$\log\frac{p_r}{p_\infty}=\frac{M}{R\theta\rho}\left(\frac{2T}{r}+\frac{dT}{dr}-\frac{e^2}{8\pi kr^4}\right). \quad (1.13)$$

Taking first the case of uncharged drops, for which $e=0$ we have

$$\log\frac{p_r}{p_\infty}=\frac{M}{R\theta\rho}\left(\frac{2T}{r}+\frac{dT}{dr}\right). \quad (1.14)$$

Now the exact way in which T varies with r is not known. For very thin films Lord Rayleigh has shown that the surface tension should be proportional to the square of the film thickness. Further from the experiments of Reinold, Rucker, and Johannot, Thomson concludes that the surface tension is zero at $r=0$ and then it increases with r, reaches a maximum value at a certain value of r and then diminishes again.

On the basis of the above assumptions, Thomson shows that the variation of

$$\log\frac{p_r}{p_\infty} \text{ or of } \frac{M}{R\theta\rho}\left(\frac{2T}{r}+\frac{dT}{dr}\right)$$

with r, may be represented by a curve of the type shown in Fig. I-2. In this modified curve $\log p_r/p_\infty$ is zero when $r=0$. Log p_r/p_∞ then increases with r, reaches a maximum value and then goes on diminishing until it vanishes and then changes sign.

It is easy to see from this modified curve corresponding to Eq. (1.14), that there will always be a drop whatever the degree of supersaturation. In order to find the radius of the drop corresponding to any supersaturation S, one has to draw a straight line parallel to the abscissa at a distance log S from the origin. The abscissa of the point where this straight line cuts the curve of Fig. I-2 determines the size of the drop. Since the straight line will always cut the curve, we shall always get drops of particular radius r corresponding to any positive value of S. There will always be condensation for the slightest supersaturation.

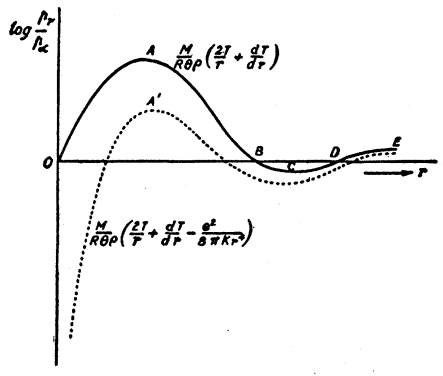

FIG. I-2. Influence of the variation of surface tension on the saturation vapor pressure over a drop.

The radius of these drops will however be too small to be visible, and moreover these drops cannot grow to a visible size as they lie on the ascending part of the curve OA. As soon as the supersaturation ceases, i.e., p_r becomes equal to or less than p_∞, the drops evaporate. But once the drop is past the point A—by producing sufficient supersaturation—p_r the saturation vapor pressure over the drop decreases as the radius increases. Hence water vapor will condense on the drops which will grow in size. The region AC is unstable, and when the drop has passed the stage A, it will soon be large enough to be visible. This is Thomson's explanation of the formation of the dense cloud at eightfold supersaturation—this supersaturation is required to carry the drop past the point A. With higher supersaturations ($S>8$) even smaller nuclei are carried into the region AC and are soon transformed into visible drops. This explains the rapid increase of the density of the cloud with expansion ratio in this range.

According to Thomson the initial droplets, which serve as nuclei for cloud-like condensation, are produced by the coalescence of molecules of water vapor. The larger ones are formed by the coalescence of the smaller ones. The small ones are therefore more numerous than the large ones; there is however a fairly definite upper limit to the size of these droplets. The number of the droplets which exceed this limit is too small to produce a visible cloud.

4. Difference between the Action of Positive and Negative Ions in Producing Condensation

C. T. R. Wilson (1899b) showed further that negatively charged ions act as better condensation nuclei than the positive ones. For air and water vapor, he found that negative ions begin to act as condensation centers when the expansion ratio is 1.25 ($s=4$), whereas the positive ions do not act as nuclei until the expansion ratio is 1.31 ($S=6$). Experimenting with water and several organic liquids, Laby (1908) found that all the vapors (except water) condensed more readily, in air, on the positively charged nuclei than on the negative. The liquids investigated were—acetic acid, amyl alcohol, chloroform, ethyl acetate, ethyl alcohol, ethyl iodide, heptyl alcohol, isoamyl alcohol, methyl butyrate, and propyl acetate.

Scharrer (1939) has again investigated the condensation of supersaturated vapors of water, ethyl, methyl alcohols, benzene, carbon tetrachloride, chloroform, chlorobenzene, and mixture of ethyl alcohol and water on nuclei, natural ions, and ions produced by x-rays. Water and chlorobenzene condense more readily on negative ions, ethyl, methyl alcohol, and chloroform vapors more readily on positive ions; benzene and CCl_4 equally well on both.

Such differences can be explained by assuming that at the surface of a drop, a double layer of electrification is formed, i.e., a layer of one sign at the surface of the drop and a layer of opposite sign in the gas, the distance between the two layers being very small. This assumption is based on the fact that splashing of drops and bubbling of air through water produce electrification.

We have seen [Eq. (1.12)] that

$$(M/R\theta\rho)[(2T/r)-(e^2/8\pi kr^4)]$$

is the excess pressure at the surface of the drop over the saturation value. The first term is the pressure due to the surface tension and the second is due to the electric field ($=kE^2/8\pi$, where $E=e/kr^2$ is the electric intensity). Now if there is a double layer, the electric tension will be modified.

If V is the potential difference between the layers because of their charge and d their separation the tension is $(k/8\pi)(V/d)^2$. The Eq. (1.12) is now modified to

$$\log_e\frac{p_r}{p_\infty}=\frac{M}{R\theta\rho}\left\{\frac{2T}{r}-\frac{k}{8\pi}\left(\frac{V}{d}+\frac{e}{kr^2}\right)^2\right\}, \quad (1.15)$$

and when $e=0$, i.e., for uncharged drops, we have the corresponding equation

$$\log_e\frac{p_r}{p_\infty}=\frac{M}{R\theta\rho}\left\{\frac{2T}{r}-\frac{kV^2}{8\pi d^2}\right\}. \quad (1.16)$$

Comparing Eqs. (1.15) and (1.16) we see that for a charged drop the terms inside the bracket on the right-hand side are diminished by

$$\frac{e^2}{8\pi kr^4}+\frac{eV}{4\pi dr^2}. \quad (1.17)$$

The first term is always positive, so we deal with the second term alone.

If $eV/4\pi dr^2$ is positive, the right-hand side of (1.15) becomes less, or p_r/p_α becomes less for a given r i.e., less supersaturation than previously is required. Thus condensation is promoted. On the other hand if $eV/4\pi dr^2$ is negative condensation will be retarded.

Now the electric field V/d due to the double layer has a fixed direction depending on the gas. So if the ion has a charge which produces a field in the same sense, the product will be positive and the ion will act as a better condensation center.

When a fresh surface of water is exposed to air, the air gets negatively electrified and an equal quantity of positive charge goes to the water surface to form the outer coating of the double layer. This double layer has negative charge on water and positive charge on the air surface. So the field is inwards. Thus a negatively charged ion would be more efficient than one positively charged, in the case of water vapor.

In some liquids, the electrification produced

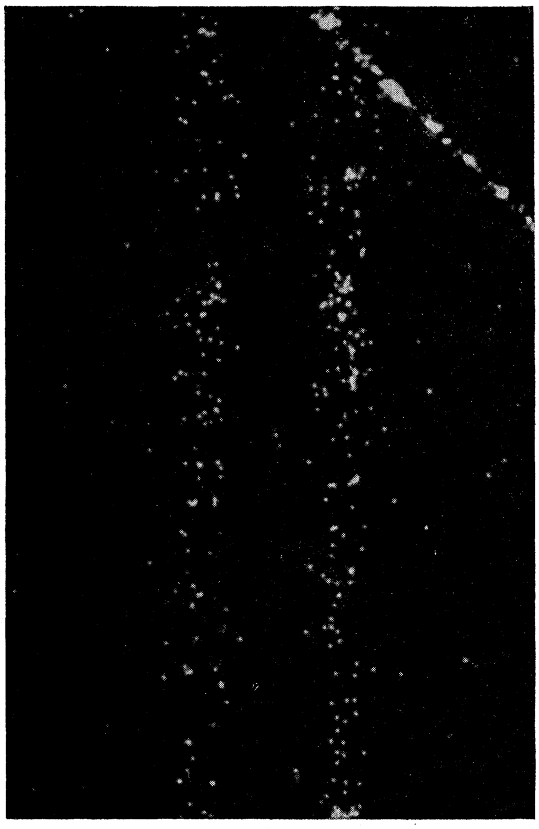

FIG. I-3. Difference in the action of positive and negative ions in producing condensation. The ions have diffused and formed into columns of positive and negative ions before the drops are formed. The denser column of drops is formed on positive ions. [From Hazen, Phys. Rev. 65, 259 (1944).]

by bubbling air through them is positive and not negative. In such cases the field is outwards and so a positive ion is more efficient as condensation center. This has been found to be true for alcohols by Laby (1908), Scharrer (1939), and Hazen (1944b). By the application of a strong electric field, it is possible to separate the drops formed on positive and negative ions as centers; Figure I-3 obtained in this way by Hazen shows clearly the difference in action of positive and negative ions. The denser column of drops is formed on positive ions.

5. Ion and Cloud Limits

Wilson found that with air-water vapor mixture and at an expansion of 1.25, rain-like condensation takes place on ions as nuclei, whereas at expansion ratios above 1.37 the condensation is cloud-like and occurs throughout the chamber possibly on associated vapor molecules as centers. These two limiting expansion ratios may be termed the *ion* and *cloud limits*. Wilson's original experimental results were confirmed and extended by Powell (1928), Volmer and Flood (1934), Flood (1934), and Beck (1941).

Powell used a gamma-ray source in order to distinguish between the ion and the cloud limits. He found that in the presence of the gamma-ray source and with air-water vapor inside the Wilson chamber, drops are produced at an expansion ratio of 1.25 by volume (supersaturation 4). On removing the gamma-ray source there is no condensation until the expansion ratio reaches the value of 1.37 (supersaturation 8).

Flood used a strong electric field to remove the natural ions as soon as they were formed. In the presence of the field, the ions are absent and the condensation takes place only on associated vapor molecules and correspond to the cloud limit. On the other hand, the minimum expansion required for the formation of the drops in the absence of the field—when the ions are present—corresponds to the ion limit. Flood also studied the variation of the cloud and the ion limits with composition of the liquid mixture used. Table I-8, compiled by Flood, indicates the variation of the cloud and the ion limits with the percentage composition of water alcohol mixture.

It will be found from Table I-8 that the ion and the cloud limits with 100 percent C_2H_5OH set in earlier than with 100 percent water. It is also seen that the expansion ratio required to reach the ion and the cloud limits is minimum for a particular composition of water alcohol mixture. Evidently this composition will be the ideal for chamber work, provided it produces a minimum background of fog.

TABLE I-8. Cloud and ion limits with different compositions.

% of C_2H_5OH by weight	% of C_2H_5OH by volume	Expansion ratio without field (ion limit)	Expansion ratio with field (cloud limit)	% of C_2H_5OH by weight	% of C_2H_5OH by volume	Expansion ratio without field (ion limit)	Expansion ratio with field (cloud limit)
00.0	00.0	1.251	1.276	58.3	63.0	1.101	1.113
9.3	11.	1.155	1.174	67.8	73.	1.105	1.114
24.9	30.	1.115	1.130	73.4	77.	1.100	1.112
44.2	49.	1.110	1.112	83.9	87.	1.114	1.128
50.4	57.	1.098	1.107	90.0	92.	1.119	1.132
52.8	59.	1.103	1.114	96.0	96.	1.142	1.158
				100.0	100.	1.152	1.172

6. Critical Supersaturation

We have seen before (see Table I-4) that for the same expansion, supersaturation is less with alcohol than with water vapor. On the basis of Flood's (1934) results, we have to conclude that the ion or cloud limit sets in for smaller supersaturation in alcohol vapor than with water vapor, and that the ion limit or the cloud limit can be pushed down further by using a mixture of 70 percent by volume of C_2H_5OH and 30 percent by volume of water. This may be explained by the fact that the ion or cloud limit is ultimately dependent on the number of drops formed per cc and for the same supersaturation this number may vary for different liquids.

The number of drops formed per cc has been calculated by Volmer and Weber (1926) and Farkas (1927). They assume with Thomson that there are always present in equilibrium a certain number of nuclei in saturated vapor. These are in a state of formation and evaporation but may act as condensation center for the drops.

The work done to form such an embryonic drop of radius "r" is given by the formula $W=4\pi r^2T/3$, which was derived by Gibbs from thermodynamic considerations. T is the surface tension of the drops.

Volmer and Weber (1926) showed from thermodynamic considerations that the number of stationary embryos is proportional to

$$Z=A\exp\left[-4\pi r^2T/3k\theta\right], \qquad (1.18)$$

where k is Boltzmann's constant. Farkas (1927) has shown that

$$A=\frac{2c}{F}\alpha p_\infty\left(\frac{T}{k\theta}\right)^{\frac{1}{2}},$$

where $C=$constant, $F=4\pi r^2$, $\alpha=N/(2\pi R\theta M)^{\frac{1}{2}}$, $M=$molecular weight of the liquid, and p_∞ =saturation pressure at the temperature θ. Hence the number of drops formed per cc, is given by

$$Z(n)=\frac{2c}{F}\alpha p_\infty\left(\frac{T}{k\theta}\right)^{\frac{1}{2}}\exp\left[-\frac{4\pi r^2T}{3k\theta}\right]. \qquad (1.19)$$

In order to compare the effective supersaturation for good tracks, we define a critical supersaturation S_c such that at the critical supersaturation the number of drops formed per cc is of the order of unity. Hence at critical supersaturation

$$\frac{4}{3}\frac{\pi r^2T}{k\theta}=\ln\left[\frac{2c}{F}\alpha p_\infty(T/k\theta)^{\frac{1}{2}}\right]. \qquad (1.20)$$

Also the critical supersaturation S_c is defined by Thomson's formula [Eq. (1.10)]

$$S_c=\frac{p_r}{p_\infty}=\exp\left[\frac{2T}{r}\frac{M}{R\theta\rho}\right]$$

or

$$\log S_c=\frac{T}{\theta}\frac{M}{\rho}\cdot\frac{2}{Rr}. \qquad (1.21)$$

Substituting for $1/r$ from Eq. (1.20), we have

$$\log S_c=\left(\frac{T}{\theta}\right)^{\frac{3}{2}}\frac{M}{\rho}\cdot\frac{2}{R}\left(\frac{4\pi}{3k}\right)^{\frac{1}{2}}\times\left\{1/\ln\left[\frac{2c}{F}\alpha p_\infty\left(\frac{T}{k\theta}\right)^{\frac{1}{2}}\right]\right\}^{\frac{1}{2}}\simeq D\left(\frac{T}{\theta}\right)^{\frac{3}{2}}\frac{M}{\rho}, \qquad (1.22)$$

where D is a constant if we neglect slight variations inside the log term.

In the case of pure liquids S_c may be calculated with the help of the Eq. (1.21) and then compared with the experimental results. Table I-9 reproduced from the work of Volmer and Flood (1934) shows that the agreement between the theoretical and experimental results is quite satisfactory. The empirical constant D has been chosen to bring agreement between the theoretical and experimental results for water at $\theta=264°$ absolute.

The ideal mixture for use in cloud-chamber work is one which has the lowest critical super-

TABLE I-9. Comparison of experimental and theoretical values of supersaturation (Volmer and Flood).

Substance	θ	M	ρ	M/ρ	T	S_c (theo.)	S_c (exp.)
Water	264	18	1.00	18.0	77.0	4.85	4.85
Ethyl alcohol	273	46	0.81	56.8	24.0	2.30	2.34
n-propyl alcohol	270	60	0.81	74.3	25.4	3.20	3.05
Isopropyl alcohol	265	60	0.82	73.4	23.1	2.90	2.80
Methyl alcohol	270	32	0.81	39.5	24.8	1.84	3.20

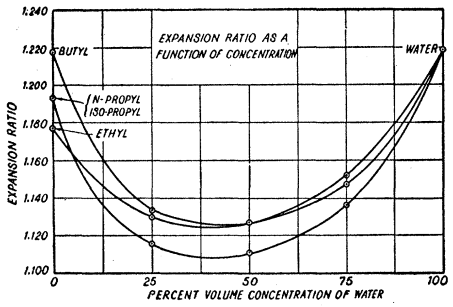

FIG. I-4. Expansion ratio for the formation of best tracks as a function of the concentration of alcohol-water mixture.

saturation, i.e., the smallest molecular volume, associated with a low surface tension. As Table I-9 shows, water has a low molecular volume but a high surface tension, while the reverse is true for alcohols. By combining water in a suitable proportion with alcohol, it is possible to obtain a lower critical supersaturation than with a pure liquid. Such a combination is ethyl alcohol and water.

When a mixture of two liquids is used, as a source of condensing vapor, the drops that are formed contain both the liquids. Flood (1934) shows that even in such cases we can still define a critical supersaturation S_c' given by an equation similar to (1.21)

$$\log S_c' = k(T'/\theta)(M/\rho)', \qquad (1.23)$$

where $(M/\rho)'$ now refers to the molecular volume of the mixture and T' the surface tension of the droplets. Knowing the molar percentage of the two liquids in the drops, it is possible to calculate S_c' with the help of above equation and to compare it with the experimental values. Flood obtained good agreement between the calculated and experimental values in the case of ethyl alcohol-water mixture. The critical supersaturation reaches a minimum value of 1.68 with a mixture containing 60 percent of alcohol, 40 percent of water by volume.

Loughridge and Trueblood (1934) have investigated several other organic liquids suitable for Wilson chamber.

Beck (1941) carried out a series of experiments in order to determine experimentally, the optimum liquid combination for use in cloud-chamber work, i.e., a liquid mixture giving low expansion ratio, low background fog, and good electron tracks in a cloud chamber filled with air at nearly atmospheric pressure. A small quantity (about 5 cc) of liquid containing alcohol and water in different concentration, is introduced into the chamber and the expansion ratios required for the appearance of tracks, best tracks, and the beginning of general fog are carefully observed. By "best tracks" is meant, that the droplets should be numerous, well-developed while the general fog which forms simultaneously with the track is inconspicuous.

Beck found that mixtures of two pure alcohols were unsuitable. They required higher expansion ratios, but produced poorer tracks and higher background fogs than for either pure alcohols or water-alcohol mixtures. Beck's results for various alcohol-water mixtures are reproduced in Fig. I-4. His investigations indicate that the condition for best tracks is obtained with a minimum expansion ratio of 1.125 for 65 percent ethyl alcohol and 35 percent water when air is used as the non-condensing gas. But still better results are obtained with 50 percent ethyl or normal propyl alcohol, 25 percent acetone, 25 percent water at an expansion ratio of 1.112. The presence of acetone increases the contrast between the tracks and the background fog.

7. Growth of Drops

Let us now consider how starting from molecules or ions, drops of cloud, rain, or fog are formed within the cloud chamber and grow to visible size.

The words "rain," "cloud," and "fog" are used in a technical sense by meteorologists. Figure (I-5) reproduced from an address by Simpson (1941) shows the size of particles with which we are concerned here. On the left of the figure is given a logarithmic scale of lengths and as land marks on this scale have been entered familiar points, e.g., the limit of unaided vision at 5×10^{-3} cm, limit of microscopic vision at 2×10^{-5} cm, and the wave-lengths of the visible light extending from 4×10^{-5} to 7×10^{-5} cm.

The sizes of cloud particles and of rain drops observed in nature vary over wide limits. This is indicated by vertical lines or brackets extending over the range in diameters. One of the lines

ends in arrows, indicating that the sizes must extend beyond the limits shown. Thus while the usual size of a cloud particle extends from 2×10^{-3} to 4×10^{-4} cm which include the most frequent diameter of the clouds, the cloud particles must extend to smaller sizes and join up with the ions on one side and also extend towards larger sizes and join up with the rain drops. This is indicated by the arrow heads. On the right-hand side of the figure are two tables. The upper one giving supersaturation required to cause condensation on nuclei of various sizes, the lower one mass and the velocity of descent of water drops of different sizes, calculated from Stokes' law.

The sizes of the particles with which we are most interested in this section are:

10^{-8} cm—molecules,
10^{-7} cm—small ions,
10^{-6} cm—medium large ions,
10^{-5} cm—ultra large ions,
10^{-4} cm to 10^{-3} cm—cloud particles,
10^{-2} cm to 10^{-1} cm—rain drops.

According to the ideas of J. J. Thomson developed in the previous sections, small drops of water of radius 5.2×10^{-8} cm or less are always being formed and then evaporating away in saturated vapor. The primary physical process which results in the formation of these drops is not very clear. The radius of a molecule of water

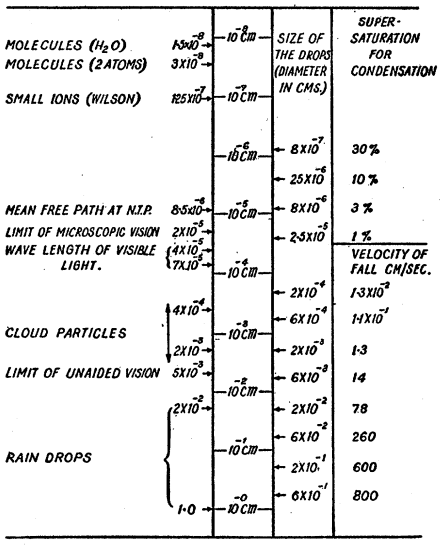

FIG. I-5. Relative sizes of molecules, ions, cloud particles, and rain drops.

vapor as deduced from viscosity measurements is 2×10^{-8} cm and a molecule of water vapor weighs about 5.4×10^{-26} g. A water drop of the size assumed by Thomson requires a coalescence of about 10^4 molecules. This number is to be compared with the number of collisions per sec. between two water molecules at N.T.P., which is of the order of $7.1\times10^{+7}$ per sec. When one remembers that the thermal velocity of a water molecule at N.T.P. is 6.15×10^4 cm/sec., it is difficult to visualize a process in which such a large number of molecules associate together after collisions without recoiling. Moreover at such small radii of the drops, the vapor pressures must be considerably greater than the saturation pressures.

But whatever the process once the small embryonic drops of radius about 5.2×10^{-8} cm are formed, they can act as centers for further condensation provided the amount of supersaturation exceeds the value of four. As explained before in this range the equilibrium vapor pressure over the drop diminishes as the drop radius increases and therefore the vapor from the surrounding space diffuses on to the surface of the drop. The growth of the drops can be calculated with the help of diffusion equations

$$dm/dt=4\pi r^2D(d\rho/dr), \qquad (1.24)$$

where D is the coefficient of diffusion and $d\rho/dr$ the density gradient at any distance r from the center of the drop. For $d\rho/dr$ one can substitute approximately $(\rho_D-\rho_2)/r_0$, assuming that the density changes from the liquid density ρ_D at the center of the drop to ρ_2 the saturated vapor density at the surface of the drop. With the above assumption, since $m=(4/3)\pi r_0^3\rho$ the Eq. (1.24) may be written as

$$dr_0^2/dt=(2D/\rho)(\rho_D-\rho_2). \qquad (1.25)$$

With the Eq. (1.24) is closely related the latent heat equation

$$\lambda(dm/dt)=4\pi r^2K(d\theta/dr), \qquad (1.26)$$

where λ is the latent heat, K conductivity, and $d\theta/dr$ the temperature gradient at any place. Here, as in the previous case, it may be assumed that the drop temperature changes from θ_D at the center to θ_2 at the surface of the drop. θ_2 is also

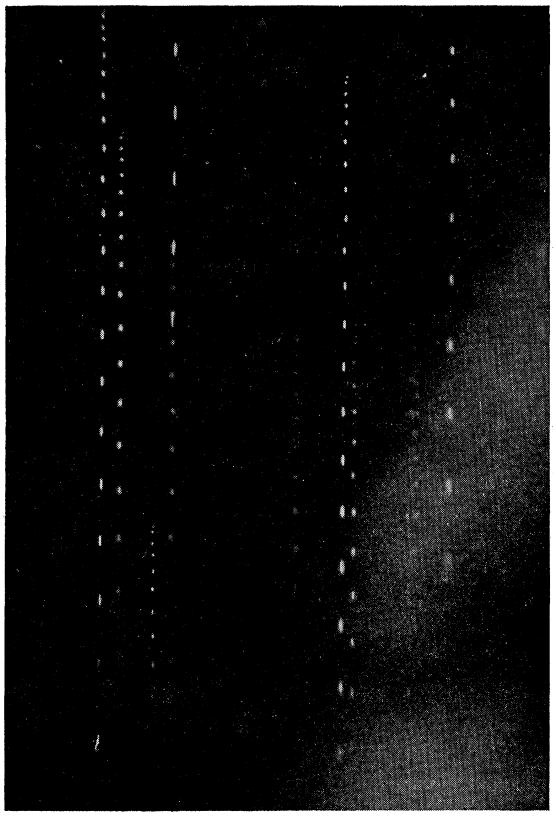

FIG. I-6. Growth of drops. Falling drops in helium and the vapor from 95 percent C_2H_5OH photographed with illumination which flashed 30 times per second. [Hazen, Rev. Sci. Inst. **13**, 247 (1942).]

the temperature of the space. Then corresponding to (1.25) we have the equation

$$dr_0^2/dt = (2K/\rho\lambda)(\theta_D - \theta_2). \qquad (1.27)$$

With the help of the equations given in Section I-1, and Eqs. (1.25) and (1.27) it is possible to obtain an expression for the rate of the growth of the drops in terms of known quantities. When this is done it can be shown that r_0^2 varies approximately linearly with time, a fact which also seems to be justified by the experimental results of Hazen which will now be described.

TABLE I-10. Temperature of drops in the vapor from 95 percent C_2H_5OH. Total pressure was between 1.1 and 1.2 atmospheres.

Permanent gas	N_2	H_2	He
Percent expansion	16	15	10
$\theta_D - \theta_2$ (Eq. (1.27))	10	4	4
$\theta_1 - \theta_2$ (adiabatic)	15.5	15	15

The size of the drops inside the cloud chamber may be determined either with the help of Stoke's law (Brode 1939) or directly from a photographic record. The sizes determined by the second method are not very reliable, because the image of the drop recorded on the film depends on the illumination, the quality of the film emulsion and on the diffraction produced by the lens.

Hazen determined the rate of growth of the drops by photographing a drop as it moves in a gravitational field with periodic illumination. A typical photograph is shown in Fig. I-6. Taking into consideration that magnification is linear with distance measured on the film, he has determined the actual values of r_0^2 at different intervals and has found that r_0^2 varies linearly with time. The actual values of dr_0^2/dt for nitrogen with 15 percent expansion is 5×10^{-6} cm^2/sec. The result is also obtained by calculation. However there is no agreement between the calculated and the experimental values for dr_0^2/dt in the case of hydrogen.

With the measured values of dr_0^2/dt, the drop temperature can be calculated from the Eq. (1.27). Table I-10 compiled by Hazen compares the values of $\theta_D - \theta_2$ obtained in this way with the adiabatic drop in temperature $\theta_1 - \theta_2$. Thus the drop temperature is always slightly higher than that of the surrounding gas, the difference being greatest in nitrogen.

CHAPTER II. DIFFERENT TYPES OF WILSON CHAMBER

1. Earlier Forms of Cloud Chamber

C. T. R. Wilson's original apparatus (Fig. II-1) has been described in many textbooks in detail, and we propose to discuss in this section only the various modifications which have been made upon Wilson's (1912) original apparatus, to make it suitable for investigating special types of phenomena.

One of the drawbacks of the original Wilson's method is that the whole process is much too slow. Nuclear phenomena are however so rare

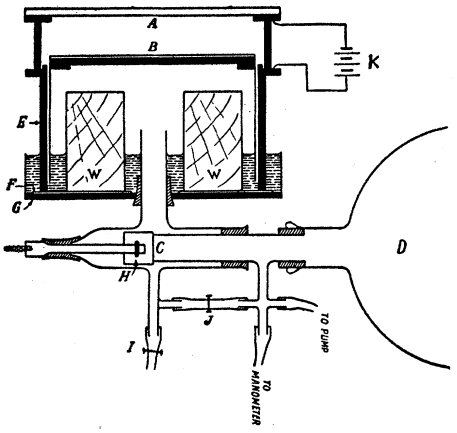

FIG. II-1. Wilson's original cloud chamber.

AB = expansion chamber, cylindrical in shape and completely closed,
B = movable base which slides inside cylinder E and serves as piston,
F = rubber sheet resting on a brass disk G to arrest downward motion of B,
D = highly evacuated vessel which may be put in communication with the space below B by opening the valve C,
WW = wooden blocks reducing the air space within the chamber,
I = stopcock on opening which space below B is connected with the atmosphere and the piston brought back to the original position,
J = pinch cock for adjusting the initial position of the piston and hence the expansion ratio,
K = battery providing the electric field to remove stray ions just before a fresh expansion.

that one must take numerous photographs before one can expect to get a picture of the phenomenon itself. Blackett (1925) records that he photographed 10^6 α-ray tracks in nitrogen out of which only in 20 cases the particle was captured by the nitrogen nucleus and protons were emitted. Obviously for photographing such rare types of nuclear phenomena an automatic arrangement is required in which the expansion can be rapidly repeated and photographs taken continuously. The earliest of such modifications is attributed to Shimizu (1921). In Shimizu's apparatus the piston executes a reciprocating motion producing alternate compressions and expansions and the operation may be continued as long as necessary without interruption.

Shimizu also developed a method for obtaining simultaneous photographs of two images of the tracks viewed from two different directions at right angles to each other. Shimizu's method was used by many subsequent investigators including Blackett, Harkins and Ryans, and Auger and Perrin in investigating the complicated collision problems caused by the passage of α- and β-rays.

Blackett showed that although Shimizu's method is very efficient for continuous photography of α-tracks the tracks obtained are not as sharp as in Wilson's original method. The excellent definition of the tracks requires very sudden expansions which are a characteristic of Wilson's original method.

Blackett (1927) modified Shimizu's apparatus by replacing the reciprocating mechanism by a simple spring action. This combines the merit of sudden expansion of Wilson's original design with the mechanism of repeating it as frequently as desired.

Other modifications were introduced by him in the control mechanism in (1927) and (1929a). With this modified chamber Blackett was able to take 1270 photographs every day, each containing about 20 α-ray tracks [Blackett and Lees (1931, 1932)].

All the cloud chambers used before 1933 are essentially of a type in which a definite volume change is produced in the expansion chamber by a sudden motion of the piston or the plunger forming the floor of the chamber. This is brought to rest by striking against a base plate, so that the volume at the completion of the expansion stroke remains constant but the pressure in the expansion volume, i.e., the working chamber increases as temperature rises after expansion (see Chapter III, Section 5). In all these cases water or oil seal is used limiting the use of the chamber in the horizontal position.

Wilson (1933) first introduced an important change in the method of producing expansion. In this modification the chamber is given a fixed floor of wire gauze backed by a thin rubber diaphragm which is pressed by compressed air in the back chamber. The expansion is effected by allowing the whole or a part of the air from the back chamber to escape into the atmosphere or into a large chamber kept at a desired final pressure; the rubber diaphragm thereby moves outwards causing an expansion of volume in the working chamber. This type of apparatus is simpler to construct and may be used in any position, horizontal or vertical. Moreover in this form of the chamber, the rise of temperature in the working chamber, because of heat conduction from the walls or condensation to form a cloud, is not so rapid as in the previous type. The piston being elastic resists sudden changes of

pressure and after expansion a longer interval of time is therefore available in which necessary supersaturation persists. All the chambers designed now-a-days belong to this modified type.

We now mention very briefly some other modifications which have been made in the design of the cloud chamber by various workers to remove particular difficulties. Dahl, Hafstad, and Tuve (1933) felt that in chambers which had small leaks, it was necessary to adjust the expansion ratio after a few days and so designed a permanently sealed chamber using sylphon bellows. This bellows forms a part of the working chamber and can be compressed or expanded mechanically or by means of a high pressure gas. This was the first sylphon bellows type of the chamber. Modifications of this form have been made by Dempster (1934), Brubaker and Bonner (1935), and Crane (1937), and most of these chambers have been used for nuclear disintegration studies. The bellows type of chamber is found to have smaller turbulences than the earlier piston type or the new rubber diaphragm type of chambers.

Another important modification of the expansion chamber was made by Wilson and Wilson (1935) in which the expansion is radial. The expansion within the cloud chamber is brought about by a sudden reduction of pressure in the annular space by opening communication with the surrounding atmosphere, the air escaping through perforation of suitable aperture. In the radial form of expansion, the chamber can be illuminated from the back and thus the problem of proper illumination becomes greatly reduced. (See Chapter III, Section 1). It is also possible to place source or targets near the axis of the chamber without causing appreciable disturbance. The advantages of the radially expanding chamber have also been discussed by Trey (1938).

Wilson and Wilson (1935) also tried to develop a falling type of chamber in which both the chamber and the camera are allowed to fall freely under gravity. The falling type of chamber has the advantage that the disturbing effect of gravity is eliminated as the droplets do not fall relatively with the gas in the chamber the convection effects are minimized. The time interval between expansion and taking of photographs may be extended without the risk of distortion because of the fall of the drops. With the falling camera, the time of exposure can be increased and a continuous source of illumination has possibilities for its use. This type of chamber has not been used by later workers because of the great mechanical difficulties. Locher (1933a) has described a rectangular chamber with which he has photographed cosmic-ray bursts. Rectangular chambers however are not much in use, because the distortions are greater for such chambers than for cylindrical chambers.

Among other important modifications of the chamber may be mentioned the attempts made to have a continuously sensitive chamber by the diffusion of warm saturated vapor through a non-condensible gas into a refrigerated space [Langsdorf (1939)]. The diffusion is vertically downwards between a horizontal heated roof and a refrigerated floor. The vapor is supplied from liquid in a glass flask heated by radiation from above. It is however difficult to produce very sharp tracks in such a chamber. Vollrath (1936) tried to produce supersaturation continuously by allowing HCl and H_2O vapor to diffuse. Trey (1940) tried to produce continuous clouds in gases by removing heat from the vapor by conduction. Brinkman (1939a, 1939b) describes a continuously running cloud chamber which makes several expansions per sec. Portable light weight chambers have been described by Locher (1933b), Livingston (1936), Bauer (1936), Rathenau (1938), Hilsch (1939), Thomas and Ramsay (1939), Kunze (1941), and Herzog (1941). Cloud chambers for projection purposes have been described by Herzog (1937), Hilsch (1939), Livingston (1936), and Rathenau (1938).

2. Counter-Controlled Chambers

For the study of nuclear phenomena, where strong sources may be employed, there is little difficulty in obtaining a number of tracks of α- or β-ray in every picture. But where the phenomena to be studied are of rare occurrence such as cosmic rays, chambers operated at random are at a disadvantage. Cosmic rays do not always traverse the chamber and may altogether be absent when the photograph is being taken.

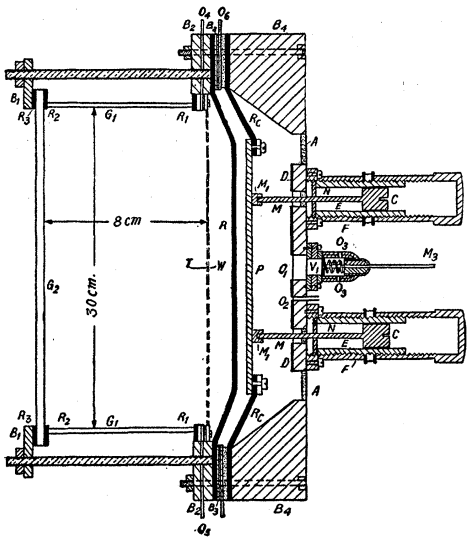

FIG. II-2. The diagram shows a vertical section of the cloud chamber through the axis of the cylinder.

G_1—section of the glass cylinder taken from the sides.
G_2—thick glass plate covering G_1, through which the picture is taken.
R_1, R_2, R_3—rubber gaskets for making the chamber air tight.
R—rubber diaphragm whose motion produces compression and expansion.
W—wire netting in front of R to reduce turbulence inside chamber.
T—a piece of black velvet soaked with alcohol water mixture to produce a perfectly dark background and also to reduce turbulence.
P—brass plate serving as piston and fixed on annular rubber cloth.
M_1—rod screwed on to P which slides inside the brass tube E when the piston works.
N—stop fixed rigidly with the brass tube E which limits the maximum forward motion of the screw head C on the compression stroke.
E—brass tube with screws on the outer surface which may be moved towards or away from P by screwing it in or out of tube F. The position of E thus controls the expansion ratio.
O_2—inlet for air into the back chamber. This is permanently connected with the compressor unit through a regulative valve V_2 shown in the following figure.
O_1—outlet for air from the back chamber. This is closed when valve is in its most forward position.
V_1—valve controlling escape of air. When V_1 is pushed back, air escapes through O_1 and O_3.
O_4—inlet for alcohol-water mixture. This is closed during the operation of the chamber.
O_5—inlet for gas into the front chamber. This also remains closed after gas mixture has been introduced.
O_6—a hole in brass piece B_3 which connects the space between the rubber diaphragm and the piston with atmospheric air. This facilitates quick forward and backward motion of the piston.

Blackett and Occhialini (1933) and Anderson (1933) almost simultaneously introduced the counter-controlled chamber, in which the chamber is normally inactive but as the cosmic ray passes through the counters placed above and below the chamber a series of mechanisms is released and the track is automatically photographed. The various incidents taking place in succession are:

(1) passage of an ionizing particle through the top counter, chamber, and the bottom counter,
(2) expansion of the chamber,
(3) flashing of the light and illumination of the drops,
(4) exposure before the drops have grown sufficiently large in size, and
(5) resetting of the chamber and making ready for another expansion.

These operations take place every time a coincidence discharge of the counters occurs. Blackett and Occhialini state that 80 percent of the plates thus exposed contain cosmic-ray tracks, and we get a larger proportion of multi-rayed or shower pictures.

In a counter-controlled chamber the mechanisms controlling the release of the piston, its resetting, and various other factors are slightly

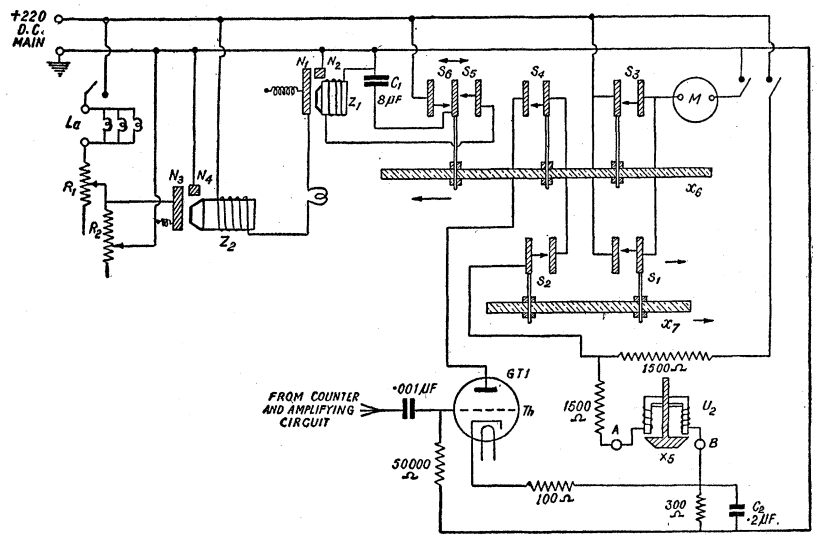

FIG. II-3a.

FIG. II-3b.

The control mechanism of automatic counter-controlled chamber is shown in Figs. II-3 and II-4.

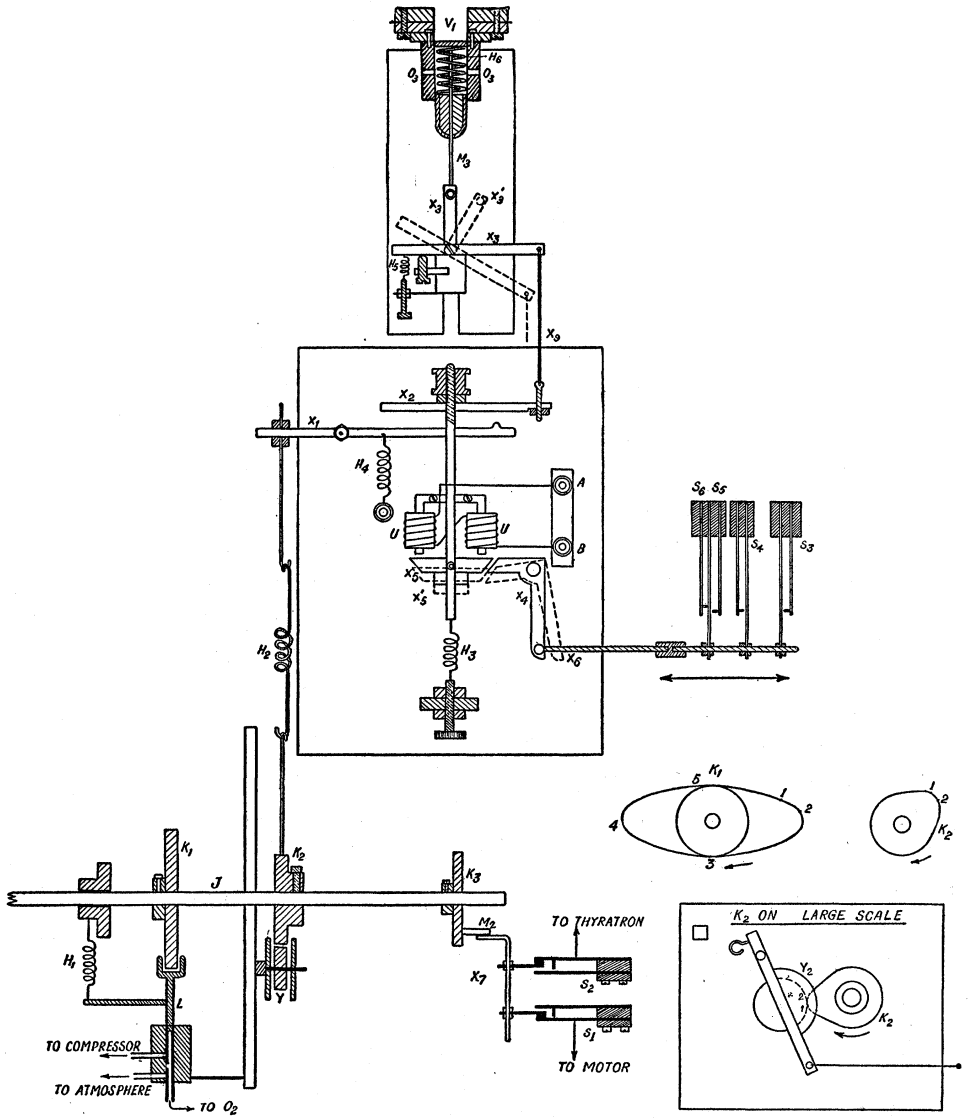

V_1—valve for producing expansion.

M_3—rod rigidly connected to the plate I and resting on one arm of a T-shaped metal piece X_3 hinged at Q. When X_3 is moved to position X_3', M_3 slips producing an expansion.

Th—gas filled relay ($GT1C$) which is connected in parallel to the electromagnet U_2 through S_2, S_4. When the coincident counter pulse is applied to the grid of the thyratron, it flashes short-circuiting the electromagnet.

U_1—electromagnet which holds the armature normally in the position X_5. When the current through the electromagnet stops, armature moves from the position X_5 to X_5' pulling with it the T piece X_3 to the displaced position X_3' which causes an expansion. This pull is communicated via X_8, X_2, X_9.

H_3—spring to pull back X_5 when the electric current through U_1 is stopped.

X_4—brass arm which communicates a lateral push to X_6 when X_5 is moving to the position X_5'. This motion of X_6 makes the switches S_5, S_3, on and switches S_6, S_4 off.

S_5—switch which discharges the condenser C_1 through the relay Z_1, thus completing the circuit $N_2N_1Z_2$ which in turn short-circuits R_2, applying the full voltage on to the lamps La. The duration of illumination is governed by the time necessary for the leakage of charge from C_1 through the inductance z_1.

R_1, R_2—current limiting resistances where $R_1 \ll R_2$.

S_3—switch which starts the motor M rotating the shaft J which carries three cams K_1, K_2, K_3.

K_2—cam for resetting the valve and armature X_5. As K_2 rotates at a certain position of K (point 2 against V), a push is communicated to X_3 (via H_2, X_1, X_2) resetting M_3 against X_3. The valve V_1 is thus closed and held so by the electromagnet U_1. Simultaneously X_4 pulls X_6 to the left closing the contacts S_4 (thyratron) and S_6 (condenser charge).

K_1—as J rotates, K_1 first comes to position 2 and begins to let in air through V_2 and O_2. When K_1 is at position 3, air is let out through O_2. One cleaning expansion is produced to remove any remaining ions before the final expansion is made. When K_1 is at position 4, air is again let in, with K_1 at 5, V_2 is full open to compressor unit. When K_1 finally comes to 1, compressor is disconnected from the chamber.

K_3—cam carrying a rod M_2 which strikes against X_7 when K_1 and K_2 are in position 1. This disconnects S_1 (motor) and connects S_2 (thyratron plate).

The chamber is now ready for an expansion. When the grid of the thyratron is excited by a coincident pulse, it is short-circuited, thereby V_1 is opened causing expansion and simultaneously the light is flashed on as explained above. The camera shutter is always kept open so that an exposure is recorded. As soon as the expansion has occured the motor circuit is completed through S_3 and the chamber is made ready for another expansion, through K_1, K_2, K_3. The spool of the film is also coupled mechanically to the shaft J, so that the camera is also made ready for a new exposure by the time the chamber is reset. The compressor unit supplying compressed air, which moves the piston, starts or stops through an automatic arrangement as soon as the pressure inside the reservoir falls below or rises above certain limits which again can be adjusted as desired.

different. The operation of the chamber will be clear from Figs. II-2, -3a, and -3b.

Different types of vacuum tube circuits for control of cloud chamber operation and also to regulate the timing of events have been described by Richardson (1938b), Barendengt and Sizoo (1939), Getting (1939), Street and Stevenson (1936), and Jones (1937).

3. Random Operated Slow Chambers

As has already been mentioned the counter-controlled chamber was designed mainly to study rarer and also some particular types of phenomena in cosmic rays, so that the expenditure to run the investigation might be minimized by an economic use of film and specially of time. But a chamber controlled in this way has some inherent drawbacks.

Firstly, it has some bias in favor or against some particular phenomenon and will not represent the normal relative frequency of the different types of particles and particles of low energy, e.g., it will record a larger number of shower particles than is statistically due and the low energy particles will be underestimated. Secondly, when a magnet is used to measure the energy of the particles recorded, either the magnet must be a permanent one, in which case it will not be possible to use a high field, or the electromagnet must be run continuously. This means a tremendous demand on electric power together with an increased difficulty in the task of properly controlling the temperature of the chamber.

Evidently the best method is to devise a chamber which will run in a completely automatic way and yet record several tracks per random expansion. The result will be a true statistical representation and the field can be switched on, one or two seconds before the expansion and switched off after the expansion has been completed.

Bearden (1935) first realized that the yield of tracks per expansion would increase with an increase in the sensitive time (see Chapter III, Section 5) of the chamber. He increased the sensitive time of a sylphon bellows type, air-driven chamber (20 cm in diameter and 4 cm deep) to about 2.0 sec. by using a slow rate of expansion and recorded about 4 cosmic particles per expansion. This was achieved by allowing the air expanding the bellows to leak slowly through a valve. Frisch (1935) also designed a chamber similar in principle to Bearden's. Bearden's chamber was water sealed and could be used only in a horizontal position and was therefore not suitable for studying cosmic rays. With such slow expansions the tracks become diffuse.

The control mechanism in random expansion chambers is similar to that in counter-controlled chambers. The electromagnet holding the release valve of the chamber is short circuited at regular intervals by a clockwork mechanism; a few seconds before this the magnetic field used to deflect the particles is established, and when the expansion is over it is cut off. The mechanism then resets the chamber.

Williams (1939a) showed that the sensitive time of a chamber could be increased by increasing the depth of the chamber and so constructed (1939b) a rubber-diaphragm type of chamber, 30 cm in diameter and 30 cm deep. This chamber recorded two or three tracks per expansion and was used in conjunction with a Helmholtz type of coil producing 2200 gauss. Williams' chamber can be used both in horizontal and vertical positions and enjoys the privilege of stronger illumination by the inclined method (see Chapter III, Section 1) because of its greater depth over Bearden's chamber. Williams and Roberts (1940) later designed a still bigger chamber 60 cm in diameter and 50 cm deep and were successful in getting a meson-decay track. This large sensitive time and volume of a chamber make it a very sensitive detector of radiations from radioactive bodies and the chamber has been used by Walke, Williams, and Evans (1939) for this purpose.

Maier-Leibnitz (1939) describes a slow chamber in which a sensitive time of about 1 sec. was attained. Hazen (1942) has constructed a deep chamber having a sensitive time of about 0.5 sec. Herzog (1935) also constructed a large chamber for this purpose.

It should be marked, that the larger yield per expansion is caused by the larger sensitive time of the chamber and the larger diameter of the chamber. The average number of cosmic-ray tracks recorded per photograph is $jdxt_S$,

where j=number of cosmic-ray particles/cm² sec.; d=diameter of the region photographed; x=depth of focus of the camera used; and t_S=sensitive time of the chamber. In Williams' chamber, $d\simeq 24$ cm, $x\simeq 5$ cm, and $t_S\simeq 0.4$ sec.; and since $j\simeq 0.03$, the number of tracks recorded per photograph was about 1.5.

4. Low and High Pressure Chambers

Sometimes a chamber is used with a low pressure inside the working volume, e.g., to obtain tracks of fission fragments. In this case more care has to be taken to make the working chamber leak-tight. The back chamber is connected to a vessel, the pressure inside which is slightly higher than that inside the working volume. The expansion is effected by connecting the back chamber to an evacuated vessel. Joliot (1934) has described a chamber which can be worked at various pressures. Low pressure chambers are essential for the study of fission fragments and other particles whose range is only a few mm in normal air (see Chapter V, Section 6).

The design of the extra high pressure Wilson chamber is the latest marked improvement in the technique of the Wilson chamber. The usual procedure for investigating interactions between very high energy particles (cosmic rays) and matter has been to observe the rays emerging from layers of dense materials after the process under investigation has taken place somewhere inside the layer. The frequency of occurrence of the phenomena is often so very low that large thicknesses of materials are necessary if the experiments are to yield any tangible result. The difficulty is that when a phenomenon occurs inside a solid, we cannot know what has happened at the time of occurrence, but we photograph the secondaries or tertiaries after they emerge from the plates. Only when the event occurs within the gas of the chamber is it possible to measure the angles and energies with the accuracy required for a comprehensive interpretation of the phenomena. Such events are, however, rare because of the low absorptive power of the gas. One such rare event of special interest is the disintegration of the mesotron as it approaches the end of its range. Definite evidence for the disintegration of the mesotron has been provided by only two or three cloud-chamber photographs of slow mesotrons disintegrating within the gas of the chamber. Another rare phenomenon is the Heisenberg explosion type of shower formation. More evidence of these effects within a reasonable time requires increasing the probability of occurrence, within the gas of the chamber, either by enlarging the volume of the chamber or by increasing the pressure. At higher pressures there will be more interactions per unit length of path of the ray and since the photographic technique becomes more difficult in very large chambers, the high pressure chamber appears to be a satisfactory solution of the problem. Such chambers would be of increasing interest for studies of nuclear effects excited by artificial radiations as the energy limit of the cyclotrons and betatrons is pushed higher and higher up.

The first high pressure chamber was designed by Mott-Smith (1934) to measure neutron energies. This chamber consists essentially of an enclosure divided into two parts by a rubber membrane, the tracks are formed in the upper part while the lower is connected to the apparatus for expansion. The body was built of a strong brass ring and the top plate was a 2.5-cm thick quartz plate which could stand up to 50 atmospheres. There was a thick glass window to let light into the chamber. Mott-Smith worked with 15 atmospheres inside this chamber. Brubaker and Bonner (1935) designed a sylphon bellows type of high pressure chamber, and they worked up to 25 atmospheres with this chamber and made arrangements to run the chamber completely automatically. Kipfer (1935) designed a 2-cm chamber in which the pressure could be up to 100 atmospheres. Williams and Evans (1940) also designed a 20-cm diameter and 16-cm deep high pressure chamber and operated it with argon at 80 atmospheres.

Johnson, Benedetti, and Shutt (1943) have lately designed a hydrostatically supported cloud chamber (30 cm in diameter and 9 cm deep) of new design for operation at pressures up to 200 or possibly up to 300 atmospheres (see Fig. II-4).

The wall thickness of the glass cylinder is 6 mm, the front is covered by a glass plate of the same diameter as the ring and is of 9-mm

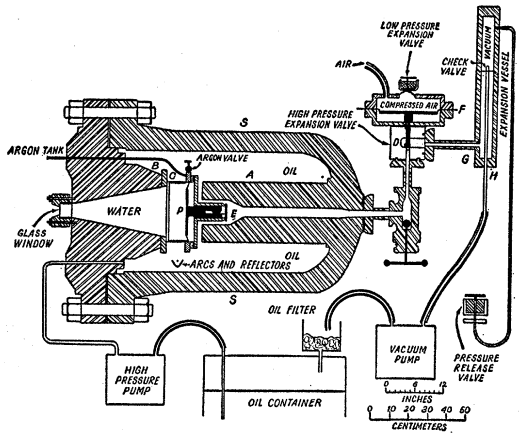

FIG. II-4. Schematic drawing of the high pressure cloud chamber of Johnson, DeBenedetti and Shutt [from Rev. Sci. Inst. **14**, 265 (1943)].

thickness. The construction is such that the high pressure is sustained by a cast steel vessel filled with transparent Eureka white oil; the glass walls of the cloud chamber are not subjected to high pressure differentials.

The shape of the tank containing the oil permits the tank to be used as a part of the magnetic circuit for an electromagnet capable of producing a strong magnetic field within the chamber. The space available can accommodate about 1 ton of copper, and it is possible to produce a field of 10,000 gauss or more without seriously heating the chamber.

The back wall of the chamber consists of a movable piston attached to the cylindrical side walls by means of a flexible synthetic rubber diaphragm. The chamber is expanded by releasing a measured volume of oil from the vessel through the high pressure expansion valve, which is controlled by low pressure (49 lb./in.) compressed air acting upon a large (13″ in diameter) aluminum piston. The chamber is filled with argon saturated with a mixture of water and isopropyl alcohol vapors. The expansion ratio for the formation of good tracks diminishes with increasing pressure so that high pressure chambers are subjected to smaller turbulence. At atmospheric pressure the volume expansion ratio is 1.07 to 1.08, but at 110 atmospheres this ratio decreases to 1.04 (see Chapter I, Section 1*b*). The maximum volume expansion ratio allowed in this chamber is about 20 percent.

At the foci of cylindrical parabolic reflectors which project a parallel beam of light across the chamber are placed capillary arcs all mounted inside the tank. Photographs are taken through a two-inch thick glass window of small diameter designed to withstand full pressure. Because of the greater density of ionization in the high pressure chamber, the intensity of illumination needed to photograph the tracks is somewhat less than that necessary in a chamber at about 1 atmosphere. But because of the absorption of light in the oil this advantage is neutralized in the high pressure chamber.

The advantage of this type of chamber over the conventional Blackett type of chamber lies in the increase of cosmic-ray track length which may be observed in a given time. At 200 atmospheres the effective track length across the diameter of the chamber is equivalent to 200 ft. of normal argon, so that the chamber can completely record the life of a particle of this large length. The efficiency, judged by good tracks, is almost 10 times greater because of the longer period over which the supersaturation is maintained inside the chamber (see Chapter III, Section 5). Such high pressure chambers require nearly fifteen minutes to elapse after each compression, in order to lose the heat produced by compression, before they are ready to record the passage of another charged particle through it.

CHAPTER III. FACTORS INFLUENCING THE QUALITY OF TRACKS

1. Illumination

It is often experienced that although very good tracks are visible inside the chamber, these do not appear in the photographs. This may be caused by: (a) improper illumination, (b) wrong adjustment of magnification, or (c) small depth of focus of the camera lens.

Let us consider an object of area S placed normally to the lens at a distance u from the optical center of the lens. If a be the diameter of the stop used, the total light from the source which passes through the lens is given very approximately by $(IS/u^2)(\pi a^2/4)$, where I is proportional to the light emitted from unit area of the object. If the area of the image be S', the

illumination on unit area of the image surface is

$$I_S' = \frac{I}{u^2}\cdot\frac{S}{S'}\frac{\pi a^2}{4} \tag{3.01}$$

provided no light is lost by reflection from or scattering by the lens surface. Introducing the linear magnification factor $m=v/u=(S'/S)^{\frac{1}{2}}$, $I_{S'}$ may be expressed as

$$I_S' = \frac{\pi I}{4}\frac{A^2}{(1+m)^2}, \tag{3.02}$$

where $A=a/f$ is the relative aperture, $v=f(1+m)$. Hence to increase $I_{S'}$, I and A must be made large and m small. The methods of increasing I with minimum use of power will be described later. We first consider the maximum permissible value of A or a/f. This is limited by the depth of focus as the following analysis will show.

If u be the object distance, v the image distance, and f the focal length of the lens, a change of δu in u will produce a change of δv in v, given by

$$\delta v/\delta u = -v^2/u^2 = -m^2. \tag{3.03}$$

The condition for sensibly perfect definition demands that the path difference between the extreme ray and the central ray should not be more than $\lambda/4$.

Now a change of δv introduces a change of path difference of $(a^2/8)(\delta v/v^2)$* so that Rayleigh's condition gives

$$\frac{\lambda}{4}=\frac{a^2}{8}\frac{\delta v}{v^2} \tag{3.04}$$

and

$$\delta u = \frac{\delta v}{m^2}=\frac{2\lambda}{A^2}\left(\frac{1+m}{m}\right)^2. \tag{3.05}$$

We see from Eqs. (3.05) and (3.02) that the depth of focus δu decreases while the illumination increases as A is increased. Hence a compromise between the two must be made. Generally the aperture is adjusted to some critical value A_c consistent with a required depth of focus, the value of A_c being given by

$$A_c=(1+1/m)(2\lambda/\delta u)^{\frac{1}{2}}. \tag{3.06}$$

* Rayleigh, *Collected papers* (Cambridge University Press, England, 1920) Vol. I, p. 415.

Thus for $m=1/12$, $\lambda=4.4\times10^{-5}$ cm and $\delta u=5$ cm. $A_c=1/18.3$, so that the lens should not be worked at a stop larger than f:18.3. For the critical aperture A_c,

$$I_{S'}=\frac{\pi I}{4}\frac{(1+m)^2}{m^2}\frac{2\lambda}{\delta u}\frac{1}{(1+m)^2}, \qquad =\frac{\pi I\lambda}{2m^2\delta u}. \tag{3.07}$$

Hence for a particular value of δu, $I_{S'}$ increases with diminishing values of m, and the smaller the value of m the easier it is to get not only sharper images, but also a larger number of tracks per exposure. The minimum value of m that can be used is limited by the resolving power (that is, the number of lines to the millimeter resolvable) of the photographic emulsions used. The lowest useful value of m is that which gives the image of a track a breadth equal to the finest lines reproducible on the films used. For very rapid emulsions this is generally of the order of 20μ. Now the breadth of the image of a track can be taken to be equal to the sum of the width ϵ of the diffraction pattern due to a line source and the width D of the geometrical image of the track. For the former, we have

$$\epsilon = 2v\lambda/a = 2\lambda(1+m)/A, \tag{3.08}$$

and for the latter mD_0, where D_0 is the width of the track itself. The total breadth Δ is therefore

$$\Delta = mD_0+2\frac{\lambda}{A}(1+m)=m[D_0+(2\lambda\delta u)^{\frac{1}{2}}], \tag{3.09}$$

where the critical value of the aperture has been used. Taking $D_0=0.1$ mm, $\lambda=4.4\times10^{-5}$ cm, and $\delta u=5$ cm, $\Delta=m\times310\mu$. Now Δ for Kodak super XX films is of the order 20μ, so that minimum useful value of m is of the order of $m\geqslant 20/310$ i.e., $m\geqslant 1/15.5$. If instead of $m=1/12$ we use this value of m, the result will be an increased depth of focus [Eq. (3.05)] or an increased illumination of the image [Eq. (3.02)]. It is always advisable to have rapid films, so that the depth of focus may be increased by using a smaller A, thereby improving the efficiency of the chamber per expansion. In the low pressure chamber where the tracks are generally fainter because of smaller

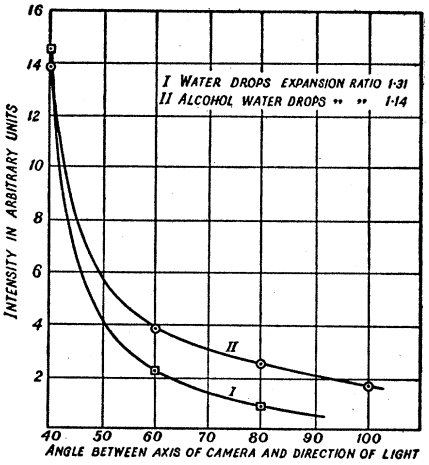

FIG. III-1. Variation of intensity of scattered light from the drops in the Wilson chamber with the angle between the camera and the direction of illumination.

number of ions being produced per centimeter of the path, the advantage of smaller magnification should be utilized in increasing the intensity rather than the depth of focus.

When the apertures used are larger than the critical aperture it is seen [Blackett (1929b)] that the breadth of the average image increases with the aperture because of lack of perfect focus, while for small apertures the breadth of the image increases as the aperture decreases because of increase in the aperture disk. It is advantageous therefore to use the critical aperture.

We now consider the methods of increasing I_S' by increasing I, all other factors remaining constant. As the increase of I does not interfere with the depth of focus, it is desirable to get as large a value of I as is possible with a minimum power used. If it is possible to make I_S' more than what is demanded by the film, by means of a strong illumination of the tracks, we can increase the depth of focus by stopping down the lens, thereby increasing the yield of tracks per expansion, as also the definition of the tracks.

Blackett (1934) used spark discharges from condensers through quartz mercury vapor lamps. Later on he substituted capillary mercury lamps connected directly to the secondary of an 8000-volt transformer connected to 220 volts main. A large current, 100 to 200 amp., was passed through the primary for 1/50 to 1/20 of a second and a flash occurred; the illumination was adequate to allow the photography of single droplets from a direction at right angles to that of illumination.

Crane (1937) has used 1000-watt, 110-volt Mazda projection lamps backed by parabolic mirrors which give ample light for an exposure of $\frac{1}{5}$ second at f: 1.9, on super X film. The lamps were flashed at 220 volts.

When the track due to a charged particle is illuminated by strong light, it is only because of the light scattered by the drops that these are visible. Webb (1935) has shown experimentally (see Fig. III-1) that the intensity of light scattered by droplets increases rapidly as the scattering angle decreases. For water drops, the intensity at 20° to the beam is about one hundred times that at 90°, while for water-alcohol drops (mixed in equal proportions) the ratio is about fifty to one. Evidently for greater illumination, the axes of the camera should be inclined at a small angle to the direction of illumination. When the depth of the chambers used is small, there is no other alternative but to have the camera axis placed at right angles to the direction of illumination, which demands strong illumination; but if the depth is increased, it may be possible to photograph the tracks from a direction inclined at a small angle to that of illumination.

As early as 1930, Williams and Terroux (1930) used a deep chamber, so that even with the camera axis parallel to the magnetic field it was possible to decrease the angle between axis of the camera and the direction of illumination. With this arrangement only 8 to 10 100-watt lamps flashed momentarily on 220 volts, produced sufficient light after condensation by lenses to illuminate a chamber 30 cm deep and 30 cm in diameter.

2. Photographic System

Investigations of nuclear phenomena and cosmic rays by means of a Wilson chamber require a method of photographing the tracks which will permit a determination of the ranges, curvature and the angles between the paths of various particles in whatever plane they may occur. This demands the same track to be photographed from two different directions. The method most com-

monly used for this purpose is the arrangement described by Shimizu (1921) (see Fig. III-2) in which two mutually perpendicular views of the tracks are registered by a single lens on the same film, by means of two mirrors B and C at right angles to each other and inclined at 45° to the plane of the chamber A. The angle between the various particles, or the actual length of the tracks may then be calculated from measurements on the two images registered [Blackett (1922), (1923)]. The method appears at first sight to be economical from the point of view of film consumptions. But since the two object planes are at right angles to each other, only a small region of the cloud chamber can be brought to sharp focus for both views and only a small number not more than a dozen tracks can be photographed at each exposure.

Blackett (1929b) has described a method of eliminating this difficulty by using two separate cameras. For the sake of easier computations and the accuracy in the determinations of the angle the image planes P and P' of the two cameras are placed perpendicular to each other, as shown in Fig. III-3. The lenses L and L' are tilted so that the plane of the chamber is conjugate with both plates. This is done by adjusting the principal plane of each lens to pass through the line of intersection of the plane of the chamber and the plane of the photographic plate.* In this method the lenses are used axially and yet sharp photographs are obtained of the whole of the chamber. The lens axis passes through the center of the chamber and makes a small angle with the normal to the plate, due to which the magnification of the image becomes non-linear in different parts of

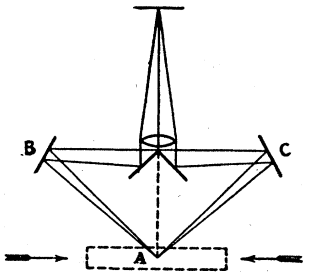

FIG. III-2. Stereoscopic photography on one film.

* R. Glazebrooke, *Dictionary of Applied Physics* (Macmillan and Company, London, 1927), Vol. IV, p. 400.

it. This defect is got rid of by the special method of analyzing the tracks which is described below.

The method of analysis consists merely in replacing the developed negatives in the film holders of the camera in the exact positions in which they were when the photographs were taken and re-projecting the two images back in

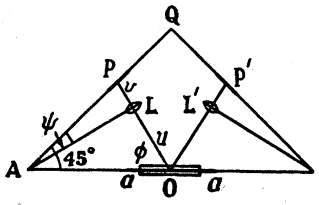

FIG. III-3. Stereoscopic photography on two films.

the object plane [Williams and Terroux (1930); Curtiss (1930)]. A thin white translucent screen is adjusted and rotated until the two images coincide on the screen, and an exact geometric reproduction of the track is obtained in the plane in which it was formed, and the rectilinear distortion is automatically corrected. Since the same cameras are used and the negatives are placed in the positions which they occupied when the exposure was made, many errors, which might arise because of bad alignments of the different parts of the cameras, are also eliminated. The white screen may then be replaced by a photographic paper and a permanent record may be obtained. For measurements on the reproduced tracks a stereo comparator has been designed by Grosev *et al.* (1936).

In actual practice the two cameras must be mounted on a single casting so that it may be removed without altering the relative positions of the cameras in any way, Curtiss (1930) and Jones and Ruark (1940) have described such an apparatus for viewing stereo pictures. To facilitate replacing the negatives in the exact positions which they occupied at the time of exposure two electromagnets are used to push a needle point through the film at the instant of exposure. The guides fit the film rather snugly and the film can be replaced by adjusting it until the needle point passes into the hole in the film made at the time of exposure. It is found that in this method, though twice as much film is used for taking a

photograph, four or five times as many tracks are obtained all in good focus.

When however it is only necessary to determine if a particular rare phenomenon occurs inside the chamber, as for example a knock-on shower, it is sufficient to use a single camera with its principal plane parallel to the plane of the chamber.

3. Sharpness of the Tracks

When a fast particle traverses a gas it produces an equal number of positive and negative ions within a narrow cylindrical column surrounding its path. If we neglect recombination and the effect of the electrical field, the ions diffuse away from their starting point and after a time τ the distribution at a distance r from the track is given by

$$n(r)=\frac{N_0}{4\pi D\tau}\exp(-r^2/4D\tau), \qquad (3.10)$$

where N_0 is the total number of ions per cm of track and D is the diffusion coefficient of the ions.

Suppose supersaturation takes place after the time τ has elapsed since the passage of the charged particle. The ions are now covered with water forming drops and their mobility is reduced to zero. The photograph taken at this instant will indicate the projection of the ions at the time τ on the plane of the photographic film (XZ plane, Z is the direction of track, X the direction perpendicular to track on the plane of photograph. Y is the direction of observation). The superficial density of the ion images is obtained by integrating $n(r)$ with respect to y from $+\infty$ to $-\infty$

$$\rho(x)=\frac{N_0}{4\pi D\tau}\int_{-\infty}^{+\infty}\exp-[(x^2+y^2)/4D\tau]dy$$

$$=\frac{N_0}{(4\pi D\tau)^{\frac{1}{2}}}\exp-[x^2/4D\tau]. \qquad (3.11)$$

It is seen that $\rho(x)$ has a gradient from the center towards the periphery of the track and it is convenient to define a width x_1 containing 90 percent of the ion images. The value of x_1 is obtained from the relation

TABLE III-1. Calculated and observed values of x_1.

Gas	D N.T.P.	D at 1.48 atmos.	x_1 calc. mm	x_1 observed mm
O_2	0.032	0.022	0.71	0.85
H_2	0.135	0.092	1.42	1.78

$$\frac{\dfrac{N_0}{(4\pi D\tau)^{\frac{1}{2}}}\displaystyle\int_0^{x_1}\exp-[x^2/4D\tau]dx}{\dfrac{N_0}{(4\pi D\tau)^{\frac{1}{2}}}\displaystyle\int_0^{\infty}\exp-[x^2/4D\tau]dx}=0.9,$$

which gives

$$x_1=4.68(D\tau)^{\frac{1}{2}}. \qquad (3.12)$$

The mean value of D for the positive and negative ions at N.T.P. for air is 0.034 cm^2 sec.$^{-1}$† so that $x_1=0.86\tau^{\frac{1}{2}}$. Hence if the track is to have a thickness of 1 mm, τ must be about 1/70 of a sec.

When the expansion mechanism is released by coincident counter discharge, some time elapses before the piston is released. The time during which the piston moves is only a fraction of τ say $\alpha\tau$. If d be the distance moved by the piston during this time

$$d=\tfrac{1}{2}(SP/m)(\alpha\tau)^2, \qquad (3.13)$$

where S = area, P = pressure difference on the two sides of the piston, m = the mass of the piston, and SP/m is the acceleration. The coefficient of diffusion D is inversely proportional to pressure and $D=k/\rho$ (say), where ρ is the density of gas inside the chamber. Eliminating D and τ from Eqs. (3.12) and (3.13) we have

$$x_1=5.5\left(\frac{k}{\rho}\right)^{\frac{1}{2}}\left(\frac{dm}{SP\alpha^2}\right)^{\frac{1}{4}}. \qquad (3.14)$$

This analysis gives us the following conditions for sharp tracks:

(i) The distance moved should be as small as possible.
(ii) The mass of the piston should be as light as can be managed.
(iii) Pressure as large as practicable.

In Table III-1 the calculated and observed values of x_1 determined by Blackett (1934) are given.

† J. J. Thomson, *Conduction of Electricity Through Gases* (Cambridge University Press, England, 1928), Vol. 1, p. 77.

In these calculations α has been put equal to unity. It is difficult to measure x_1 accurately, but the calculated values are in rough agreement with the measured ones.

4. Distortion of the Tracks

The tracks inside the cloud chamber may be distorted owing to any of the following causes: (a) distortion caused by the optical system, (b) distortion by the front glass plate of the chamber, and (c) distortion due to gas motions inside the chamber.

(a) *Lens Distortion*

This distortion is caused by the fact that large aperture lenses have to be used firstly to get sufficient illumination and secondly to get longer tracks when the tracks are photographed through a hole in the pole piece of the magnet. Even very high quality lenses are found to have distortions, which again are positive in some cases and negative in others. Consequently, unless the distortion is taken into account a very high energy negative particle having a very small displacement might be mistaken as a positive particle of about the same energy.

Blackett and Brode (1936) have considered the distortion produced by a lens in some detail. In Fig. III-4, 0 is the optical center of the image,

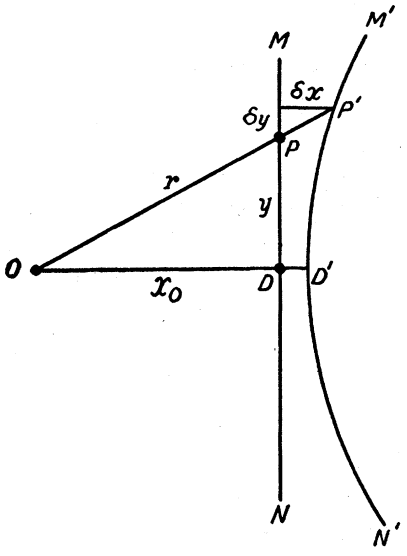

FIG. III-4. Distortion in the image of a linear object produced by a lens.

i.e., the point where the axis of the lens meets the photographic plate or film. If the object be a straight line, the undistorted image will be straight and the distorted one will be curved. Let MN be the image of straight object produced by a lens if there were no distortions and $M'N'$ be the actual distorted image. The point $P(x_0, y_0)$ is the true position of the image of a point in the object space, and $P'(x_0+\delta x, y_0+\delta y)$ is its actual position. Then

$$\delta x = x_0(\delta r/r). \tag{3.15}$$

But δr, which is the displacement of the true image P because of distortion, can be expressed as a series of odd powers of the distance of P from the axial point 0.* We may write therefore

$$\delta r = a_1 r^3 + a_2 r^5 + \cdots \tag{3.16}$$

so that

$$\begin{aligned}\delta x &= x_0(a_1 r^2 + a_2 r^4),\\ &= A + By^2 + Cy^4,\end{aligned} \tag{3.17}$$

where

$$A = a_1 x_0^3 + a_2 x_0^5, \quad B = a_1 x_0 + 2a_2 x_0^3, \quad C = a_2 x_0.$$

Putting

$$y = 0, \quad \text{we get} \quad DD' = \delta x = A.$$

If therefore we measure the X coordinates of P' with respect to a line through D' parallel to MN, the equation of $M'D'N'$ is given by

$$\begin{aligned}x &= By^2 + Cy^4,\\ &= (a_1 x_0 + 2a_2 x_0^3)y^2 + a_2 x_0 y^4,\end{aligned} \tag{3.18}$$

when

$$a_2 = 0, \quad x = {}_1x_0 y^2. \tag{3.19}$$

The curvature is parabolic and increases linearly with the distance x_0 from the axis. The curvature is positive or negative according as a_1 is positive or negative. If we assume the curve to be nearly circular, then $\sigma = 2x/y^2 = 2a_1 x_0$, where σ is the curvature. When $a_2 \neq 0$ the distorted curve may be approximately taken to be circular only for small values of y in the neighborhood of D', and we may write

$$x \simeq (a_1 x_0 + 2a_2 x_0^3)y^2 \tag{3.20}$$

and

$$\sigma_{\text{central}} = 2a_1 x_0 + 4a_2 x_0^3. \tag{3.21}$$

When a_1 and a_2 are of the same sign, the curvature is a minimum at D' and increases along the

* R. Glazebrooke, *Dictionary of Applied Physics* (Macmillan and Company, London, 1927), Vol. 4, p. 403.

track. When a_1 and a_2 are of opposite sign, the curvature is a maximum at D' and decreases towards the edge of the track and may even change sign.

The curvature due to distortion as shown above is found to agree quite well with the values determined experimentally [Blackett and Brode (1936)], Fig. III-5.

To determine the distortion due to the lens used, several parallel wires are photographed and the curvature of the images measured. Then since the camera axis is parallel to the magnetic field, the curvature of a track on the plate is the sum of the true curvature of the track and the distortion curvature produced by the lens. Subtracting the distortions curvature from the total curvature we get the true curvature of the track. This distortion may be minimized by using a specially designed lens system for a particular front plate.

(*b*) *Distortion Caused by the Front Plate*

Again when a parallel plate of the thickness t and refractive index μ is inserted at right angles to the lens axis between the object and the lens, a ray making an angle θ with the axis will be given an angular displacement of the amount

$$\delta\theta=\frac{t}{u}\sin\theta\{1-\cos\theta(\mu^2-\sin^2\theta)^{-\frac{1}{2}}\}, \quad (3.22)$$

where u is the object distance. The effect of $\delta\theta$ will be to shift the image by an amount δr which can be shown to be given by

$$\delta r=A_0 r+A_1 r^3 \quad (3.23)$$

where

$$A_0=\frac{t}{u}\left(1-\frac{1}{\mu}\right),$$

and

$$A_1=\frac{t}{2uv^2}\left(1-\frac{1}{\mu^3}\right),$$

and $v=$image distance. It can be shown that the curvature due to the glass plate of the image of a straight line is given by $\sigma=2A_1x_0$, where $x_0=$distance of the image if it were undistorted, from the center of the plate. The plate introduces a positive distortion and any lens which is specially designed to be free from distortion must be designed to be used with a glass plate. There is a possibility therefore of compensating a small negative distortion of the lens when it is matched properly with a suitable plate. The distortion due to the glass plate may be determined by measuring the image curvature of a straight wire, with and without the glass plate between the wire and the lens.

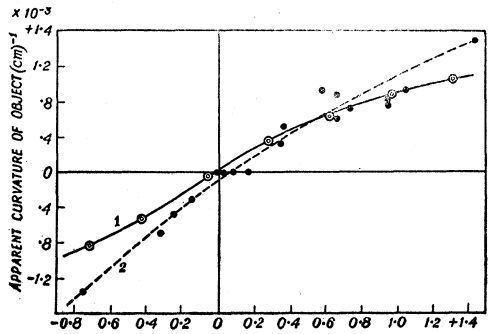

FIG. III-5. Comparison between the calculated and the experimentally observed distortions.

(*c*) *Chamber Distortion*

In a counter-controlled chamber the interval between the passage of the ray and the instant of the photographing is about 10^{-2} sec.; during this interval the gas in the chamber expands and any irregularity in this expansion will distort the tracks. It is found that a copper gauze or a perforated plate, the surface of which is covered with a black velvet wet with the alcohol-water mixture, placed in front of the rubber diaphragm, smoothes to a great extent the turbulent motion of the gas during and after the expansion. The tracks will also be distorted if any convection current exists before expansion. After each expansion the gas near the walls warms up first, so that convection current develops causing a rapid fall of the central mass of cold gas. This motion is much greater in a vertical than in a horizontal chamber and the forces to which the motion is due, increase with time as t^3. It is necessary therefore to photograph very soon after the expansion is over.

The fall of drops through the gas also distorts the tracks, and it is never possible to photograph the tracks undistorted later than about 0.25 sec. after the expansion. Another type of distortion owes its origin to the swirling motion of the gas,

the exact reason for whose origin is yet unknown. The chamber distortion increases not only at distances away from the lens axis, but also as the inclination of the tracks to the vertical increases, and for good results the tracks should be limited to the vertical direction as much as possible. The distortion is higher at higher temperatures and the variation in the chamber distortion due to the variation in the room temperature can be eliminated if the metal casings of the chamber be enclosed in a copper box cooled with running water [Blackett and Wilson (1937), (1938)]. It is better to enclose the chamber in a heat insulating box of fiber board, into which the pole pieces of the magnet protrude. The camera is built into one side of the box and the illumination is admitted through a thick glass window on the other side. It is also found necessary to keep the temperature of the enclosure within 1°C of that of the magnet, which is effected by keeping the temperature of the room very near that of the magnet. A small amount of water cooling at the bottom of the chamber keeps both moisture off the glass walls and the thermal condition inside the chamber stable. Large expenditure of power should be avoided, for the curvature of tracks thus increased is vitiated by the increased distortion due to the less favorable thermal conditions arising from the warming up of the magnet. Thus controlled, the chamber distortions may be greatly reduced even when a plate of metal is inserted in the chamber. By measuring the curvature of tracks in a chamber without the magnetic field, the over-all curvature due to the several sources of distortions may be found [see Chapter IV, Section 4 in this connection].

5. The Sensitive Time of a Cloud Chamber

After the expansion had taken place, heat gradually leaks into the chamber, supersaturation diminishes, and after a time condensation can no longer take place on the ions. The sensitive time may be defined as the length of time for which supersaturation remains sufficient to cause condensation along the tracks of the ionizing particles [Williams (1939a)]. Experimental estimate of this time may be made by observing the formation of tracks by a radioactive source, which may be uncovered at different times after the expansion, the expansion ratio being the maximum consistent with that not forming a cloud.

The sensitive time of a chamber has been determined by Hazen (1942) by using a different method. A radioactive source containing Cl is rapidly moved through the gas in the cloud chamber during and after expansion. The successive positions of the source are photographed by periodic illumination and the tracks are also photographed on the same film. The sensitive time is then determined from the photograph as the time interval after the expansion during which tracks of a certain density are still formed.

Let us consider the physical process in the cloud chamber after expansion. Immediately after expansion, the gas is at a lower temperature θ_2, but the surrounding walls are at a higher temperature θ_1. Owing to the much greater heat capacity and greater conductivity of the walls, the temperature of the surface practically remains steady at θ_1. The gas immediately close to the wall, therefore begins to heat up because of convection. The heating is maximum near the wall and falls off as we go farther away from the walls. Because of this heating, the boundary layer expands and compresses the gas inside and heats it.

The problem of heat leakage which we have here is similar to the classical case of heat leakage into the interior of the earth given by Lord Kelvin, which can be found in all standard treatises on heat.† The temperature θ_x at a distance x from the boundary, after a time t, is given by

$$\theta_x=\theta_1-(\theta_1-\theta_2)\frac{2}{\pi^{\frac{1}{2}}}\int_0^{\xi}\exp(-\xi^2)d\xi, \quad (3.24)$$

where $\xi=x/2ht^{\frac{1}{2}}$, $h^2=K/c\rho$, $K=$heat conductivity, $c=$specific heat, $\rho=$density, and $h^2=$diffusivity.

Let us now find out the increase in volume of the boundary layer. For a given layer of thickness dx this is given by $Sdx\Delta\theta/\theta_2$, where $\Delta\theta=\theta_x-\theta_2$. We have therefore the increase in volume of the layer

† M. N. Saha and B. N. Srivastava, *Treatise on Heat* (Indian Press, Allahabad, India, 1935).

$$d\Delta V=\frac{S\Delta\theta}{\theta_2}dx$$

$$=\frac{S(\theta_1-\theta_2)}{\theta_2}\int\left\{1-\frac{2}{\pi^{\frac{1}{2}}}\int_0^{\xi}\exp(-\xi^2)d\xi\right\}dx.$$

The total increase in volume ΔV is obtained by integrating the expression over x from 0 to ∞, i.e.,

$$\Delta V=\frac{S(\theta_1-\theta_2)}{\theta_2}2ht^{\frac{1}{2}}\int_0^{\infty}\left\{1-\frac{2}{\pi^{\frac{1}{2}}}\int_0^{y}\times\exp(-\xi^2)d\xi\right\}dy,$$

$$=1.14\frac{S(\theta_1-\theta_2)}{\theta_2}ht^{\frac{1}{2}}. \quad (3.25)$$

The expansion of the boundary layer tends to compress the main volume V of the gas. The gain in temperature thereby is

$$\Delta\theta=(\gamma-1)\frac{\Delta V}{V}\theta_2=1.14\frac{S}{V}(\theta_1-\theta_2)ht^{\frac{1}{2}}(\gamma-1). \quad (3.26)$$

Let $\delta\theta_S$ be the limiting increase in temperature after which the chamber becomes insensitive. We have then

$$t_S=\left(\frac{\Delta\theta_S}{\theta_1-\theta_2}\right)^2\left(\frac{V}{S}\right)^2\times\left(\frac{\rho c}{K}\right)\left(\frac{1}{\gamma-1}\right)^2\left(\frac{1}{1.14}\right)^2. \quad (3.27)$$

We have now to find out the value of $\Delta\theta_S$. Let us suppose that $1+\epsilon$ is the original expansion which was just sufficient to cause formation of tracks. Let $1+\epsilon+\Delta\epsilon$ be the maximum expansion which can be used without producing a fog. Since we have

$$\theta_2/\theta_1=(1+\epsilon)^{-(\gamma-1)}, \quad (3.28)$$

we have approximately, taking logarithms,

$$(\theta_2-\theta_1)/\theta_1=-(\gamma-1)\epsilon=\theta/\theta_1 \text{ say}, \quad (3.28')$$

where θ is the temperature difference produced. We have therefore

$$\Delta\theta/\theta=\Delta\epsilon/\epsilon. \quad (3.29)$$

Hence,

$$t_S=\left(\frac{\Delta\epsilon}{\epsilon}\right)^2\left(\frac{V}{S}\right)^2\left(\frac{\rho c}{K}\right)\left(\frac{1}{\gamma-1}\right)^2\cdot 77. \quad (3.30)$$

The above expression shows that the sensitive time of a chamber increases with:

(i) ρ the density of the gas,
(ii) $(V/S)^2$ the square of the ratio of the volume/surface and,
(iii) $(\Delta\epsilon/\epsilon)^2$.

The first inference is in accordance with the observations of Joliot (1934) who found that t_S varies with p, from $p=40$ to 76 cm. For very low pressures t_S decreases less rapidly. This is probably caused partly by an increase in $\Delta\epsilon/\epsilon$ as the ratio of the vapor pressure to the gas pressure increases and partly caused by a rapid decrease in γ with the decrease in the total pressure (see Chapter I, Section 1*b*).

The second inference is verified by a comparison of t_S observed by different workers. Williams (1939b) found that for a chamber 4 cm deep and 16 cm diameter, $V/S\simeq 1.3$ cm; while for a chamber 30 cm deep and 30 cm in diameter, $V/S\simeq 4$ cm, so that t_S in the latter case should be about 10 times greater. A value of t_S determined experimentally for the former was ~ 0.05 sec., while that for the latter was ~ 0.4 sec. Hazen's investigations were carried out with two chambers, for one of which V/S was double that of the other. The experimental values for t_S were as 1.7:1.0.

The third inference that t_S varies with $(\Delta\epsilon/\epsilon)^2$ was tested experimentally by Hazen (1942). Here the value of $\Delta\epsilon$ has to be inferred. We have

$$\left.\begin{aligned}&\theta=\theta_1-\theta_2=-\theta_1(\gamma-1)\epsilon\simeq 100\epsilon\\ \text{and}\quad&\Delta\epsilon=(\epsilon/\theta)\delta\theta=0.01\Delta\theta.\end{aligned}\right\}. \quad (3.31)$$

If we assume that $\Delta\epsilon$ has a nearly constant value $\simeq 0.03$, we have $t_S\propto(1/\epsilon^2)$. Hazen (see his Fig. 4) plotted t_S against ϵ and found the relation (3.30) to hold good for ϵ up to 0.126. After this, t_S after reaching a maximum began to decline. This has been explained to be caused by the fact that for $\epsilon\geqslant 0.126$ the background fog is present. Williams' equations are then no longer applicable, because of the exhaustion of moisture by the

TABLE III-2. Data on magnets for cloud chambers.

Investigators	Type of magnets	Weight of coils	Power used	Field produced	Size of the chamber
Kunze (1933)	Solenoidal, water cooled	1100 kg copper	500 kw	18,400 gauss	16.4 cm in diameter
Anderson (1933)	Heavy, water cooled copper coils with relatively light iron yoke	896 kg copper, 500 kg yoke iron	440 kw	15,000 gauss	16 cm in diameter
Blackett (1936)	Water cooled copper coils with heavy iron yoke	3000 kg copper, 8000 kg iron yoke	25 kw	14,000 gauss	17 cm in diameter
Jones and Hughes (1940)	Oil cooled iron core type 9100 kg steel	1000 kg copper, 9100 kg yoke	35 to 125 kw	12,400 to 16,000 gauss	30 cm×4.2 cm

large number of drops formed and also because of the heating effect of these drops. But as long as condensation takes place only on ionic nuclei, the sensitive time is determined correctly by the Eq. (3.30).

(a) Pressure Changes after Adiabatic Expansion

Let us now consider how the pressure inside the chamber varies after expansion. If the expansion is sufficiently rapid, the fall of pressure due to the expansion is given by the adiabetic relation. On reaching the minimum value immediately after the expansion, the pressure begins to rise because of the heat flow from the chamber walls considered above.

$$(\Delta P/P) = -\gamma(\Delta V/V),$$

where P is the gas pressure

$$\Delta P = -(\gamma P/V)\Delta V = -1.14\gamma(PS/V)[(\theta_1-\theta_2)/\theta_2]ht^{\frac{1}{2}}, \quad (3.32)$$

substituting for ΔV from Eq. (3.25). Hence ΔP will increase as $t^{\frac{1}{2}}$.

This deduction was put to test by Hazen (1942). The pressure changes occuring inside the chamber were investigated by putting an aneroid type of barometer inside the chamber and photographing the movement of the pointer. Hazen found that for a short interval after the expansion, the relation (3.32) is verified.

If the rate of expansion is slow, one has to take into account the amount of heat flow during the finite time of expansion. Allowance may be made for this heat flow during expansion, by producing a little extra expansion. Equation (3.31) shows that every one degree rise in temperature would require one percent increase in the expansion ratio.

6. Magnets for Cloud-Chamber Work

The observation of cosmic-ray tracks in a Wilson cloud chamber placed between the pole pieces of an electromagnet led Anderson (1932) to discover the "positron" a twin counterpart of the electron. This single fact points to the importance of the use of a magnetic field in investigations with the cloud chamber. Apart from the discrimination between the positively and negatively charged particles, the magnetic field has its utility in the measurement of the momentum of the particle passing through the chamber (see Chapter IV, Section 2).

To investigate the momentum of the particles in the energy range 10^5 to 10^7 ev, a field of 1000 gauss is quite sufficient to produce a measurable curvature in the ion track induced by the particle. To deflect very high energy particles having energy of the order of 10^{10} ev, even a field of the order of 20,000 gauss fails in its action. Evidently the magnetic field to be used must be selected very carefully, so that the curvature produced is neither very large causing the particle to revolve several times nor very small so that the particle passes almost undeflected. We shall discuss here mainly the magnetic fields used in the study of cosmic rays. Similar arrangements are to be made in the case of α-ray or β-ray studies, only the strength of the field to be used should be chosen properly.

The energy of the cosmic-ray particles has been determined from the curvature of their tracks in a strong magnetic field by Kunze (1933a), (1933b), Anderson (1933), Blackett (1936), (1937), Blackett and Brode (1936), Jones and Hughes (1940), and Jones (1939). Williams (1939b) has used a smaller magnetic field. The

types of magnets used and the fields obtained there by various workers have been tabulated in Table III-2.

It will be seen from the table, that prior to Blackett, the magnets used were not properly designed. Because of this not only a considerable fraction of the power used was lost without any proportionate gain in the strength of the field produced but difficulties regarding the cooling of the chamber were enhanced. This loss in power can however be overlooked in the case of a randomly operated chamber where the field is turned on only a few seconds before the expansion occurs; but for counter-controlled chambers where the field must always be present, the magnet should be properly designed. When the chamber is very deep ($\sim$30 cm) it is not possible to design an electromagnet which would yield a large field strength without using very high power. It has been customary therefore to place a deep chamber in the field produced by a pair of coils of the Helmholtz type. The field in these cases is uniform only over the region determined by the depth of focus of the camera used to photograph the tracks produced. The shallow chambers are only used for the measurement of very high energies. It may be marked that the field produced by a solenoid is less homogeneous than that of an iron core electromagnet, so the energies measured with a solenoidal field are less accurate.

Since the deflection is at right angles to the magnetic field and since the camera axis should be perpendicular to the path of the particle, usually the front pole piece of the electromagnet is bored through its length and the camera views the chamber through this bore. When it is necessary to record a stereoscopic view of the tracks, plane mirrors are attached to the walls of the bore, and the cameras photograph the images through the mirrors.

CHAPTER IV. PHYSICAL MEASUREMENTS CARRIED OUT WITH THE HELP OF A CLOUD CHAMBER

1. Specific Ionization

The term *specific ionization* indicates the number of ions produced per unit length of the track of a charged particle during its passage through a medium. According to Bloch (1933a), (1933b) the specific ionization depends directly on the square of the charge of the moving particle and to a large extent inversely on the square of the velocity of the incident particle [see Eq. (6.01), Appendix 3]. As regards the medium it depends directly on the number of electrons per cc of the medium. Hence heavy molecules like those of xenon produce far more ionization than lighter ones.

Particles with smaller velocities and the same charge passing through the same medium will produce therefore more ions per unit length of the track than higher velocity particles. Or in other words the former will have shorter ranges than the latter.

The energy imparted by the incident charged particle to the liberated electrons may be sufficiently larger than the ionization potential of the electrons in the different levels of atoms of the medium. The first liberated electrons known as primary electrons may further ionize atoms and molecules in the medium. This process of secondary ionization continues, so long as the energy of the liberated electrons is greater than the ionization potential of the outermost electron. Consequently some tracks are found to have branch lines starting from points along their lengths.

The specific ionization of a charged particle may be determined by various methods such as the use of the ionization chamber, Geiger-Muller counters, etc. The cloud-chamber method however is the only one that enables one to determine the primary and the total ionization separately. When the charged particle passes through the cloud chamber just after expansion, condensation takes place on ions before they have time to diffuse from their points of formation. The breadth of the track under such condition is given by $x_1=4.68(D\tau)^{\frac{1}{2}}$. A primary ionization in which the ejected electron has sufficient energy to produce, say 20 secondaries, will appear as a blob. The measurements of specific primary ionization therefore consists in counting the number of blobs and clusters of ions along the main track—the track being sharp and undiffused. If a magnetic field is used to deflect the particles, the primary specific ionization may be obtained as a function of $H\rho$, or the momentum of the particles.

If the ionizing particle passes through the chamber a short time before the expansion, the ions will spread by diffusion and each blob will appear now as cluster of ions. The resolution of the drops will depend on the delay-time, i.e., the interval between the passage of the particle and the expansion of the chamber. For a given delay this spreading of a blob will vary from medium to medium, directly as $D^{\frac{1}{2}}$, where D is the diffusion coefficient of ions in the medium. If the delay is too small, the primary ions will not be resolved into their secondary components; and if very large, the ions produced will diffuse so much from their origin that they will be lost in the background drops of the chamber which always exist. In practice the delay is adjusted depending on the gaseous medium used. When a magnetic field is used simultaneously, the delay must be critically adjusted so that while the ions are quite resolved, the track is not so much distorted because of gas motions that the error in curvature measurements is considerable. Using Eq. (3.12) we see that for O_2, since $D\sim 0.022$ $cm^2\cdot sec.^{-1}$, $x\sim 3.1$ mm for $\tau\sim 0.2$ sec. and air for which $D\sim 0.034$ cm^2 $sec.^{-1}$, $x\sim 3.9$ mm for the same value of τ.

Since for the determination of total ionization the delay method is essential, only counter-controlled chambers can be used for the determination of total specific ionization. The delay may be introduced by short circuiting the electromagnet U a desired interval after the coincidence of the counters. This may be effected with the help of a time delay circuit operated by the thyratron, or by a cam mechanism set into operation by the tripping of the counters. The successive stages in the delayed expansion mechanism with a delay of about 0.2 sec. are: cosmic-ray passage at $t=0.0$ sec., clearing field shorted at 0.01 sec., expansion at 0.2 sec., and light on at 0.245 sec. and off at 0.250 sec. With this sequence of events Brode (1939) has measured clusters containing up to 250 ions.

The illumination of the chamber for delayed expansions must be stronger than for immediate expansions of the chamber. In the latter case the individual ions are packed closed together, consequently the scattering effect of the concentrated column makes a track that can easily be photographed even when the scattering by the individual droplets is small. A larger aperture will make the drops brighter, but the distortion caused by the lens system increases. Because of the action of gravity on the droplets the duration of illumination cannot be increased as desired.

After the tracks have been photographed, the plates or films are developed and the total number of drops are counted. By reprojecting the images obtained back into the object space, their lengths are measured; dividing the total number of ions by the length of the track, we get the average specific ionization of the particle recorded.

Because of the small depth of focus (since larger apertures are used), the ions of the general background that lie in the same region of the track but in a different plane can easily be distinguished. By counting the number of background drops in a region equal in size and adjacent to the track the error due to the background density is determined. The background density may be diminished by using smaller expansion ratio.

When the tracks are photographed in a magnetic field, the chance of recombination between the positive and negative ions is considerably diminished, for ions of opposite charges are completely separated from each other.

2. Momentum and Magnetic Curvature

A particle of mass M, charge ze (e.s.u.), and momentum p moving at right angles to the magnetic field of H gauss describes a track with a radius of curvature ρ cm where

$$\left.\begin{aligned} pc &= \frac{M\beta c^2}{(1-\beta^2)^{\frac{1}{2}}} = zeH\rho \\ \text{and}\qquad pc)_{ev} &= 300zH\rho, \end{aligned}\right\} \quad (4.01)$$

where $pc)_{ev}$ is written for pc expressed in electron-volts, and $H\rho$ is expressed in gauss-cm. Hence from a measurement of $H\rho$, the momentum of the particle may be obtained directly provided z is known.

The corresponding equations connecting $H\rho$ with the energy and the velocity of the particle are given below. If E, T, and βc be the total energy, kinetic energy, and the velocity of the

particle,

$$E=Mc^2\left\{1+\left(\frac{zeH\rho}{Mc^2}\right)^2\right\}^{\frac{1}{2}}, \tag{4.02}$$

$$T=Mc^2\left[\left\{1+\left(\frac{zeH\rho}{Mc^2}\right)^2\right\}^{\frac{1}{2}}-1\right], \tag{4.03}$$

$$\beta=\frac{zeH\rho}{Mc^2\left\{1+\left(\frac{zeH\rho}{Mc^2}\right)^2\right\}^{\frac{1}{2}}}. \tag{4.04}$$

If $T\ll Mc^2$, we have

$$T\simeq\frac{(zeH\rho)^2}{2Mc^2} \text{ and } T)_{ev}=0.088\frac{m}{M}(zH\rho)^2, \tag{4.05}$$

$$\beta\simeq\frac{zeH\rho}{Mc^2}=5.86\times10^{-4}\frac{m}{M}zH\rho. \tag{4.06}$$

If $T\gg Mc^2$, we have

$$T=zeH\rho-Mc^2$$

and

$$T_{ev}\simeq300zH\rho-Mc_{ev}^2, \tag{4.07}$$

where T_{ev} is written for kinetic energy expressed in electron-volts and $H\rho$ is expressed in gauss-cm.

In order to determine the velocity or the energy of the particle from a measurement of $H\rho$, the mass must be known in general [Eqs. (4.01) and (4.06)]. Only when the kinetic energy is so high that the rest energy may be neglected in comparison, does Eq. (4.07) enable one to deduce the kinetic energy from a measurement of $H\rho$.

The values of β, $H\rho$, p/Mc, and T for the well-known particles are given in Appendix II [see in this connection Bhattacharya (1941)].*

It can be easily seen from Eq. (4.01) that a particle with $pc=10^8$ ev energy and $z=1$, will be deflected by a field of 1000 gauss to produce a radius of curvature 3.3 meters. About 10^4 gauss will be needed to produce the same curvature for a particle of energy 10^9 ev. In the study of cosmic particles where the energies are very high and high fields must be used, special precautions have to be taken for the construction of the magnet and for heat insulation of the chamber in order to avoid distortion due to convection currents in the chamber. The details of the construction of magnets for cloud-chamber work and its arrangement for cosmic-ray studies have been given in Chapter III, Section 6. Here we proceed to discuss the methods used for the determination of very small curvatures and the errors in the estimation of energy or momentum caused by spurious curvatures in the cloud chamber.

To measure the curvature of a track, the plates or films are replaced in the cameras and illuminated from behind, so as to throw two images back into the object space. If P and P' be the image points on the two photographs corresponding to a point O in the object space, the point of intersection of PL and $P'L'$ where L, L' are the optical centers of the corresponding lenses is the point O. Wire models could thus be built up of full size in the object space. In practice an arrangement of pin points A, B, C, $\cdots$ mounted on arms with universal joints is placed in front of the camera. To locate the position of O one of the pins is moved, so that its point coincides with the intersection of PL and $P'L'$. The relative positions of a number of points on a track may be recorded by using several pins. Measurements on the pins may then be made by projecting images of them on a screen.

Instead of going through this trouble, since we know that the track of a particle in a counter-controlled chamber lies on a plane at right angles to the magnetic field and hence at right angles to the axis of symmetry of the photographic system, the reprojected images can be made to coincide on a screen whose plane is at right angles to the magnetic field. Then by rotating the screen about its vertical axis and on horizontal axis the two images can be placed in exact coincidence. The coordinates of the points on the track thus obtained may be measured by a microscope with a micrometer eyepiece; these are then plotted on a paper in a magnified scale and ρ obtained. Blackett (1936), Anderson (1933), and others have used this method.

Jones and Hughes (1940) have used a special arrangement (see Fig. IV-1) instead of a microscope with a micrometer eyepiece. The reprojected track intersects the ruled straight line DE at two points A and C; the displacement of the center of the track is then measured by setting the disk on the movable central platform to coincide with the track. The displacement, read

* J. B. Hoag, *Electron and Nuclear Physics* (D. Van Nostrand Company, Inc., New York, 1938) pp. 464–466.

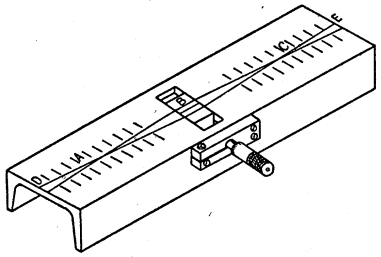

FIG. IV-1. An arrangement for quick measurement of of the radius of curvature.

from the micrometer screw which drives the platform, can be measured to within 0.005 cm, i.e., the smallest measurable deflection is of this magnitude. For a 20-cm track and a field strength of 16,000 gauss such a displacement corresponds to an energy of 5×10^{10} ev. The value of ρ determined by this method agrees well with the method stated above. For the less curved tracks a different method is adopted, which has some advantage both in speed and accuracy. The principle is based on the remarkable accuracy with which the straightness of a line can be judged when viewed obliquely along its length. The curvature can be compensated by some optical device, so as to reduce the actual measurement to a judgment of straightness. A convenient way of applying this principle is to reproject the image on a white screen and then to place in front of the lens a suitable curvature producing device. For very small curvature an inclined parallel plate glass [Blackett and Brode (1936)] is quite efficient. For medium curvatures some type of achromatic prism is convenient. For small curvatures the amount of curvature $1/\rho$ introduced into the image of a straight line by such a prism is given by

$$\rho=\rho_0 \operatorname{cosec}\theta, \tag{4.08}$$

where θ is the angle between the line and the principal plane of the prism. To measure the curvature of a curved track, the value of θ is determined which produces a straight image on the screen. The accuracy of the judgment of the straightness increases as the angle of viewing the screen is decreased; with a coating of MgO on the screen and strong source of light this angle can be reduced to 2° or 3°. The apparatus is calibrated by the use of lines of known curvature, and the value of ρ_0 can be evaluated. Then either from Eq. (4.08) or $\rho-\theta$ calibration curve the value of ρ corresponding to a particular θ can be determined immediately.

The theory of the curvature introduced by a combination of a lens and a prism is very complicated; for minimum deviation position the expression for the radius of curvature ρ, introduced by a prism of refractive index μ and angle 2α, is, according to Rohr (1920),

$$\rho_0=\frac{\mu f(1-\mu^2\sin^2\alpha)^{\frac{1}{2}}}{2(\mu^2-1)\sin\alpha}, \tag{4.09}$$

where f is the focal length of the lens used.

Using a 35 mm $f:2$ lens at magnification 1/5.6 and an achromatic prism consisting of 29° crown and 16° flint component placed normal to the axis and in front of the camera lens, Blackett (1937) has measured radii of curvatures up to a maximum value of 0.33 m with probable error of about 0.0016 m.

The maximum energy that can be measured depends upon the accuracy with which curvatures can be measured. The measurement of small curvatures depends upon the measurement of the central displacement d of a track length l. If ρ be the radius of curvature, then

$$\rho=l^2/8d \quad \text{and} \quad pc=300Hl^2/8d. \tag{4.10}$$

Because of distortions of the tracks due to gas motions, or various factors discussed in the previous sections, there is always some curvature of the tracks even in the absence of magnetic fields. Figure IV-2, reproduced from Hughes' work (1940), shows distortions caused by these effects when there is no magnetic field. The figure shows the observed distribution as a function of the displacement d of 110 tracks taken without the magnetic field. From such a study of the tracks without the magnetic field the probable error in d may be estimated. In this particular case it was 0.012 cm. The displacements corresponding to different energies can be estimated from Eq. (4.10) and then the probable errors in energy measurements obtained. In this case $H=12400$ gauss, $l=20$ cm, hence displacement for an energy of 10^9 ev was 0.186 cm and that for 10^{10} ev was 0.0186 cm. These displacements correspond to errors of 6 percent at 10^9 ev, 66 percent at 10^{10} ev, 100 percent at 2.10^{10} ev. This represents

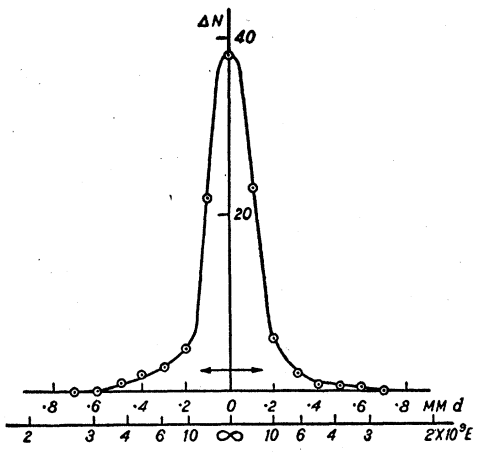

FIG. IV-2. Distribution of the central displacement of tracks inherent in a chamber.

the maximum energy that can be measured by this arrangement.

(a) Measurement of Rate of Change of Momentum

The rate of change of momentum is another important physical measurement that may be carried out with the help of a cloud chamber. If the particle moves through a material medium, it will be continuously losing energy and hence momentum along its path by ionization, radiation, etc., consequent to which the value of $H\rho$ for the particle would change from point to point along its track. For a medium of low density, the various losses per cm of track are very small, so that the change in ρ from point to point can hardly be recognized and the particle maintains a constant (average) curvature over a fairly long path; the curvature of any track inside a Wilson chamber placed in a magnetic field may with good reasons be assumed as constant.

But for media of higher density (e.g., Pb, Au) the energy lost per cm depending on the nature of the particle, is comparatively high. If therefore a Pb plate 1 or 2 cm thick be inserted in the path of the particle within the chamber, the curvature of the track below and above the plate will generally be different, the former being greater than the latter. From a measurement of the curvatures above and below the Pb plate, the rate of change of momentum may be obtained. It follows directly from Eq. (4.01).

$$c(dp/dx) = 300zH(d\rho/dx). \qquad (4.11)$$

For low energy particles the thickness of the plate must be chosen carefully. For the same field the curvature of the track above the plate will be less than that below it. If the difference in curvatures in the two halves of the chamber be very great, the curvatures in both the halves cannot be measured accurately, and the accuracy in the determination of the momentum loss will be small.

The insertion of a plate inside the chamber greatly increases the chamber distortions which must be minimized as far as possible. The distortions in the two compartments of the chamber are generally different so that distortion curvatures are to be determined simultaneously for each half of the chamber, by taking no-field tracks during each run, interspaced in time with the field tracks. From these no-field tracks the distortion curves giving the curvature correction as a function of position in the chamber, for each half of the chamber and for each separate run are constructed.

Because of this difference in behavior in the two halves of the chamber, some tracks are photographed, in which a particle apparently gains momentum after emerging out of the plate, or even appears to change its charge from negative to positive and *vice versa*. The determination of the errors introduced in curvature are therefore of primary importance.

When the chamber is placed in the field of a magnet, this difference of curvature above and below an absorber plate, tells immediately the incident direction of the particle, thereby indicating the nature of charge of the particle. Anderson (1933) discovered the positron by this method.

3. Range

The range of a particle is of great significance, as in many cases in nuclear physics, the energy and the nature of the particle are deduced from an observation of its range inside Wilson's cloud chamber.

For the purpose of reference, range is usually given in terms of dry air at 15°C and 76-cm pressure measured under standard barometric conditions, i.e., mercury column reduced to equivalent height at 0°C at the sea level and at

45° latitude. The relative stopping power of water vapor with respect to dry air at the same temperature and pressure is assumed to be 0.74. The corrections due to temperature, pressure, latitude, and humidity may be quite appreciable in different cases and must be carefully carried out.

The following procedure enables a quick determination of air range. The length L_0 of the image of a full length α-ray track of range R_0 cm in air at 15°C and 760 mm is measured on the film. Then if La be the apparent length of any track, its reduced air range Ra is given by

$$Ra = La(R_0/L_0). \tag{4.12}$$

We assume that the stopping power of the gas mixture relative to air is constant along the range.

Unfortunately the exact determination of range is rendered difficult because of the self-absorption of the particles inside the source and also straggling. Rutherford, Ward, and Lewis (1931) observed that the slightest tarnish on the source reduced the mean range of 9-cm tracks by about 0.3 mm.

Because of fluctuations in the number of collisions, an initially homogeneous beam becomes inhomogeneous after traversal through any thickness of matter. If on the average the particles make n collisions while passing through the layer, the fluctuation in the number of collisions is $n^{\frac{1}{2}}$ and the fluctuation in the energy of individual particles after traversal through the layer is $n^{\frac{1}{2}}I$, where I is the average energy required for the production of an ion pair. Actually there is also fluctuation in I in addition to the fluctuation in n. Hence the ranges of the individual particles of a homogeneous beam are not the same but are distributed around an average value according to a Gaussian law.

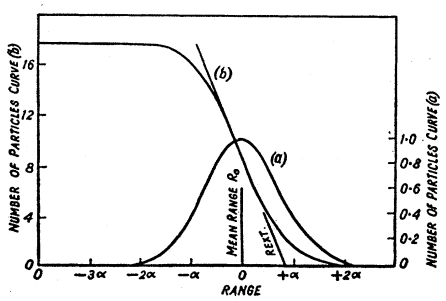

FIG. IV-3. Relation between the extrapolated and the mean range; curve (a) differential range distribution $p(R)dR$; curve (b) integral range distribution $P(R)$.

Curie (1923), Meitner (1926), Feather and Nimmo (1929), and Freitag* studied the effect of straggling on α-particle ranges with the expansion method. A narrow horizontal beam of homogeneous α-rays is introduced into the Wilson chamber and photographed. The average range and the distribution in the ranges are then measured. The results of these experiments show that the range distribution follows closely the Gaussian distribution

$$p(R)dR = \frac{\alpha}{\pi^{\frac{1}{2}}} \exp\left[-\alpha^2(R-R_0)^2\right]dR, \tag{4.13}$$

where R_0 is the mean range, α the linear straggling parameter relative to the particles and the medium concerned, and $p(R)dR$ the probability of occurrence of a group with range between R and $R+dR$.

The differential range distribution curve is shown in Fig. IV-3, curve (a). The mean range R_0 is the range which is reached by just half the particles. The mean range has a meaning only when we start with an initially homogeneous beam (as in some radioactive substances), and infinitely thin emitter (so as to prevent self-absorption). For artificial radioactive substances, the emitter must be suitably thick from intensity considerations. Moreover the energy of the emitted particle depends on the angle of emission—hence the beam is non-homogeneous at the start. In such cases, the particles of longer range, are more significant and the extrapolated range is used.

The extrapolated range is easily obtained from the number-range distribution $P(R)$, i.e., from a diagram giving the number of particles as ordinate which have ranges exceeding the value indicated in the abscissa

$$P(R) = \int_R^{\alpha} p(R)dR = \tfrac{1}{2}[1-\phi\{\alpha(R-R_0)\}], \tag{4.14}$$

where ϕ is the error integral.

This curve which may also be called the integral distribution in range, has the form as shown in Fig. IV-3, curve (b) because of the

* See General reference 5, p. 95.

effect of straggling. The intersection of the steepest tangent to the number-range curve with the range axis gives the extrapolated range (R_{ext}).

Since the integral distribution curve $P(R)$ has the steepest slope at $R=R_0$, it can be easily shown that

$$R_{ext}=R_0+\frac{1}{2}\frac{\pi^{\frac{1}{2}}}{\alpha}=R_0+S. \qquad (4.15)$$

The differences between the mean and extrapolated ranges have been measured for α-particles from ThC′ and RaC′. Good agreement between the observed and calculated values particularly for high energies, justifies the use of calculated values of S for determining the mean range R_0 from the measured extrapolated range R_{ext}. The straggling for α-particles varies from 1.2 percent of their ranges at 4 Mev to 0.85 percent at 50 Mev. S for different energies of protons and α-particles is given by Livingston and Bethe (1937).

The theoretical relationship between the mean range and the energy for α-particles and protons has been discussed in detail by Livingston and Bethe (1937). See also Appendix 3(b) in this connection where an approximate range-velocity relation has been deduced. It has been shown that the range of a particle is approximately proportional to (M/z^2) and to the velocity.

Unfortunately, the theoretical range-energy relation is rather uncertain because of:

(a) interchange of charge, i.e., capture and recaptures electrons during the last few mm of the track and

(b) uncertainty in the value of I, the average excitation potential.

On account of these difficulties, Livingston and Bethe use the following method in order to fix a conventional range-energy scale. The average excitation energy I and the constant in the Eq. (6.01) are so fixed that the range calculated theoretically agrees on the average with the observed range of the natural α-groups whose energies have been measured with great care from their magnetic curvatures [Rutherford, Lewis, and Bowden (1933)]. The range-energy relation for α-rays is fixed in this way between 5.3–11.5 Mev. For lower energies of α-particles and protons, the theory is much less certain and hence only the experimental data of Blackett and Lees (1932a), (1932b) are used. For higher energies the theoretical relation is again used as the theory is more reliable in this part. The complete range-energy curve for α-particles and protons obtained in this way up to a maximum energy of 15 Mev has been given by Livingston and Bethe.† This relation is generally used for obtaining the energy of a particle corresponding to any measured range.

In Appendix 2 the ranges, the corresponding velocities, and the energies of electrons, α-particles, and protons have been tabulated. With the help of these tables the energies or the velocities of these particles may be determined from their ranges measured in a Wilson cloud chamber. In Table VI-8 are collected the values of $[Rz^2/(M/m)]$ as a function of $\beta/(1-\beta^2)^{\frac{1}{2}}$. These results are quite general and should be applicable to any heavy particle.

4. Determination of Mass from Cloud-Chamber Measurements

The energy of the charged heavy particles with which we have to deal in nuclear physics rarely exceeds a few million electron volts and this energy is insignificant compared with their rest-energy. The velocity is then small compared to c and varies inversely with the mass of the particle.

$$\beta=pc/(p^2c^2+M^2c^4)^{\frac{1}{2}}\simeq pc/Mc^2. \qquad (4.16)$$

For such low velocity particles, the density of ionization which varies inversely as the square of the velocity will be very different for different particles, even when their kinetic energies are comparable. An inspection of the density of ionization along the track or the range inside the cloud chamber is sufficient to identify the nature of the particle.

In the case of cosmic particles, the kinetic energies may be as great or even greater than the rest energies. In such cases the velocities of all particles—electrons, mesotrons, or protons—approach appreciably close to that of light and the density of ionization is nearly the same for all particles. The determination of mass then becomes a problem. Moreover the other usual

† M. S. Livingston and H. A. Bethe, Rev. Mod. Phys. 9, 245 (1937), Figs. 29 and 30.

methods of mass determination, *viz.*, from electrostatic and magnetic deflections, fail for such high energy particles.

In the following pages a description is given of the methods developed recently, for the determination of the mass of the high energy cosmic particles from the cloud-chamber data. The methods have mainly been applied to determine the mass of the newly discovered mesotron and it is found that the values of the mass deduced by these different methods are not very consistent. This may be caused by the inaccuracies inherent in the experimental methods to be described below. It may also be possible that cosmic-ray mesotrons are not all of one rest mass.

The mass of an unknown particle may be deduced from the following cloud-chamber measurements:

(a) specific ionization I and curvature in a magnetic field $H\rho$,
(b) specific ionization I and range R,
(c) magnetic curvature $H\rho$ and range R,
(d) rate of change of magnetic curvature when the particle penetrates an absorber plate placed across the chamber $d(H\rho)/dx$, and
(e) magnetic curvature $H\rho$ and collision electrons e in the path of the heavy particle.

(a) *Determination of Mass from a Measurement of Specific Ionization and Magnetic Curvature*

Under certain assumptions (see Appendix 3(a), the energy loss per cm due to collisions, $(-dE/dx)_{\text{ion}}$ is independent of the mass and is a function only of the velocity of the particle. This function is given by Eq. (6.09), Appendix 3.

We can put in general

$$\left(-\frac{dE}{dx}\right)_{\text{ion}} = f\left(\frac{\beta}{(1-\beta^2)^{\frac{1}{2}}}\right). \qquad (4.17)$$

The calculated values of $(-dE/dx)_{\text{ion}}$ for different values of $\beta/(1-\beta^2)^{\frac{1}{2}}$ are listed in Table VI-7. In Fig. IV-4 curve (1) the calculated values of $(dE/dx)_{\text{ion}}$ have been plotted as a function of $\beta/(1-\beta^2)^{\frac{1}{2}}$, where βc is the velocity of the particle, i.e., the curve represents $f(\beta/(1-\beta^2)^{\frac{1}{2}})$ *vs.* $\beta/(1-\beta^2)^{\frac{1}{2}}$.

In Section 1 of this chapter we have discussed in detail how the number of ions produced per cm can be obtained from delayed expansion tracks. When the track is sharp, the number of primary ions may be estimated in an indirect way attributed to Williams (1939b). If I_0 be the true specific ionization, the mean free path between two ions is $1/I_0$. If a total track length L is now observed in the Wilson cloud chamber, the number of mean free paths in this length L, will be I_0L. The probability p that a gap of length l will occur in the total length L of the track, is given by

$$p = I_0 L \exp\left[-I_0 l\right]. \qquad (4.18)$$

Hence if the number of gaps greater than l cm occurring in the measured total cosmic-ray track length L is observed, one can deduce the value of I_0 with the help of Eq. (4.18). From a knowledge of I_0 the average number of ions produced per cm track length, the average value of the energy loss $-dE/dx$ can be determined by assuming that 32 electron volts are needed for the production of each ion pair.

Mass of the unknown high energy particle may be obtained if simultaneously with the measurement of specific energy loss, the curvature of the particle in magnetic field is also measured. It should be mentioned however that accurate measurement of curvature requires a sharp track whereas determination of $-dE/dx$ by the method of droplet-counting implies a broadened track. Both of these cannot be simultaneously determined with great accuracy and a compromise has to be made.

From Eq. (4.01) if we assume $z=1$ we have

$$\frac{M}{m} = \frac{eH\rho}{mc^2} \Big/ \frac{\beta}{(1-\beta^2)^{\frac{1}{2}}} = \frac{H\rho}{1704} \Big/ \frac{\beta}{(1-\beta^2)^{\frac{1}{2}}}, \qquad (4.19)$$

where $H\rho$ is expressed in gauss-cm, M/m is the mass number of the unknown particle in terms of the electron mass. Hence if $\beta/(1-\beta^2)^{\frac{1}{2}}$ is determined from a measurement of dE/dx, one can obtain directly M/m from $H\rho$ measurement.

In Fig. IV-4 $H\rho/(M/m)$ has been plotted against $\beta/(1-\beta^2)^{\frac{1}{2}}$ (curve 2). Hence from a measurement of dE/dx and $H\rho$, M/m can be read off directly from the curve without any calculation.

A few of the determinations of mass of mesotron by the use of this method are given in Table IV-1.

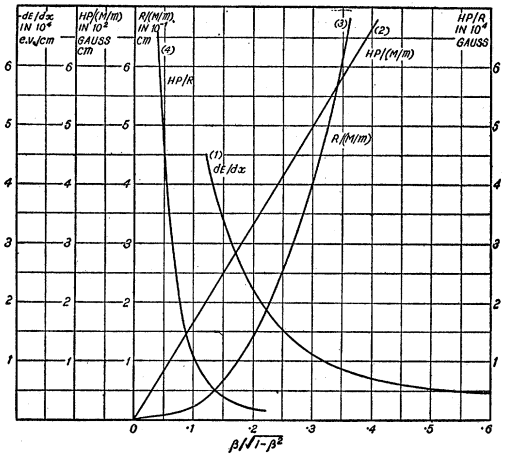

FIG. IV-4. dE/dx, $H\rho/(M/m)$, $R/(M/m)$, $H\rho/R$ plotted as a function of $\beta/(1-\beta^2)^{\frac{1}{2}}$.

(b) *Determination of Mass from Specific Ionization and Range*

Radiative losses are negligible for particles of mass much greater than that of an electron even up to very high energies ($\beta=0.9$) and in substances of large atomic numbers ($z=82$). Thus for a mesotron of energy 1.5×10^8 ev, the radiation loss in 1 cm Pb is

$$(\delta E)_{\text{rad}}=\frac{\ln 2E}{200^2\times0.5}\simeq0.01 \text{ Mev}.$$

This is entirely negligible when compared with the ionization loss of 10 Mev in the same thickness. Thus the total energy loss of a heavy particle is entirely determined by the ionization loss. Under this condition as shown in Appendix 3(a) and (b) the range may be represented in general by an equation of the type:

$$R=\frac{M}{m}g\left(\frac{\beta}{(1-\beta^2)^{\frac{1}{2}}}\right), \qquad (4.20)$$

where z has been assumed to be 1. It follows from Eq. (4.20) that $R/(M/m)$ should be a function of only $\beta/(1-\beta^2)^{\frac{1}{2}}$. The values of $R/(M/m)$ for different values of $\beta(1-\beta^2)^{\frac{1}{2}}$ have been compiled in Table VI-8. These values are also plotted as curve 3 in Fig. IV-4. This curve should be quite general and apply to a heavy particle of any mass. Hence if $\beta/(1-\beta^2)^{\frac{1}{2}}$ and the range of the particle are determined the curve will enable one to determine the mass of the particle in terms of the electron mass.

As explained previously the specific ionization $-dE/dx$ determines $\beta/(1-\beta^2)^{\frac{1}{2}}$ uniquely. Hence a simultaneous measurement of the specific ionization and the range of the particle inside the cloud chamber, enables one to determine mass of the particle. However this method cannot be very accurate as both the ionization as well as the range are more likely to be underestimated, and the two errors acting in the same direction tend to give only a lower limit of the mass of the particle.

As examples of the use of this method, we give in Table IV-2 a few estimates of the mass of the mesotron by different workers [see references given in Wheeler and Ladenberg (1942)].

(c) *Determination of Mass from a Measurement of Magnetic Curvature and Range*

Neither $H\rho$ nor range R determines the velocity directly. But $H\rho/R$ is a function of only the velocity which can be calculated theoretically.

From Eq. (4.19) we have

$$H\rho=1704\frac{M}{m}\frac{\beta}{(1-\beta^2)^{\frac{1}{2}}}$$

and from Eq. (4.20)

$$R=\frac{M}{m}g\left(\frac{\beta}{(1-\beta^2)^{\frac{1}{2}}}\right).$$

TABLE IV-1. Estimate of the mass of mesotron from specific ionization and magnetic curvature.

Observers	$-dE/dx$ in 10^3 ev per cm air	$H\rho$ in 10^5 gauss-cm	M/m from curves (1) and (2)
Williams and Pickup (1938)	12.5 7.5	1.1 1.47	230 210
Street and Stevenson (1937)	15.0	.96	230
Hughes (1941)	12.5	1.00	214
Brode, Macpherson, and Starr (1936)	25.0	.55	184
Anderson and Neddermeyer (1936)	25.0 7.5	.60 2.5	200 370

TABLE IV-2. Estimate of mass from specific ionization and range.

Observers	$-dE/dx$ in 10^3 ev per cm air	$R/(M/m)$ deduced from curves (1) and (3) Fig IV-4	R in cm air observed	M/m
Brode, Macpherson, and Starr (1936)	25.0	0.11	>18	>167
Corson and Brode (1938)	13.7	0.29	>15	>50
Street and Stevenson (1936)	15.0	0.25	>7	>28
Anderson and Neddermeyer (1936)	25.0	0.11	<8	<73

Hence,

$$H\rho/R=1704\frac{\beta}{(1-\beta^2)^{\frac{1}{2}}}\Big/g\left(\frac{\beta}{(1-\beta^2)^{\frac{1}{2}}}\right)$$
$$=h[\beta/(1-\beta^2)^{\frac{1}{2}}], \quad (4.21)$$

where $H\rho$ is expressed in gauss-cm and R in cm air. The function $h[\beta/(1-\beta^2)^{\frac{1}{2}}]$ can be easily calculated. The calculated values have been plotted in Fig. IV-4 curve (4). A measurement of $H\rho$ and R therefore indicates $\beta/(1-\beta^2)^{\frac{1}{2}}$. M/m may then be obtained either from Eq. (4.19) or (4.20).

It should be mentioned that this is the most accurate of the several methods described here, as both the curvature and the range may be measured fairly accurately from sharp tracks. It is however often possible to make only a lower estimate of the range, in such cases this method gives an upper limit of the mass of the particle. Table IV-3 shows the values of M/m deduced for mesotrons from the curvature and range measurements by several workers. The consistency of the results obtained is also a proof of the accuracy of the method.

(d) *Determination of Mass from the Rate of Change of Curvature*

We have described in Chapter IV, Section 2, how the rate of change of momentum of a particle can be determined by inserting a metal plate inside the cloud chamber. The rate of change of momentum is an important parameter which lead to a determination of the mass of the particle. This method has been used by

TABLE IV-3. Mesotron mass from curvature and range.

Observers	$H\rho$ in Gauss-cm	R in cm air	$H\rho/R$	$H\rho/(M/m)$	M/m
Brode, Macpherson, and Starr (1936)	5.5×10^4	>18	$<3.06\times10^3$	$>2.7\times10^2$	<204
Corson and Brode (1938)	5.5	>4	<13.5	>1.55	<350
Nishina and Takeuchi (1937)	3.87	6.5	5.95	2.1	184
Anderson and Neddermeyer (1936)	1.74	770.	0.226		220

TABLE IV-4. Estimate of mesotron mass from $d(H\rho)/dx$.

$(H\rho)_{\text{mean}}$	$d(H\rho)/dx$	M/m
3.27×10^5	0.67×10^5	161
2.20	2.67	250
6.15	0.522	226

Corson and Brode (1938) and discussed in detail by Wheeler and Ladenburg (1941).

From Eq. (4.11) and (6.11′)

$$\frac{d(H\rho)}{dx}=\frac{1}{300}c\frac{dp}{dx}$$
$$=\frac{1}{300}\frac{1}{\beta}\frac{dE}{dx}=i[\beta/(1-\beta^2)^{\frac{1}{2}}], \quad (4.22)$$

if $z=1$.

Since the variation of $(dE/dx)_{\text{ion}}$ with $\beta/(1-\beta^2)^{\frac{1}{2}}$ is known, (6.09), the values of $d(H\rho)/dx$ corresponding to any value of $\beta/(1-\beta^2)^{\frac{1}{2}}$ can be calculated. The calculated values of $d(H\rho)/dx$ are given in Table VI-9, and are shown graphically in Fig. IV-5. With the help of this curve and the measured value of $d(H\rho)/dx$, $[\beta/(1-\beta^2)^{\frac{1}{2}}]$ may be estimated. M/m may then be obtained from Eq. (4.19).

A few calculated values of M/m based on the observations of Anderson and Neddermeyer (1936) are shown in Table IV-4.

(e) *Determination of Mass from the Method of Elastic Collision*

One of the most direct methods of determining the mass of a particle is from its elastic collisions with an electron. It has been shown in Appendix 3(a), that if T be the kinetic energy imparted to a free electron as a result of collision with a primary of mass M, momentum p and if θ be the angle between the direction of ejection of

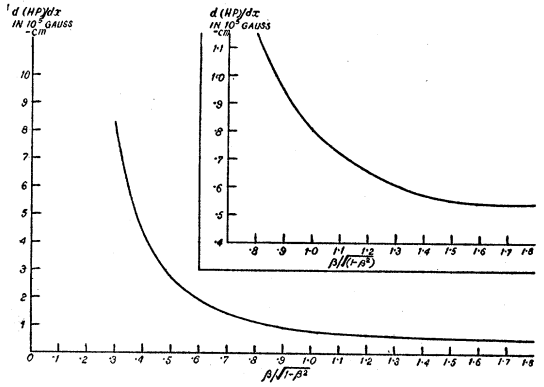

FIG. IV-5. $d(H\rho)/dx$ plotted as a function of $\beta/(1-\beta^2)^{\frac{1}{2}}$.

the secondary electron and that of the primary, then

$$T=2mc^2\frac{p^2c^2\cos^2\theta}{\{mc^2+(p^2c^2+M^2c^4)^{\frac{1}{2}}\}^2-p^2c^2\cos^2\theta}. \tag{4.23}$$

With the help of a cloud chamber placed in a strong magnetic field the tracks of the incident particle, the secondary electron and the direction of emission of this electron may be observed. A measurement of p and T from the curvature of these tracks of the primary and secondary particle together with θ, indicates the mass (M) of the primary particle.

Advantages of this method over the previous ones are that this method involves only the fundamental laws in physics, *viz.*, the principle of conservation of energy and momentum, while the previous ones depend on the use of formulas which have been verified only up to a limit. The applicability of the method is however limited because of rarity of the phenomenon. Recently Hughes (1941) and Leprince-Ringuet, *et al.* (1941) have obtained tracks of mesotrons producing secondary electrons inside the cloud chamber. The mass of the primary particle determined with the help of this method were 180 m and 240 m, respectively.

CHAPTER V. APPLICATION OF WILSON CHAMBER

1. Wilson Chamber in the Study of α-Rays

Alpha-rays were among the first to be photographed soon after the invention of Wilson chamber technique in 1911. On account of greater charge and slow speed, α-rays produce thick tracks in the cloud chamber which may be photographed easily.

The α-tracks show that occasionally an α-ray makes a close encounter with an electron which is thrown out with considerable velocity and is known as delta-rays. From theoretical considerations, it can be shown that such electrons may have velocities as great as twice the α-velocity and ranges approximately about 3 mm.

Meitner (1926) and Feather and Nimmo (1929) first applied cloud track method to investigate the complexity of α-ray spectra of ThC and RaC. From a statistical study of the ranges one can determine the number of particles of any range. Kurie (1932) has discussed the use of Wilson chamber for measuring ranges of α-particles from weak sources.

α-ray tracks are usually straight except near its end where the track shows kinks due to collisions of the α-particle with oxygen or nitrogen nuclei. When this occurs, one can usually discern the presence of another particle. The probability of such an event is extremely small, for the charged particle must pass very close to the nucleus—say within a distance of 10^{-12} cm. The probability of such a collision is about 10^{-8}. This is borne out by statistics of forked collisions. We usually get one such collision in say 100 tracks. A single track contains about 3×10^5 dots, nearly $\frac{1}{3}$ of which are caused by primary transference of energy to electron. Hence the probability works out to be 10^{-7}. When such a forked track occurs, from a measurement of the angles, one can deduce the ratio of masses of the two particles involved in the collision.

If a particle of mass M and initial velocity V collides with another of mass m initially at rest and the two particles after collision make angles ϕ and θ with V, then from the principles of conservation of energy and momentum we have,

$$m/M=\sin\phi/\sin(2\theta+\phi). \tag{5.01}$$

Blackett (1925) and (1932) studied elastic encounters of α-particles with hydrogen, helium, and nitrogen nuclei. In every case the values of m/M calculated from a measurement of ϕ and θ agreed with the accepted values. Such agreement

shows that elastic encounters really take place in which energy and momentum are conserved.

Occasionally abnormal forks occur in which α-particles suffer inelastic collisions. Blackett (1932) observed about 20 cases in 10^6 where the α-particles were captured by nitrogen nuclei which emitted protons. After collision only the proton track and that of the resulting nuclei were visible.† In such cases the momentum is conserved but not the energy. Assuming ψ and ω to be the angles between the initial track of the α-particle and the tracks of proton and of resulting nucleus, we have

$$\left.\begin{aligned} m_p V_p &= MV \sin\omega/\sin(\psi+\omega) \\ m_n V_n &= MV \sin\psi/\sin(\psi+\omega) \end{aligned}\right\}, \quad (5.02)$$

where m_p and m_n are the masses and V_p, V_n the velocities of proton and the final nucleus, M, V the mass and velocity of α-particle. ψ and ω may be measured, V calculated from the distance from the source at which fork occurs. Knowing m_p, V_p may then be obtained.

In the same way the cloud chamber may be used to study the range and distribution of α-particles when they are emitted as one of the disintegration products. To take one example, Murrel and Smith (1939) observed that two groups of α-rays with ranges 5 and 3.4 cm are emitted in the reaction $Na^{23}(d\alpha)Ne^{21}$. From the range of α-rays observed their energy may be deduced and an estimate can be made of the mass of Na^{23}.

2. Wilson Chamber in the Study of β-Rays

Compared to α-rays, β-rays produce thinner tracks (about 50 ions per cm) inside the Wilson chamber and are therefore more difficult to be photographed. β-ray tracks are of beaded nature owing to the separation between individual ions. Because of such sparseness of ionization, it is possible to count the total number of ions produced by a β-particle per cm path and hence its specific ionization. We have already mentioned how under suitable conditions, it is possible to determine approximately the velocity of the β-particle from a measurement of its specific ionization. The number of collisions increases as the β-particle slows down, hence the path of a slow β-particle appears curved because of a great number of random deflections. When a slow moving β-particle collides with another electron the angle between two tracks is approximately 90°, as the masses are equal. With the increase of energy of the colliding particle, its relativity mass increases and angle in space between two tracks diminishes. Champion (1932a), (1932b) from stereoscopic measurement of the angles between two tracks in space studied the variation of relativity mass with the energy of the β-particle.

Collision of a β-particle with the nucleus produces no recoil track of the struck nucleus, its mass being so great compared with that of the electron that very little momentum is transferred in the impact [Champion (1936)].

The cloud chamber has been used in the study of the continuous β-ray spectrum. The fields used in such work may be of the order of 1000 gauss. The energies are deduced from curvature measurements. If the radioactive source is introduced into the chamber deposited on a metal surface the secondary β-rays from the source holder are also present along with the primary ones, and thus a great confusion may be caused. This difficulty was avoided by Richardson and Leigh Smith (1937) by introducing the radioactive substance in the form of a gas inside the chamber.

The shape of the β-spectrum is obtained by a direct measurement of the number *vs.* energy distribution from cloud-chamber data. In order to obtain the end-point of the β-spectrum one has to take the help of either Fermi or Konopinski-Uhlenbeck theory. According to these theories:

$$(N/F)^{1/k} = K[(1+\eta_0^2)^{\frac{1}{2}} - (1+\eta^2)^{\frac{1}{2}}], \quad (5.03)$$

where N = number of electrons with momenta, $\eta = H\rho/1704$, η_0 = momentum of fastest electrons,

$$F = f(z\eta) = \frac{2\pi\alpha z\eta(1+\eta^2)^{\frac{1}{2}}}{1-\exp[-2\pi\alpha z(1+\eta^2)^{\frac{1}{2}}]/\eta}. \quad (5.04)$$

K is a constant of proportionality depending on the total number of electrons counted, $k=2$ in the Fermi theory and $k=4$ in the K.U. theory.

In some cases as in RaE, $(N/F)^{\frac{1}{4}}$ *vs.* $(1+\eta^2)^{\frac{1}{2}}$ is a straight line suggesting a simple spectrum. In

† Blackett and Lees, Proc. Roy. Soc. **136**, 338 (1932), Plate 7.

other cases such as Mn^{56}, I^{128} no such simple line is obtained, which suggest β-rays may be divided into two or more groups [Bacon, *et al.* (1941)].

Cloud-chamber work on β-rays suffers from several disadvantages. First the number of tracks examined must be large and the amount of time and labor involved enormous. Secondly it is almost impossible to eliminate completely the secondary electrons produced either from gas or chamber walls by the action of γ-rays, primary electrons, etc. Scattering of the electrons or positrons by the gas inside the chamber introduces considerable error when the energy is low. This is minimized by using hydrogen instead of other gases inside the chamber. It has been further shown by Bacon, *et al.* (1941) that when the source is in the form of a layer on the inner surface of the chamber wall, the track cannot enter the visible portion of the chamber at all if $\rho<(A-B)/2$, where ρ=radius of the horizontal projection of the electron track, A=inside radius of the cloud chamber, and B=radius of the visible portion of the chamber. It is possible for a particle to enter the visible portion only when the angle made by the horizontal component of its initial momentum with the horizontal tangent to the emitting surface, lies within a certain range. Now since B is a function of the position of the point of emission, the finite width of the source affects the energy spectrum. It has been shown by them that the yield of low energy tracks was the same for different sources but for high energy tracks it was proportional to the width of the source.

In spite of these difficulties the cloud chamber has been used extensively for the study of artificially produced β-activity. We know that almost all elements can be induced to be radioactive by bombarding them with α, d, p, or n of suitable energy. These bodies emit electrons, positrons, or γ-rays before they come to a stable form. These electrons and positrons have been studied and their energy distribution has been determined with a cloud chamber in a magnetic field. The various radioactive bodies and the maximum energy of the β-particles studied by this method have been listed by Seaborg (1944).

Among other applications of the Wilson chamber in the study of β-rays may be mentioned the attempts of Crane and Halpern (1934) to obtain evidence of the presence of the neutrino. Crane and Halpern introduced radiochlorine into the cloud chamber and measured simultaneously the momenta of the electron and the recoil nuclei involved in β-disintegration. This experiment, though of limited accuracy, seems to indicate that momentum is not conserved between the electron and the nucleus alone and emission of a third particle—the elusive neutrino—seems highly probable.

Sizoo and Barendregt (1939) with the help of a cloud chamber obtained evidence of the production of positive electrons by internal and external conversion of the kinetic energy of β-rays from radioactive substances. A drop of $RaBr_2$ placed in a thin capillary glass tube about 70 microns thick and closed at both ends, is placed at the center of the Wilson chamber in a magnetic field of about 400 gauss. The glass tube is so thin that it stops all α-particles but only a negligible fraction of β-rays. It is found that together with the electrons, positrons also emerge from the glass tube, the number and energy distribution of which can be determined from curvature measurements. The number of positrons is found to be much greater than can be accounted for by the theory of Jaeger and Hulme, if we assume they are produced by the creation of pairs by γ-rays.

3. Application of Wilson Chamber in the Study of X-Rays and γ-Rays

A beam of x-rays and γ-rays does not produce continuous tracks inside the chamber; only the electrons which these beams release either from the gas in the chamber or from its walls can be photographed.

Two types of electron tracks are found to be associated with the passage of an x-ray beam through the cloud chamber. The long tracks are due to photoelectrons which take up the whole energy of the x-ray or γ-ray quantum. There is also found a second type of very short tracks resembling "dots." These are caused by recoil electrons generated by the Compton process.

As the energy of x-ray quanta increases, the number of photoelectron tracks diminishes and that of recoil electrons increases. The short tracks

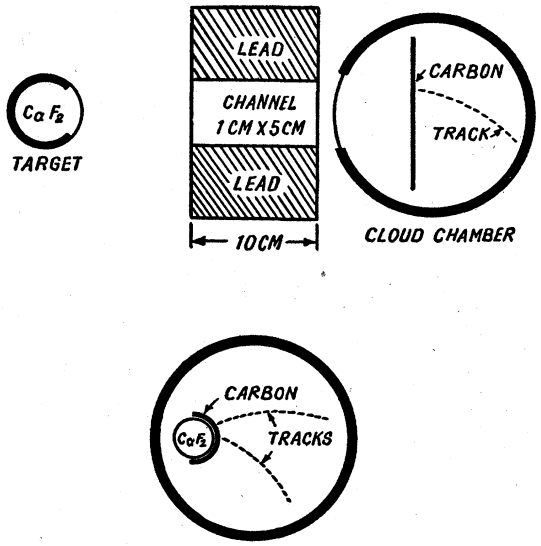

FIG. V-1. Experimental arrangement for measuring γ-ray energies with the help of the recoil electrons released in a cloud chamber.

due to recoil electrons are also found to develop tails as the energy of the quantum increases. These have been named "comma" or "fish" tracks [see Wilson (1923)].

Sometimes the photoelectron may be ejected from the K level of the atom. As a consequence of this, secondary K-radiation is emitted by the atom. This radiation may be absorbed in the same atoms thereby releasing tertiary electrons from higher levels. This effect, first discovered by Auger, has been photographed in the Wilson chamber [see Auger (1925)]. The photograph shows clearly (1) a secondary ejected by primary x-rays, (2) tertiary ejected from the L level by the K-radiation of Xe atom, and (3) and (4) two other electrons released from the M level by two separate quanta of L radiation.

By comparing the number of cases in which the electron tracks are paired with those when the tracks are single one can estimate the relative frequency of Auger effect for different atoms.

The energies of the γ-rays may be determined from a study of photo, Compton, or pair electrons released by the rays in their passage through a cloud chamber placed in a magnetic field. Skobelzyn (1927) used this method in the investigation of the complex γ-spectra of RaC'. The energies of the Compton electrons released from the gas inside the chamber are determined from their curvatures in a field. From a knowledge of the direction of emission ϕ and the energies of Compton recoils T, the energies $h\nu$ of the γ-rays responsible for them are deduced by means of the scattering formula

$$\gamma_2=\frac{2\gamma^2}{1+2\gamma+(1+\gamma)^2\tan^2\varphi},$$

[see Eqs. (6.16) and (6.19), Appendix 4].

Figure V-1 shows the experimental arrangement used by Halpern and Crane (1939). γ-rays of energy 5.8×10^6 ev from Ne^{20} in the reaction $F^{19}(p\gamma)Ne^{20}$ are first collimated by means of a Pb canal and then allowed to fall on a carbon or lead slab inside the Wilson chamber. For weak sources, target and the radiator may be placed inside the chamber. The chamber is in a magnetic field, the electrons released from the carbon radiator by photoelectric action, Compton effect or pair production are bent by the magnetic field. The curvature of the tracks is measured and a statistical study is made of the number of particles whose tracks have $H\rho$ lying between definite limits. One of the representative curves $n(H\rho)$ as ordinate and $H\rho$ as abscissa is shown in Fig. V-2. [Fowler, *et al.* (1938), Richardson (1938a, 1939), Curtiss and Richardson (1940).]

For understanding these curves, one must remember that in the energy range considered Compton collision is the predominating factor. Others may be neglected. Corresponding to the angle of emission of the Compton electron ϕ, and energy T_φ, there is a definite probability of emission $\sigma(\epsilon, \varphi)$. These experimental curves give $\sigma(\epsilon\varphi)\sim T_\varphi$. It will be shown in Appendix 4, Eq. (6.23) that theoretically $\sigma(\epsilon\varphi)$ should reach a maximum value at the electron energy $\gamma_2=2\gamma^2/1+2\gamma$ corresponding to $\varphi=0$.

The experimental curves differ somewhat from theoretical ones because of the finite thickness of the absorber. Because of this the electrons liberated from inside the radiator have to suffer energy losses because of scattering. The maximum intensity is not obtained at the point $\phi=0$, but somewhat earlier. $n(H\rho)$ drops to zero at a value of $H\rho$ corresponding to $\gamma_2=2\gamma^2/(1+2\gamma)$. From a determination of $H\rho$ at which the maxi-

mum occurs the energy of the γ-ray may be calculated (see Table VI-10).

From an inspection of these curves it is possible sometimes to decide whether there is one or more than one γ-ray. In the case of V^{48} for example, the curve of secondary electrons is found to be composed of two curves. One with the limit at $H\rho=2400$ is owing to the γ-ray of 0.53 Mev; the other peak in the β-distribution curve (Fig. V-2) is caused by a strong γ-ray of 1-Mev energy. Gaerttner and Pardue (1940) investigated γ-rays from N bombarded with H^2. From the distribution of pairs and recoil electrons ejected from a Pb lamina 0.026 cm thick, they deduced that there were two γ-rays of 7.2×10^6 ev and 5.3×10^6 ev. The distribution of recoil electrons from a carbon lamina (0.12 cm) indicate two other γ-rays of 4.2 and 2.2 Mev.

The area of the experimental curves represents the total number of electrons released by γ-quanta. This area will be larger the larger the number of γ-quanta emitted per disintegration. From an estimate of the areas relative intensities of the γ-ray quanta may be deduced.

Direct proof of formation of pairs of positive and negative electrons in a cloud chamber has been obtained by various workers [see the references given in Heitler (1937) and in Delsasso, Fowler, and Lauritsen (1937a) and (1937b) and Gaerttner and Pardue (1940)]. The early workers used γ-rays from ThC$''$ D($h\nu=2.62\times10^6$ ev), from $F^{19}(\alpha p)Ne^{22}$ reaction ($h\nu=2\times10^6$ ev) and those from $Be^9(\alpha n)C^{12}$($h\nu=6.7$, 4.2, 2.7 Mev). The recent workers have used the high energy γ-rays resulting from a bombardment by protons of lithium ($h\nu=16\times10^6$ ev), boron ($h\nu=16\times10^6$ ev) and fluorine ($h\nu=6\times10^6$ ev). Gaerttner and Pardue used 7-Mev γ-rays from N^{14} bombarded with deuterons. The electrons released from lead sheets placed inside the cloud chamber are deflected by a magnetic field and their energies studied. In all cases the total kinetic energy of the two electrons when added to their rest energy agrees with the energy of the γ-quantum as known from other measurements.

Another interesting photograph in this connection is that obtained by Shinohara and Hatoyama (1941). They obtained a picture in which two electrons and one positron start from a common point in the gas filling the cloud chamber. This is believed to be an example of pair production by γ-rays in the field of the electron. The γ-ray used was that of F bombarded by a proton. Adding the energy of the two electrons to that of the positron, these workers obtained a value of 5.95×10^6 ev which is in close agreement with the accepted γ-ray energy of F.

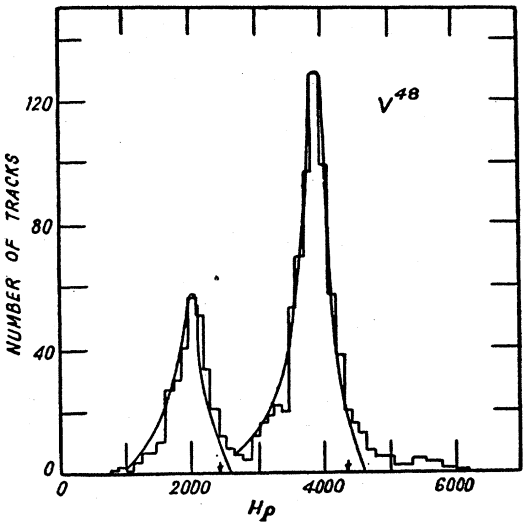

FIG. V-2. Energy distribution of recoil electrons released by γ-ray bombardment.

Approximate values for the cross section for pair production can be derived from the measurement of the number of positive and negative electrons inside the chamber. It is assumed that all positrons and some electrons are produced in pairs while the rest of the electrons are generated either by recoil or photoelectric process. This assumption is justified by the finding of Blackett that the upper limit of the electron distribution is about 1 Mv higher than that of the positron distribution.

Since the cross sections for photoelectric and Compton effect are known fairly accurately, one can deduce the cross section for pair production from the observed number of positive and negative electrons.

γ-rays arising from the annihilation of positive electrons have been studied with the help of the cloud chamber by J. R. Richardson (1938a) and Richardson and Kurie (1936). Sources of positron emitters, e.g., N^{13}, Cu^{64}, V^{48} are covered with thick absorbers so as to stop all positrons. The

γ-rays given out from these substances are then examined by analysis of the secondary electrons released from a target placed inside a cloud chamber in a magnetic field. The experimental set up has been described in detail earlier. From a study of the energy distribution of these electrons the energies of the parent γ-rays are deduced. In each of the above positron emitters evidence of continuous distribution of energies from 5×10^6 ev upwards has been obtained. These are probably caused by annihilation of positive electrons in motion.

Chadwick, Feather, and Bretscher (1937) and Richardson and Emo (1938) have studied the photo-disintegrations produced by γ-rays. The former used γ-rays from ThC$''D$ and $Li^7(p\alpha)He^4$ reaction and the latter used γ-rays from $Na^{23}(dp)Na^{24}$ reaction.

In these experiments the cloud chamber is filled with ${}_1H^2$ at a pressure of 1 atmos. When radioactive Na is brought close to the cloud chamber proton tracks are observed. The mean energy of the protons deduced from their ranges is about 410 kev. From this result the difference between the energies of Na^{24} γ-ray and the binding energy of ${}_1H^2$ is 810 kev. If we assume the energy of Na^{24} γ-ray as 3×10^6 (from Compton recoil method) the binding energy comes out to be 2.18×10^6 ev. The distribution of tracks implies a considerable preponderance of photoelectric over photomagnetic type of reaction and the cross section is found to be of the order of 10^{-27} cm^2.

4. Application of Wilson Chamber in the Study of Neutrons

Neutrons being uncharged do not ionize directly and hence cannot be photographed. Neutrons are detected in the Wilson chamber only when they collide with other nuclei producing thereby nuclear recoils. Curie and Joliot (1934) were the first to photograph in a Wilson chamber the tracks of recoil protons driven by the impact of radiation from Rn and Be mixture. They had hydrogen gas inside the chamber. Chadwick found that the radiation from Rn and Be mixture was also capable of conferring great speeds to other nuclei of light elements, e.g., Li, He, B, C, N, O, A, etc. The ranges of recoil-nuclei may be measured inside the cloud chamber from which their velocities are deduced from the well-known range-velocity relation. When the nature and velocity of the struck nuclei are known, the energy of the particles responsible for the production of such recoils may be calculated from the laws of conservation of energy and momentum.

The energy distribution of neutrons has been investigated by studying the energy distribution and the ranges of ejected protons in a Wilson cloud chamber [Bonner (1941) and see reference 3 in that paper]. The energies of neutrons are obtained from the range of recoil protons in a methane filled chamber. Neutrons have practically the same mass as protons. The maximum energy that is transferred to a proton in a single head-on collision is therefore equal to the neutron energy and the measurement of neutron energy distribution reduces to that of measuring the energies of protons from the well-established energy-range relation. Only those protons are observed which make extremely small angles (0° to 10°) with the direction of the neutron beam. Since the recoil proton tracks may be very long, high pressures have to be used inside the chamber. Bonner used a pressure of 14.7 atmospheres and thus could measure proton ranges as long as 126-cm air with his 8.8-cm chamber. Interposing sheets of mica of known thicknesses, range as great as 190-cm normal air could be photographed. For small proton ranges hydrogen at $\frac{1}{2}$ atmosphere was used as the chamber gas.

Figure V-3 represents the results obtained with neutrons from $Li^7(dn)2\alpha$ reaction. The upper curve giving the distribution of recoil protons has to be corrected for the variation of neutron-proton collision cross section with the energy of the neutron. With such correction one obtains the dotted curve giving the probable distribution of neutron energies.

The hump near 13 Mev is explained to be due to neutrons from Li^7 produced by the reaction $Li^7(dn)Be^8$. The neutrons from this second reaction are nearly homogeneous with a maximum at 13.5 Mev. From the relative areas it is possible to estimate the relative probabilities of the two disintegrations.

The same technique has been used in the

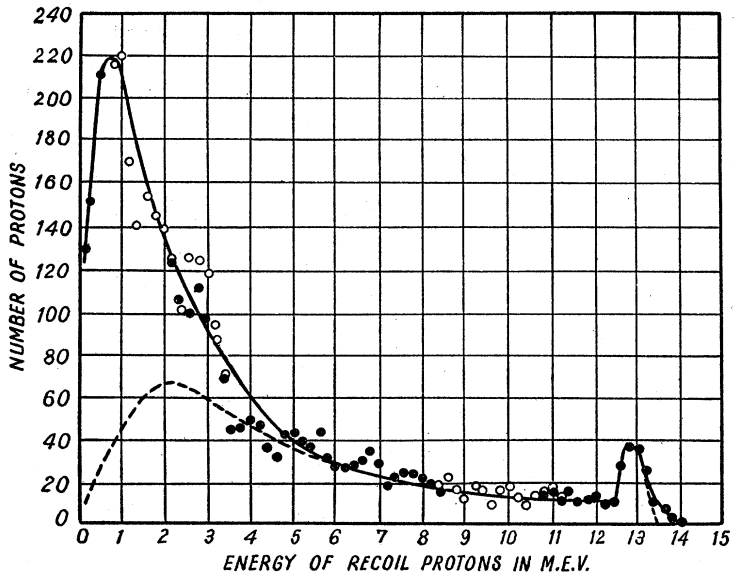

FIG. V-3. Energy distribution of recoil protons resulting from collisions with a neutron beam.

study of neutrons from other nuclear reactions. Neutrons from the reactions $Be^9(\alpha n)C^{12}$, $F^{19}(\alpha n)Na^{22}$ have been studied by Dunning (1934) and Mott-Smith and Bonner (1934) who found that groups of neutrons are emitted corresponding to the excited states of the product nuclei. In the case of $H^2(dn)He^3$, $Li^7(dn)Be^8$, $C^{12}(dn)N^{13}$, and $C^{13}(dn)N^{14}$ mono-energetic neutrons are found to be emitted. Four groups of neutrons are found to be emitted by B^{10} in the reaction $Be^9(dn)B^{10}$.

Application of Wilson chamber technique in the study of photo-neutrons from $(\gamma-n)$ type of reactions have already been considered under γ-rays.

5. Wilson Chamber in the Study of Artificial Disintegrations

The investigation of the disintegration particles emitted during the bombardment of elements by means of artificially accelerated particles is carried out mainly by the use of either electrical counting devices or of an expansion chamber. The former methods are best suited for a rapid investigation of the types and ranges of the emitted particles, while the latter method, once the correct set of experimental arrangement has been realized, gives direct evidence of the ranges and also of relative directions of emission of the particles in space. The choice of experimental conditions is greatly simplified by a knowledge of the results of a "test" experiment by the counting method and so a chamber method is sometimes preceded by counting experiments.

The expansion chamber used for artificial disintegration experiments may be of the standard horizontal or vertical type. The bombarding beam of ions falls upon the target contained in a small tube which passes through the top of the chamber [Dee (1935)]. The target is a few square millimeters in area and has generally a very small stopping power. It is inclined to the incident beam of bombarding particles. When the range of the disintegration products is larger than the dimensions of the chamber, the target is surrounded by a window system (usually of mica) which has to withstand the pressure inside the chamber and at the same time admit the products of disintegration into the chamber. The stopping power of the window system varies according to the range of the products in the gaseous medium used in the chamber. Sometimes the high pressures used are sufficient to keep the range inside the chamber, so that the window system is unnecessary. The pressure may be adjusted according to the energy of the products. For very small range products, gases of small stopping powers or a mixture of denser gases diluted with lighter ones are used. This method

is very useful for studying neutron produced disintegrations which lead to forked tracks.

The bombarding beam is shielded from the target by a light shutter which is held closed by an electromagnet inside the beam tube. It is opened at the desired instant relative to the expansion by short circuiting the electromagnet by a thyratron. The method is similar to that used for randomly operated chamber in the study of cosmic rays.

It should be mentioned here that the shortness of the interval during which the chamber remains sensitive, combined with the thin and small targets used, require the beam of bombarding ions to be of very high intensity.

When the scattered incident particles have a fairly large chance (depending on the energy of the particle) to mask the product particles, a magnetic deflection method as used by Becker, Fowler, and Lauritsen (1942) is adopted. The target is placed outside the chamber, and the produced particles together with the incident particles scattered in this direction, are allowed to pass through a magnetic field at right angles to the direction of motion. The two beams are then separated depending on their e/m and velocity. The beams thus separated then enter the chamber through a mica window in the cylindrical wall of the chamber. The space between the target and the window is kept evacuated. A knowledge of the stopping power of the window sheet and the gas inside the chamber then allows one to determine the energy of the particles.

Photographs are taken through the front plate of glass of the chamber, with two cameras which are mounted in a way as described in Chapter III, Section 2. Measurements are made upon the images of the tracks reproduced in the object space. The tracks are reproduced in the model and those passing through the same point are supposed to belong to one nuclear reaction. But a large portion of the target where the incident beam impinges on it, appears as dazzling white. The determination of the point of intersection of the produced tracks, as also their angles of emission with the direction of the incident beam is not without error. Experimental conditions are therefore set by increasing the energy and decreasing the number of particles in the incident beam and by properly collimating the beam so that comparatively few tracks are recorded per expansion. It is then easier to decide which tracks belong to the same nuclear process, and how many tracks belong to any single process. If the rate of occurrence of a system of tracks with the same distribution of range and angular separation between them is greater than it would be by mere chance, it is concluded that the system has evolved out of one nuclear process.

Once the products belonging to the same nuclear process have been determined, probable charge and mass are attributed to them balancing the nuclear equation. Then from the measured ranges energies are determined (see Chapter IV, Section 3), and hence their velocities of emission, care being taken to see if the momentum and energy of the system formed of the bombarding particle and the struck nucleus is conserved. If it is so, the assumed mass and charge are accepted as valid and the nuclear transformation is supposed to be effected in the manner assumed.

In any nuclear process, charge, mass number, energy, and momentum must be conserved. In the most common type of nuclear phenomena both the initial and end products consist of two particles. Usually one of the end products is a light particle, which has a greater velocity and hence a longer range. It is therefore easier to be observed and is generally known as the emitted particle. Let the subscript 0 refer to the initial nucleus, 1 to the incident particle, 2 to the produced, and 3 to the residual nucleus. Then if M stands for the mass and T for kinetic energy,

$$M_0+M_1=M_2+M_3+Q, \qquad (5.05)$$

where Q is the total energy evolved in the process and is given by

$$Q=T_2+T_3-T_1. \qquad (5.06)$$

If now T_2 and T_3 can be determined from the observation of ranges of the two produced particles, Q may be obtained from Eq. (5.06), since T_1 is known. The value of Q thus obtained may be substituted in Eq. (5.05) and the exact mass of any of the products determined when the mass of the others are known accurately.

The ranges of both the produced particles and that of the incident one can be observed simul-

taneously in cloud-chamber photographs only very rarely. If the range of only the emitted particle together with its angle of emission is observed, T may be calculated from the principle of conservation of momentum.

Since the momenta of the two produced particles must balance that of the incident one, we have

$$M_3T_3=M_1T_1+M_2T_2 -2(M_1T_1M_2T_2)^{\frac{1}{2}}\cos\theta, \quad (5.07)$$

where θ is the angle between the directions of motion of incident and emitted particle.

Eliminating T_3 between (5.05) and (5.06) Q can be obtained in terms of M_1, M_2, T_1, T_2, and θ. Thus

$$Q=\frac{M_2+M_3}{M_3}T_2-\frac{M_3-M_1}{M_3}T_1 - \frac{2(M_1M_2T_1T_2)^{\frac{1}{2}}}{M_3}\cos\theta. \quad (5.08)$$

T_1 and θ are known from the conditions of the experiment and in almost all cases the exact nuclear weights M_1, M_2, M_3, etc., may be replaced by the mass numbers. If now T_2 is determined from range measurement in Wilson chamber track, Q may be calculated.

For an example, the experiments of Dee and Gilbert (1935) on $d-d$ reaction may be mentioned. They observed two groups of particles with almost collinear ranges of 14.7 cm and 1.6 cm when measured at right angles to a beam of 0.24-Mev deuterons.

The reaction is identified as

$$H^2+H^2\rightarrow H^1+H^3+Q. \quad (A)$$

When $\theta=90°$, the Eq. (5.08) is simplified into

$$Q=\frac{M_2+M_3}{M_3}T_2-\frac{M_3-M_1}{M_3}T_1. \quad (5.08')$$

Identifying the long range groups with the protons and after application of corrections for straggling in the thick target, the energy of the protons (T_2) is deduced to be 3.04 Mev from the range and the corresponding Q value is 3.98 ± 0.02 Mev. This value of Q may be used to calculate the mass of H^3 since all other masses occurring in Eq. (A) are known.

Many other reactions in which the emitted particle leaves a visible track have been similarly studied with the help of a cloud chamber. Of these we mention below only a few representative ones:

(a) $N^{14}(\alpha p)O^{17}$ Blackett and Lees (1932);
(b) $Li^6(d\alpha)He^4$ Dee and Walton (1933);
(c) $H^2(dp)H^3$ Dee (1934),
$Li^6(dp)Li^7$ Delsasso, Fowler, and Lauritsen (1935),
$Li^7(dp)Li^8$ Fowler and Lauritsen (1937), and
$B^{11}(dp)B^{12}$ Fowler, Delsasso, and Lauritsen (1936);
(d) $Li^7(p\alpha)He^4$ Dee and Walton (1933),
$Li^6(p\alpha)He^3$ Neuert (1935),
$Be^9(p\alpha)Li^6$ Krichner and Neuert (1935), and
$B^{11}(p\alpha)Be^8$ Dee and Gilbert (1936).

When the emitted particle is a neutron neither its direction of emission θ nor T_2 can be determined from observation. In such cases if the direction of motion of the residual nucleus ϕ and its energy T_3 are observed, then T_2 and Q may be deduced from the equations

$$M_2T_2=M_1T_1+M_3T_3 -2(M_1T_1M_3T_3)^{\frac{1}{2}}\cos\phi \quad (5.09)$$

and

$$Q=\frac{M_3+M_2}{M_2}T_3+\frac{M_1-M_2}{M_2}T_1 - \frac{2(M_1T_1M_3T_3)^{\frac{1}{2}}}{M_2}\cos\phi. \quad (5.10)$$

As an example we consider the alternative $d-d$ reaction studied by Dee and Gilbert (1935).

$$H^2+H^2\rightarrow n'+He^3. \quad (A')$$

Their Fig. 6 shows one of the pictures obtained by the authors. The long tracks are caused by H^1, and H^2 produced in the reaction (A) and the short ones are caused by He^3. On account of the very short range of He^3, it was found necessary to fill the expansion chamber with deuterium gas and to introduce the deuteron beam into the chamber itself.

The Q value calculated from the measured range of He^3 is 2.88 Mev [Dee and Gilbert (1935)]. Bonner and Brubaker (1936b) observed 2.53 Mev for neutron energy at right angles to

the beam. This yields a Q value of 3.17 Mev and is possibly more correct.

(αn), (pn), and (dn) reactions may be studied in this way. But when the residual nucleus is heavy, it is not easy to observe its track or direction of emission with any accuracy. In such cases it is more convenient to investigate the energies of neutrons by the method of recoil protons in a hydrogen- or methane-filled cloud chamber (see Chapter V, Section 4). Neutrons from the following reactions have been investigated in this way.

(a) $Be^9(\alpha n)C^{12}$, $B^{11}(\alpha n)N^{14}$, $F^{19}(\alpha n)Na^{22}$ [Bonner and Mott-Smith (1934)].

(b) $Li^7(dn)Be^8$, $Li^7(dn)2He^4$ [Bonner and Brubaker (1935)], $Be^9(dn)B^{10}$, $B^{10}(dn)C^{11}$, $B^{11}(dn)C^{12}$, $C^{12}(dn)N^{13}$ [Bonner and Brubaker (1936b)].

When the bombarding particle is a neutron, the incident particle leaves no track and the disintegration tracks appear as a fork, one arm of which is usually longer and thinner than the other.† In this case it is not possible to determine either θ or ϕ separately, but a knowledge of the range of each of the two arms together with the angle between them allows us to determine the energy of the incident particle, for we know that

$$M_1T_1=M_2T_2+M_3T_3 +2(M_2M_3T_2T_3)^{\frac{1}{2}}\cos(\theta+\phi) \quad (5.11)$$

and

$$Q=\frac{M_1-M_2}{M_1}T_2+\frac{M_1-M_3}{M_1}T_3 -\frac{2(M_2M_3T_2T_3)^{\frac{1}{2}}}{M_1}\cos(\theta+\phi). \quad (5.12)$$

Many elements (e.g., C, N, O, F, and Ne) can be introduced into the chamber in the form of gases and subjected to neutron irradiation. A single fork track under controlled conditions is then sufficient to establish a reaction. However, the method is tedious, many thousands of photographs must be taken to record a single fork. Moreover, since the direction of motion of the neutron is not known, there may be considerable error in energy measurements because of the scattering of the neutron.

Feather (1932) was the first to photograph a fast neutron fork caused by the disintegration $N^{14}(n\alpha)B^{11}$. Since then, many other observers have photographed fork tracks caused by the following reactions: (a) $C^{12}(n\alpha)Be^9$ [Feather (1933), Harkins, Gans, and Newson (1935)]. (b) $C^{12}(n3\alpha)n$ [Chadwick, Feather, and Davies, (1934)], (c) $O^{16}(n\alpha)C^{13}$ [Meitner and Philip (1934)], (d) $F^{19}(n\alpha)N^{16}$, $N^{20}(n\alpha)O^{17}$ [Harkins, Gans, and Newson (1935)], and (e) $N^{14}(np)C^{12}$ [Kurie (1934), Bonner and Brubaker (1936a)].

With slow neutrons the complication due to neutron momentum does not arise. These reactions result in a single track of a length equal to the sum of the ranges of the ejected particle and recoil nucleus [Roaf (1936)].

Sometimes nuclear reactions occur in which more than two particles appear as end products. In these cases the momentum and energy conservation relations are insufficient to determine the energy of each end product as a function of the angle of emission. The change in total mass determines only the total kinetic energy of the end products. This kinetic energy may be distributed among the products in an infinite number of ways. Hence a characteristic feature of this type of reaction is a continuous velocity distribution of the produced particles.

Dee and Gilbert (1936) tried to detect triple α-emission from the reaction

$$B^{11}+H^1\rightarrow He^4+He^4+He^4+Q.$$

First they looked for pairs originating from the same point of the target and then calculated the range and the angle of emission of a third particle, if it formed one member of a triad. The momentum of the third particle must close the triangle formed by the momentum of the impinging proton and the sum of the momentum vectors of the two detected α-particles. Thus all momenta and the kinetic energies are known, and Q may be estimated and compared with the Q value of the reaction known already from the masses.

Dee and Gilbert found that, out of 79 pairs, 56 gave Q values so close to 9 Mev that they

† N. Feather, Proc. Roy. Soc. **136**, 209 (1932), Plate 16.

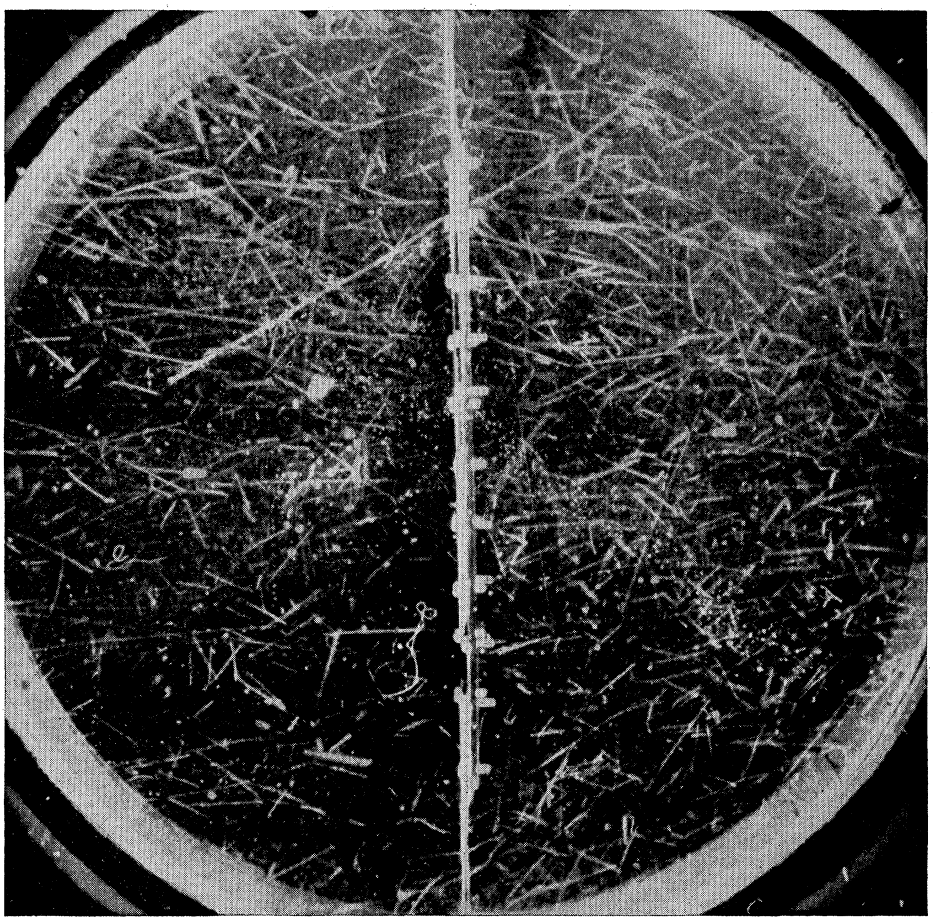

FIG. V-4. Typical pair fragments produced on fission.

must be regarded as true pairs forming a part of triads. In 48 of these 56 cases, the direction and length of the calculated α-particle track was such that it could not have been photographed, in six of the remaining eight the third track appeared within 3° degrees of the calculated direction and only in two cases it could be followed to its end.

A similar and interesting case of triple emission studied with a Wilson chamber by Dee and Gilbert (1936) is that of

$$B^{10}+H^{2}\rightarrow He^{4}+He^{4}+He^{4}+18 \text{ Mev.}$$

When one of the multiple products of a reaction is a neutron, its continuous distribution of energy may also be studied from the recoil proton tracks. Neutrons from the following reactions have been investigated in this way:

$Li^{6}(dn)He^{4}$, He^{3}
$Li^{7}(dn)2He^{4}$
$B^{11}(dn)3He^{4}$

6. Application of Wilson Chamber in the Study of U Fission

The fission phenomenon has been studied in suitably designed Wilson chambers by Hahn and Strassman (1939), Joliot (1939), Corson and Thornton (1939), and Brostrom *et al.* (1940, 1941) and the explanation of the phenomenon attempted by Bohr (1940), Bohr *et al.* (1940, 1941), Lamb (1940, 1941), and others.

The apparatus used by Boggild, Brostrom, and Lauritsen (1940) consists of a 25-cm Wilson chamber filled with various gases (H_2 or A) at

low pressure (~5 cm air). The evaporated layers (0.2 mg/cm²) of U on mica foils mounted in the center of the Wilson chamber are bombarded with slow neutrons and the tracks of both fragments photographed. (See Fig. V-4.) The photograph is taken stereoscopically.*

Fission tracks differ from proton and alpha-tracks in the intensity of ionization, very frequent branching and irregular bending throughout the tracks. Owing to much higher mass and charge, nuclear collisions are a rule rather than an exception with fission tracks. The branches due to close nuclear collisions occur several times in each track instead of once in several thousand tracks (cf. α-rays). Less violent collisions result in nuclear scattering which is the cause of irregular gradual bending of the track. This phenomenon is also very rare with α-rays or protons whose stopping is caused by the interaction between the particles and the electrons.

A careful examination of the branches show that there are two groups of tracks corresponding to two kinds of fragments. The shorter range with two to three times as many branches as the other, corresponds to the heavier particle with greater mass and lower initial velocity. The mean ranges of the two groups are found to be 19 and 25 mm normal air.

Under suitable conditions the velocity of the fission fragment may be estimated. From the observed range of a branch the velocity of the A or O nuclei (responsible for the branch) may be estimated by using the range-velocity relation of Blackett and Lees (1931). If now the angle of branching is estimated, the velocity of the fission fragment may be obtained from the principles of conservation of momentum and energy. The range-velocity relation for fission fragments may also be obtained in the following way. Since the sum of the lengths of branches is proportional to the energy loss due to branching, a measurement of the total length of branches in different parts of the track gives a rough indication of the variation of velocity with range for fission fragments.

The range velocity relation for fission fragments is found to differ considerably from that of α-particles. This peculiarity has been explained by Bohr to be caused by frequent capture and loss of electrons. Taking a typical case where $M_1=133$, $Z_1=51$, $M_2=100$, and $Z_2=41$, we have $Q=170$ Mev, $Q_1=73$ Mev, and $Q_2=97$ Mev. This has also been confirmed by the ionization chamber experiments of Jenstchke and Prankal (1939) who found that the two fragments produce 2.80×10^6 and 1.70×10^6 ion pairs in air. As the energy required on the average per ion pair is about 35 ev, the energy of the ionizing particles comes out to be 98 and 60 Mev.

Since $Q_1=\frac{1}{2}MV_1^2$ we can easily see that $V_1=10.6\times10^8$ cm/sec. $=4.85c\alpha$ and $V_2=14\times10^8$ cm/sec. $=6.5c\alpha$, where $\alpha=2\pi e^2/ch=$Sommerfeld constant and $c\alpha$ is the velocity with which the electron travels in the first Bohr orbit.

The velocities with which the ions are hurled are comparable to the orbital velocities of the inner electrons of the atoms Z_1 and Z_2, in fact they are several times larger than that of the outermost electrons. Owing to this fact, the ions will start as stripped atoms, i.e., they will have shed off many of their orbital electrons. Bohr assumes that they shed all such outer electrons whose orbital velocity $\leqslant V_1$. Taking $Z_1=51$ it is possible that all O, and some N electrons are lost and for $Z_1=41$ all O, N, and some M electrons are lost.

The ions therefore start with a high net charge (Z_1-p_1), (Z_2-p_2), where p_1 and p_2 are the numbers of electrons lost ($p_1=10$, $p_2=14$). Their ionizing power is therefore much larger than that of α-particles which start with $Z=2$.

In the case of α-particles any electron that is captured will have an orbital velocity less than the α-velocity and the probability of electron capture is much less than that of subsequent loss. The α-particle therefore travels stripped of electrons to the very end of its range. With these assumptions Bohr obtains for the ratio between the ranges of a fission fragment and of an α-particle of the same initial velocity V_1

$$R_F/R_\alpha=5\frac{M_1}{z_1^{\frac{2}{3}}}\left(\frac{V_0}{V_1}\right)^2, \qquad (5.13)$$

where $V_0=e^2/\hbar$ is the velocity of electrons in the hydrogen atom. For the same velocity the lighter fragment will have smaller range.

* See Boggild, Brostrom, and Lauristen, Phys. Rev. **59**, 276 (1941).

This relation which is found to be in agreement with experimental results is not applicable to the end portion of the range because nuclear interaction is more important there and causes a very rapid decrease in the velocity.

7. Application of Wilson Chamber in the Study of Cosmic Rays

Skobelzyn (1927) appears to be the first man who photographed a cosmic-ray track in a Wilson chamber. His chamber was placed with its axis vertical in a magnetic field the axis of the camera being parallel to the magnetic field. Since 1927, a large number of workers have used the cloud chamber for investigating cosmic rays, and the technique has been vastly improved. The latest forms of the counter-controlled and random expansion chambers for the study of cosmic rays and their mode of operation have already been described (Chapter II, Sections 3 and 4). We have also discussed in detail how from a measurement of the specific ionization, range, momentum loss, and curvature of a cosmic-ray track, it is possible to know about the charge, mass, and energy of the particle to which the track is due, or in other words, to identify the particle (Chapter IV, Section 4).

By use of this method of identification the positron or the positive electron was first discovered by Anderson (1932), directly from Wilson chamber photographs of cosmic rays in which a lead plate was inserted across the chamber as a barrier to the rays and a magnetic field was used to measure the momentum of the particle. From the curvature above and below the plate it was possible to determine the direction of motion of the particle and hence the sign of the charge. It was found to be equal in magnitude but opposite in sign to that of the electron.

The presence of another fundamental particle in the cosmic rays was also similarly detected from cloud-chamber studies by Neddermeyer and Anderson (1937). Measurement of magnetic curvature, specific ionization, and range showed that some of the cosmic-ray tracks could only be caused by particles whose charge is equal to that of electrons and mass intermediate between those of electrons and protons. The first estimate of its mass was made by Street and Stevenson (1937)

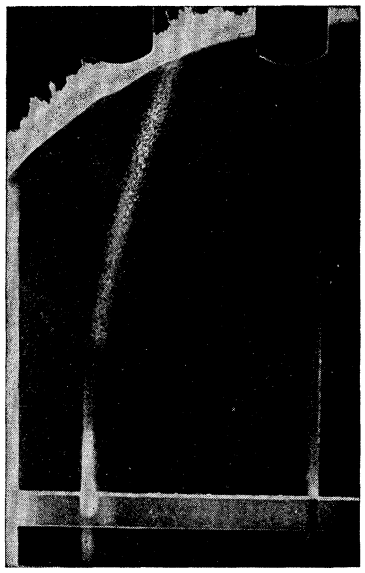

FIG. V-5. Track of particle of intermediate mass.

(see Fig. V-5) and later by many workers including Nishina *et al.*, Ehrenfest, Corson and Brode, Williams and Pickup, and Neddermeyer and Anderson [see report by Peierls (1939)].

Some other cosmic-ray observations seem to indicate that this newly discovered particle named meson or mesotron is unstable and disintegrates after a short life into an electron and a neutrino. The instability of the mesotron which is a factor of primary importance in the theory of nuclear forces is only indirectly evident from counter experiments. However, a few instances in which a mesotron has been caught at the end of its range inside a Wilson cloud chamber and an electron is found to originate where the mesotron track ends, confirms the truth of this idea [Williams and Roberts (1940), and Shutt, *et al.* (1942)].

The energy spectrum of cosmic-ray electrons and mesotrons has been studied with the help of a cloud chamber by Kunze (1933a, 1933b), Anderson (1933), Blackett (1936), Williams (1939b), Jones (1939), and Hughes (1940). A statistical survey of the cloud-chamber data indicates an excess of positive particles [Hughes (1940)] over the negatives, the reason for which is not yet quite clear.

Scattering of the cosmic-ray mesotrons has been studied by Blackett and Wilson (1938),

Wilson (1940), and Code (1941). A thick absorber in which scattering is to be investigated is placed within the chamber. Then from the direction of the track above and below the plate the scattering angle may be measured. If a high magnetic field is used in conjunction, variation of scattering with the energy of the particle may be obtained.

Blackett and Occhialini (1933), Anderson (1933), Anderson and Neddermeyer (1936), and several other workers later on have studied with a Wilson chamber the complicated shower phenomenon produced by high energy cosmic electrons, positrons, and photons in their passage through matter.

Occasionally photographs are obtained in which a shower is found to originate from a metal plate placed across the chamber without any incident particle being apparently present. These are cases of shower production by photons [Auger and Ehrenfest (1937)]. From the number of shower particles produced, it is possible to form an idea of the energy of the incident photon. Street and Stevenson and Fussel and Street obtained remarkable photographs of the growth of showers by placing several sheets of Pb one below the other in a cloud chamber [see Froman and Stearns (1938) and Hazen (1944a)]. The photographs show clearly how starting with a single cosmic particle, the number of shower particles increases, reaches a maximum and finally diminishes, as demanded by theories.

The electron showers sometimes rise to the magnitude of large bursts containing many thousands of particles. Sometimes these bursts cover an area of 300 ft. across; the energy required to initiate such a burst may be as great as 10^{16} ev. Cloud-chamber photographs of cosmic-ray bursts have been obtained by Fussel and Street [see Froman and Stearns (1938)], Anderson and Neddermeyer (1936), Sinha (1943), and also by many other observers.

Though the mesotrons cannot produce cascade showers Bhabha (1938) pointed out that a mesotron may release an electron from an atom by a direct collision, and this electron may subsequently initiate a shower. Such showers known as knock-on showers, have been investigated by Wilson (1938), Lovell (1939), Trumpy (1939), Seren (1942), and Hazen (1943). The results of their investigations show satisfactory agreement with the theory developed by Bhabha.

The cloud chamber is unique in such investigations in the fact that it enables a study of the phenomena in three dimensions. Simultaneously with the measurement of the direction of emission of the shower particles, a cloud-chamber photograph gives information regarding the nature and the energy of the particles from their ionization, range, further multiplication, etc. Such studies have brought to light many rarer types of showers, explosions, and atomic disintegrations produced by cosmic rays [see Anderson (1936), Brode, *et al.* (1936), Auger, *et al.* (1937), Powell (1940 and 1942), Herzog (1941), Bostic (1942), Nielsen and Powell (1943), and Hazen (1944)]. Experiments with light weight chambers carried in aeroplanes indicate that the number of slow mesotrons, protons, neutrons, and other possible atomic disintegration products increases rapidly with height. It is not possible without large uncertainty to identify these particles. Some of these tracks show δ-rays along their path. It is possible to determine from the number of δ-rays per cm of path, the velocity of the particle producing the δ-rays. Then from the range and velocity of the particle its nature can be guessed. It has thus been found that some of the heavy tracks belong to alpha-particles which have been produced in the nuclear disintegrations. But the nature of the primary particles remains still unknown.

The mechanism as to how the mesotrons are produced is still a mystery. High altitude cloud-chamber photographs of Herzog (1941), Herzog and Bostick (1941), Bostick (1942), Janossy (1943), Hazen (1944a), and Bose, *et al.* (1944) show that sometimes more than one mesotron starts from the same point. Bostick (1942) concludes from the angular distribution of the slow mesotrons that these are not produced by nuclear evaporation. Janossy (1943) suggests that the mesotrons might be produced by a proton colliding several times inside the same nucleus, with the nucleon, while Hamilton, Heitler, and Peng (1943) put the suggestion that the mesotrons are produced by a cascade nuclear process. But Hazen's (1944a) observations lend no support to

the theory of cascade production of mesotrons while Bose (1944) has recorded a cascade production of a mesotron. Rossi *et al.* (1940) having controlled a chamber by an anti-coincidence circuit tried to obtain evidence of the production of mesotrons by neutral particles in cosmic radiation. But they obtained a negative result.

The cloud chamber thus has been instrumental in solving many riddles of cosmic-ray research. Two of the fundamental particles of nature owe their discovery to cloud-chamber technique. It has yet to solve the problem of production of mesotrons and the nature of the primary cosmic rays. Who knows that the investigation of cosmic rays with the cloud chamber will not again add to our present knowledge of fundamental particles and unravel the mysteries of the primary cosmic rays.

CHAPTER VI. APPENDIX

1. Vapor Pressure of Ethyl Alcohol and Water at Different Temperatures and Composition of the Mixture

TABLE VI-1. Vapor pressures of water and ethyl alcohol at different temperatures (from Landolt and Bornstein's *Phys. Chem. Tabellen*).

Temperature in degree centigrade	Pressure in mm Hg		Temperature in degree centigrade	Pressure in mm Hg	
	Water	Ethyl alcohol		Water	Ethyl alcohol
			5	6.54	17.70
35	42.188		4	6.01	16.62
30	31.834	78.41	3	5.68	15.69
28	28.35	70.09	2	5.29	14.60
25	23.76	59.03	1	4.92	13.65
24	22.38	55.70	0	4.58	12.73
23	21.07	52.54	−1	4.25	
22	19.83	49.54	−2	3.95	
21	18.65	46.69	−2.8		9.49
20	17.54	44.00	−3.0	3.67	
19	16.48	41.45	−4.0	3.40	
18	15.48	39.05	−5.0	3.16	
17	14.53	36.77	−6.0	2.93	
16	13.64	34.62	−7.0	2.71	
15	12.79	32.60	−8.0	2.51	
14	11.99	30.69	−9.0	2.32	
13	11.23	28.89	−10.0	2.14	6.47
12	10.52	27.19	−10.6		5.20
11	9.84	25.59	−11.0	1.98	
10	9.21	24.08	−12.0	1.83	
9	8.61	22.66	−13.0	1.68	
8	8.05	21.31	−16.5		3.23
7	7.51	20.04	−24.6		1.72
6	7.01	18.84			

TABLE VI-2. Vapor pressure of ethyl alcohol and water at different compositions of the liquid mixture.*

Weight percent of ethyl alcohol in the mixture	Partial vapor pressure in mm Hg at 20°C		40°C	
	Water	Ethyl alcohol	Water	Ethyl alcohol
0	17.5	0.0	54.3	0.0
10	16.8	6.7	51.6	26.9
20	15.9	12.6	47.6	43.5
30	15.1	17.1	46.2	54.7
40	14.7	20.7	45.5	62.5
50	14.5	23.5	44.6	68.2
60	14.1	25.6	42.9	74.8
70	13.1	28.0	40.5	82.8
80	11.3	31.2	35.9	91.8
90	7.5	35.8	24.7	106.4
98	1.9	42.4	6.5	123.0
100	0.0	43.6	0.0	134.0

* The $\log p_{\text{water}}$ or $\log p_{\text{alcohol}}$ for any given composition is a linear function of $1/(t+273.1)$ between any two values in the above table.

TABLE VI-3. Values of D_p/c_v.

Substance	$\gamma=c_p/c_v$	Substance	$\gamma=c_p/c_v$
Air	1.401	Methyl alcohol	1.256
Argon	1.667	Ethyl alcohol	1.133
CO_2	1.300	Water vapor	1.305

2. Energy, Range, Velocity, $H\rho$ Relationships for Electrons, Protons, and α-Particles

TABLE VI-4. Energy, range, velocity, and magnetic curvature for electrons.

β	p/Mc or $\beta/(1-\beta^2)^{\frac{1}{2}}$	Energy in 10^6 ev	$H\rho$ in 10^5 gauss-cm	Range in cm air at 76 cm 15°C	Range in g/cm² Al
0.10	0.1005	0.00257	0.00171	0.04	0.00005
0.15	0.1517	0.00584	0.00258		
0.20	0.2042	0.01053	0.00348	0.23	0.00027
0.25	0.2582	0.01675	0.00440		
0.30	0.3145	0.02466	0.00536	1.00	0.0012
0.35	0.3736	0.03448	0.00636		
0.40	0.4364	0.04652	0.00743	3.40	0.0041
0.45	0.5039	0.06117	0.00858		
0.50	0.5773	0.07900	0.00893	7.3	0.0087
0.525	0.6168	0.08934	0.01051		
0.550	0.6585	0.1008	0.01122		
0.575	0.7276	0.1135	0.01197		
0.600	0.750	0.1277	0.01278	17.9	0.0215
0.625	0.800	0.1435	0.01365		
0.650	0.8554	0.1613	0.01458		
0.675	0.915	0.1815	0.01559		
0.700	0.980	0.2044	0.01670	37.5	0.045
0.725	1.052	0.2308	0.01793		
0.750	1.134	0.2614	0.01931		
0.775	1.23	0.2984	0.02089		

TABLE VI-4. *Continued.*

β	p/Mc or $\beta/(1-\beta^2)^{\frac{1}{2}}$	Energy in 10^9 ev	$H\rho$ in 10^5 gauss-cm	Range in cm air at 76 cm 15°C	Range in g/cm² Al
0.800	1.33	0.3404	0.02271	83.0	0.10
0.810	1.38	0.3602	0.02353		
0.820	1.43	0.3816	0.02440		
0.830	1.49	0.4049	0.02535		
0.840	1.55	0.4305	0.02637		
0.850	1.61	0.4587	0.02749		
0.860	1.69	0.4901	0.02871		
0.870	1.77	0.5251	0.03006		
0.880	1.85	0.5645	0.03156		
0.890	1.95	0.6093	0.03325		
0.900	2.06	0.6609	0.03517	217.0	0.26
0.910	2.195	0.7230	0.03739		
0.920	2.34	0.7923	0.03999		
0.930	2.53	0.8787	0.04310		
0.940	2.76	0.9861	0.04693		
0.950	3.04	1.125	0.05182	437.0	0.525
0.960	3.43	1.313	0.05842		
0.970	3.98	1.590	0.06797		
0.980	4.93	2.056	0.08389	860.0	1.03
0.990	7.018	3.109	0.11950	1300.0	1.57
0.995	9.962	4.602	0.16970		
0.996	11.147	5.204	0.19060		
0.997	12.881	6.087	0.21940		
0.998	15.788	7.568	0.26890		
0.999	22.344	10.911	0.38060		

TABLE VI-5. Energy, range, and velocity relation for protons.

V_0 in 10^9 cm/sec.	$\beta^2\times10^3$	p/Mc or $\beta/(1-\beta^2)^{\frac{1}{2}}$	Energy in 10^6 ev	$H\rho$ in 10^5 gauss-cm	Range in cm air at 76 cm, 15°C
1.0	1.113	0.03334	0.522	1.044	0.8
1.2	1.602	0.04005	0.753	1.253	1.4
1.4	2.181	0.04675	1.025	1.463	2.3
1.6	2.849	0.05343	1.340	1.673	3.6
1.8	3.605	0.06014	1.697	1.883	5.3
2.0	4.451	0.0668	2.095	2.093	7.5
2.2	5.386	0.0737	2.536	2.304	10.4
2.4	6.410	0.0804	3.021	2.514	14.0
2.6	7.523	0.0872	3.649	2.725	18.4
2.8	8.724	0.0938	4.120	2.936	23.9
3.0	10.015	0.1008	4.734	3.148	30.4
3.2	11.395	0.1077	5.391	3.360	38.2
3.4	12.863	0.1142	6.092	3.573	47.4
3.6	14.422	0.1212	6.838	3.786	58.2
3.8	16.068	0.1280	7.628	4.000	70.5
4.0	17.804	0.1350	8.463	4.214	84.8
4.2	19.629	0.1420	9.343	4.428	101.3
4.4	21.543	0.1482	10.270	4.643	119.9
4.6	23.547	0.1558	11.240	4.858	140.8
4.8	25.638	0.1622	12.250	5.075	164.6
5.0	27.819	0.1690	13.310	5.293	191.1

TABLE VI-6. Energy, range, and velocity relation for α-particles.

Velocity in 10^9 cm/sec.	$\beta^2\times10^3$	p/Mc or $\beta/(1-\beta^2)^{\frac{1}{2}}$	Energy in 10^6 ev	$H\rho$ in 10^5 gauss-cm	Range in cm air at 760 mm 15°C
0.75	0.626	0.0249	1.167	1.555	0.55
0.80	0.712	0.0266	1.328	1.659	0.62
0.85	0.804	0.0282	1.499	1.763	0.70
0.90	0.901	0.030	1.681	1.867	0.80
0.95	1.004	0.0316	1.873	1.971	0.91
1.00	1.113	0.0332	2.075	2.074	1.04
1.05	1.227	0.0348	2.288	2.178	1.18
1.10	1.346	0.0366	2.511	2.282	1.32
1.15	1.471	0.0382	2.745	2.386	1.48
1.20	1.602	0.0398	2.989	2.490	1.67
1.25	1.739	0.0415	3.244	2.594	1.87
1.30	1.881	0.0432	3.509	2.698	2.09
1.35	2.028	0.0447	3.785	2.802	2.33
1.40	2.181	0.0464	4.071	2.906	2.58
1.45	2.340	0.0480	4.368	3.010	2.86
1.50	2.504	0.0497	4.674	3.114	3.17
1.55	2.673	0.0515	4.991	3.218	3.50
1.60	2.849	0.0531	5.319	3.322	3.85
1.65	3.029	0.0548	5.658	3.426	4.24
1.70	3.216	0.0565	6.008	3.530	4.65
1.75	3.408	0.0581	6.367	3.635	5.09
1.80	3.605	0.0598	6.737	3.739	5.57
1.85	3.808	0.0614	7.117	3.843	6.08
1.90	4.017	0.0632	7.508	3.947	6.62
1.95	4.231	0.0648	7.910	4.052	7.20
2.00	4.451	0.0666	8.322	4.156	7.82
2.05	4.677	0.0681	8.745	4.260	8.48
2.10	4.907	0.0700	9.178	4.365	9.18
2.15	5.144	0.0714	9.622	4.469	9.92
2.20	5.386	0.0730	10.077	4.574	10.71
2.25	5.633	0.0749	10.543	4.678	11.54
2.30	5.887	0.0765	11.018	4.783	12.42
2.35	6.145	0.0780	11.504	4.888	13.43
2.40	6.410	0.0800	12.001	4.992	14.32
2.45	6.680	0.0821	12.508	5.137	15.35
2.50	6.955	0.0831	13.027	5.202	16.44

3. Specific Ionization, Range, and Momentum Loss as a Function of the Velocity of the Particle

(a) *Specific Ionization*

The average rate of dissipation of energy through ionization and excitation by a fast primary particle of mass M, velocity $V=\beta c$, and charge ze is given by the following relation [see Rossi and Greisen (1941)]

$$\left(-\frac{dE}{dx}\right)_{\text{ion}}=\frac{2\pi ne^4z^2}{mV^2}\times\left\{\ln\frac{2mV^2T_m}{I^2(1-V^2/c^2)}-2\frac{V^2}{c^2}\right\},\quad(6.01)$$

where n = number of electrons per cm^3 of the stopping material, I = mean excitation energy of these electrons = $11.5Z$ or 82.6 ev for air [see Wilson (1941)], and T_m = maximum kinetic energy that may be transferred to an electron in elastic impact. The mass of the primary particle enters only in T_m, otherwise the energy loss is independent of the mass of the primary particle.

T_m may be deduced from the principles of the conservation of energy and momentum. If T be the kinetic energy of the electron after collision with a primary of the total energy E, then from the principle of conservation of energy, we have

$$(E-T)^2=E_r^2=(p_rc)^2+M^2c^4, \qquad (6.02)$$

where E_r and p_r are the residual energy and momentum of the primary particle after transfer of energy T to the electron. p_r may be deduced from the principle of conservation on momentum, and we have

$$p_r^2c^2=p_e^2c^2+p^2c^2-2pc\cos\theta p_ec, \qquad (6.03)$$

where p_e is the momentum of the electron after collision and θ the angle between the direction of emission of the electron and the trajectory of the primary particle.

Eliminating p_r and expressing p_e in terms of the kinetic energy T of the electron, we get

$$T(E+mc^2)=pc\cos\theta[T(T+2mc^2)]^{\frac{1}{2}}. \qquad (6.04)$$

After simplification

$$T=2mc^2\frac{p^2c^2\cos^2\theta}{(E+mc^2)^2-p^2c^2\cos^2\theta} \qquad (6.05)$$

and

$$T_m=2mc^2\frac{p^2c^2}{m^2c^4+M^2c^4+2Emc^2}. \qquad (6.06)$$

If now $M\gg m$, and $E\ll(\frac{1}{2}M/m)\cdot Mc^2$

$$T_m=2mc^2\frac{p^2}{M^2c^2}=2mc^2\frac{\beta^2}{(1-\beta^2)}. \qquad (6.07)$$

The critical energy E_c below which the relation (6.07) holds, is 10^{10} ev for a mesotron of mass 200 and 10^{12} ev for a proton. Hence for all practical purposes T_m is given by Eq. (6.07), and T_m is independent of the mass of the primary particle and is a function of the viscosity only.

Substituting the value of T_m from (6.07) in (6.01) we have

$$-\frac{dE}{dx}=\frac{4\pi ne^4z^2}{m\beta^2c^2}\left\{\ln\frac{2m\beta^2c^2}{I(1-\beta^2)}-\beta^2\right\}. \qquad (6.08)$$

For air $n=3.9\times10^{20}$, $I=82.6$ ev [see Wilson (1941)], and assuming $z=1$, we get after substituting the numerical values

$$-\frac{dE}{dx}=\frac{2\times10^2}{\beta^2}\left\{9.43+2\ln\frac{\beta}{(1-\beta^2)^{\frac{1}{2}}}-\beta^2\right\}$$

in ev per cm air. (6.09)

In Table VI-7 the calculated values of $-dE/dx$ are given for different values of p/Mc or $\beta/(1-\beta^2)^{\frac{1}{2}}$.

The calculated values of the energy loss are valid for all particles for which the radiation loss may be neglected. These values are shown plotted in Fig. IV-4 as curve 1, and this curve may be used to determine the mass of an unknown heavy particle from a measurement of the ionization produced (see Chapter IV, Section 4).

(*b*) *Calculation of Range as a Function of* p/Mc.

In Table VI-8 are collected the values of $Rz^2/(M/m)$ against p/Mc or $\beta/(1-\beta^2)^{\frac{1}{2}}$. The first nine values are taken from the curve given by Livingston and Bethe (1937) and are based on the experimental range determination of α-particles and protons. To obtain the range of a high energy cosmic particle as a function of its energy we have used the following approximate calculation by Euler and Heisenberg (1938).

We neglect the slow variation of dE/dx with $\log\beta/(1-\beta^2)^{\frac{1}{2}}$ in Eq. (6.08) and put approximately

$$-dE/dx=az^2/\beta^2, \qquad (6.10)$$

where $a=2.5\times10^3$ ev per cm air. Then we have

$$R=\int\frac{dE}{-dE/dx}=\frac{1}{z^2a}\int\beta^2dE. \qquad (6.11)$$

Since $E^2=p^2c^2+M^2c^4$, we have

$$dE=\frac{pc^2}{E}dp=\beta cdp. \qquad (6.11')$$

TABLE VI-7. Values of $-dE/dx$ as function of p/Mc.

p/Mc or $\beta/(1-\beta^2)^{\frac{1}{2}}$	$-dE/dx$ in 10^3 ev per cm air
0.126	45.2
0.18	25.9
0.255	14.8
0.315	10.8
0.366	8.7
0.411	7.4
0.60	4.68
0.894	3.28
1.15	2.83
1.39	2.69
1.61	2.52
2.68	2.41
4.74	2.49

Hence

$$R=\frac{c}{z^2a}\int_0^p \beta^3 dp=\frac{c}{z^2a}\int_0^p \frac{p^3dp}{(p^2+M^2c^2)^{\frac{3}{2}}}$$
$$=\frac{c}{z^2a}\left[\frac{2M^2c^2+p^2}{(M^2c^2+p^2)^{\frac{1}{2}}}\right]_0^p$$
$$=\frac{Mc^2}{z^2a}\left[\frac{2+(p/Mc)^2}{[1+(p/Mc)^2]^{\frac{1}{2}}}-2\right]. \quad (6.12)$$

The values of $Rz^2/(M/m)$ have been plotted in Fig. IV-4 against $\beta/(1-\beta^2)^{\frac{1}{2}}$. These values may be used for the determination of the mass of an unknown particle (see Chapter IV, Section 4).

(c) *Calculation of $d(H\rho)/dx$ as a Function of $\beta/(1-\beta^2)^{\frac{1}{2}}$*

From the calculated values of dE/dx, $d(H\rho)/dx$ as function of $\beta/(1-\beta^2)^{\frac{1}{2}}$ may be easily obtained with the help of Eq. (4.22). The values calculated for lead in this way are given in Table VI-9.

From the measured values of the rate of change of curvature when a particle penetrates a lead plate placed across a cloud chamber, the mass of the particle can be determined. For examples of the use of this method see Chapter IV, Section 4.

Table VI-8. Values of $Rz^2/(M/m)$ as function of p/Mc.

p/Mc or $\beta/(1-\beta^2)^{\frac{1}{2}}$	$Rz^2/(M/m)$ R expressed in cm air N.T.P.	Remarks
0.02	0.05×10^{-2}	From Livingston and Bethe (1937)
0.04	0.10	
0.06	0.275	
0.08	0.70	
0.10	1.60	
0.12	3.0	
0.14	5.25	
0.16	8.40	
0.18	12.35	
0.25	21.00×10^{-2}	From Euler and Heisenberg's approximate formula
0.30	41	
0.35	61	
0.40	102	
0.45	183	
0.50	265	

4. Gamma-Ray Equations for Compton Scattering

The elementary theory of Compton effect is well known. Let $h\nu$, $h\nu'$ be the energies of the incident and scattered quanta and θ and ϕ the angles which the scattered quantum and recoil electron make with the direction of the primary quantum.

$$h\nu=h\nu'+mc^2\left(\frac{1}{(1-\beta^2)^{\frac{1}{2}}}-1\right), \quad (6.13)$$

$$\frac{h\nu}{c}=\frac{h\nu'}{c}\cos\theta+\frac{m\beta c}{(1-\beta^2)^{\frac{1}{2}}}\cos\phi, \quad (6.14)$$

$$0=\frac{h\nu'}{c}\sin\theta-\frac{m\beta c}{(1-\beta^2)^{\frac{1}{2}}}\sin\phi. \quad (6.15)$$

If

$$h\nu/mc^2=\gamma, \quad h\nu'/mc^2=\gamma_1,$$
$$1/(1-\beta^2)^{\frac{1}{2}}-1=T/mc^2=\gamma_2; \quad (6.16)$$

$$\left.\begin{aligned}\gamma&=\gamma_1+\gamma_2;\\ &=\gamma_1\cos\theta+(\gamma_2^2+2\gamma_2)^{\frac{1}{2}}\cos\phi;\\ &=\gamma_1\sin\theta-(\gamma_2^2+2\gamma_2)^{\frac{1}{2}}\sin\phi.\end{aligned}\right\} \quad (6.17)$$

TABLE VI-9. Values of $d(H\rho)/dx$ in lead as function of p/Mc.

p/Mc or $\beta/(1-\beta^2)^{\frac{1}{2}}$	β	$d(H\rho)/dx$ in gauss-cm per cm lead
0.3	0.288	8.33×10^5
0.4	0.372	4.33
0.5	0.449	2.71
0.6	0.515	1.91
0.7	0.574	1.45
0.8	0.625	1.15
0.9	0.667	0.94
1.0	0.706	0.80
1.1	0.739	0.72
1.2	0.768	0.67
1.3	0.793	0.62
1.4	0.814	0.56
1.5	0.832	0.545
1.6	0.848	0.543
1.8	0.874	0.542

Eliminating ϕ, γ_2 between three equations

$$\gamma_1=\frac{\gamma}{1+\gamma(1-\cos\theta)}, \tag{6.18}$$

$$\gamma_2=\frac{\gamma^2(1-\cos\theta)}{1+\gamma(1-\cos\theta)}$$

$$=\frac{2\gamma^2}{1+2\gamma+(1+\gamma)^2\tan^2\phi}, \tag{6.19}$$

$$\cot\phi=(1+\gamma)\tan(\theta/2). \tag{6.20}$$

While θ varies from 0–180°, ϕ changes from 90° to 0°. As ϕ changes from 90° to 0°, the energy imparted to the electron varies from 0 to a maximum of $2\gamma^2/(1+2\gamma)$, i.e., a fraction $2\gamma/(1+2\gamma)$ of the energy of the incident quantum. At small values of γ very little energy goes to the electron.

The differential cross section for the deflection of a quantum between θ and $\theta+d\theta$ per unit solid angle per electron is given by

$$\sigma(\gamma\theta)=\frac{r_0^2}{2}\frac{(1+\cos^2\theta)}{\{1+\gamma(1-\cos\theta)^2\}}$$

$$\times\left\{1+\frac{\gamma^2(1-\cos\theta)^2}{(1+\cos^2\theta)}\frac{1}{1+\gamma(1-\cos\theta)}\right\}, \tag{6.21}$$

where

$$r_0=e^2/mc^2.$$

The differential cross section for emission of Compton electrons in the direction ϕ, per unit solid angle per electron is given by

$$\sigma(\epsilon\phi)=\frac{[2(1+x)]^{\frac{1}{2}}}{\pi}\frac{32r_0^2(1+\gamma)^2}{\{\gamma^2+4\gamma+2-\gamma^2\cos 2\phi\}^2}$$

$$\times\left[1+\frac{2(1+\cos 2\phi)}{(\gamma^2+2\gamma+2)-(\gamma^2+2\gamma)\cos 2\phi}\right.$$

$$\times\left\{\frac{\gamma^2(1+\cos 2\phi)}{\gamma^2+4\gamma+2-\gamma^2\cos 2\phi}\right.$$

$$\left.\left.-\frac{(\gamma+1)^2(1-\cos 2\phi)}{\gamma^2+2\gamma+2-(\gamma^2+2\gamma)\cos 2\phi}\right\}\right]. \tag{6.22}$$

Figure VI-1 gives $\sigma(\epsilon\phi)$ against E_ϕ for $\gamma=5$, i.e., $h\nu=2.5\times10^6$ ev. Corresponding to $\phi=0$, $\sigma(\epsilon\rho)$ and E_ϕ are both maximum, and energy of the electron is then given by

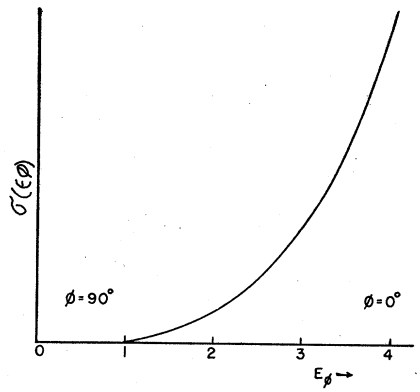

FIG VI-1. Differential cross section for emission of Compton electrons against E_ϕ for $h\nu=2.5\times10^6$ ev.

$$(\gamma_2)_{\max}=\frac{2\gamma^2}{1+2\gamma}. \tag{6.23}$$

If the $H\rho$ value corresponding to this maximum energy is determined experimentally, then the energy of the quantum responsible for this recoil electron may be estimated.

$$\gamma=\frac{\gamma_2+(\gamma_2^2+2\gamma_2)^{\frac{1}{2}}}{2}. \tag{6.24}$$

$$T=E-mc^2=[(eH\rho)^2+m^2c^4]^{\frac{1}{2}}-mc^2$$

or

$$\gamma_2+1=[(eH\rho/mc^2)^2+1]^{\frac{1}{2}}$$

or

$$\gamma_2(\gamma_2+2)=(eH\rho/mc^2)^2=y^2 \text{ (say)}.$$

From Eq. (6.24)

$$\gamma=\frac{(y^2+1)^{\frac{1}{2}}-1+y}{2}, \quad \text{where} \quad y=\frac{eH\rho}{mc^2}. \tag{6.25}$$

In Table VI-10 we have listed the values of $H\rho$ of the emitted electron in gauss-cm and the corresponding energies of the electron and γ-rays in 10^6 ev. With the help of this table, the energy of the γ-ray quantum may be deduced from a measurement of the magnetic curvatures of the Compton electrons released by it.

BIBLIOGRAPHY AND ACKNOWLEDGMENTS

References to those papers and general works mentioned in the text are given in the following

pages. While it is not exhaustive, it contains references to representative articles on all aspects of cloud-chamber work. Certain papers from which experimental facts have been used but are not referred to explicitly in the text have also been included. Indeed the Wilson chamber technique has been used so extensively in so many different laboratories of the world and the results obtained are so numerous that the writers regret that with the limited space and time at their disposal they have not been able to do full justice to all workers in this field.

In the preparation of this report the writers have drawn freely from the general references and the papers published in various scientific journals mentioned in the text. Most of the diagrams have been reproduced from the originals published in these journals and reference works. The writers wish to acknowledge their indebtedness to the writers of these various papers.

In conclusion it gives a great pleasure to the authors to express their sincere thanks to Professor M. N. Saha, F.R.S. for his valuable discussions and assistance in writing parts of the report. They are also indebted to Dr. D. M. Bose, Director, Bose Research Institute, to the members of the Palit Laboratory in Physics, Calcutta University, for many useful criticisms and suggestions, and to Professors P. Kirkpatrick and L. Marton of Stanford University for help in the correction of proofs.

TABLE VI-10. Values of $H\rho$ of the electron and corresponding energies of the electron and γ-ray.

$H\rho$ in 10^3 gauss cm	T in 10^6 ev	γ-ray energy in 10^6 ev
1.00	0.08	0.19
1.50	0.17	0.309
2.00	0.28	0.436
2.50	0.40	0.570
3.00	0.52	0.710
3.50	0.65	0.850
4.00	0.80	0.99
4.50	0.93	1.14
5.00	1.08	1.28
5.50	1.22	1.43
6.00	1.37	1.57
6.50	1.51	1.72
7.00	1.65	1.86
7.50	1.80	2.01
8.00	1.95	2.16
8.50	2.09	2.31
9.00	2.24	2.46
9.50	2.31	2.60
10.00	2.53	2.76

References

J. Aitken, *Collected Scientific Papers 1880–1916* (Cambridge University Press, Cambridge, England, 1923).

T. Alper, "On the δ-rays and the range-velocity relation of slow electrons," Zeits. f. Physik **76**, 172 (1932).

C. D. Anderson, "Energies of cosmic-ray particles," Phys. Rev. **41**, 405 (1932).

C. D. Anderson, "Cosmic-ray negative and positive electrons," Phys. Rev. **44**, 406 (1933).

C. D. Anderson and S. H. Neddermeyer, "Cloud-chamber observations of cosmic rays at 4300 meters elevation and at sea level," Phys. Rev. **50**, 263 (1936).

P. Auger, "On composite photoelectric effect," J. de phys. et rad. **6**, 208 (1925).

P. Auger and P. Ehrenfest, "Counter controlled cloud-chamber results at different altitudes," J. de phys. et rad. **6**, 285 (1935).

P. Auger and P. Ehrenfest, "Showers produced by cosmic rays," J. de phys. et rad. **8**, 204 (1937).

R. H. Bacon, E. N. Grisewood, and C. W. Merwe, "The Radioactivity of Mn^{56} and I^{128}," Phys. Rev. **59**, 531 (1941).

F. Barendengt and G. F. Sizoo, "Cloud chamber with electrical automatic control," Physica **6**, 1077 (1939).

H. Bauer, "Portable Wilson cloud chamber," Physik. Zeits. **37**, 627 (1936).

J. A. Bearden, "Wilson chamber with an increased time of sensitivity," Rev. Sci. Inst. **6**, 256 (1935).

C. Beck, "Optimum liquid combination for cloud chamber," Rev. Sci. Inst. **12**, 602 (1941).

R. A. Becker, W. A. Fowler, and C. C. Lauritsen, "Short range α-particles from flourine bombarded with protons," Phys. Rev. **62**, 186 (1942).

H. J. Bhabha, "On the theory of heavy electrons and nuclear forces," Proc. Roy. Soc. **166**, 501 (1938).

P. C. Bhattacharya, "A search for the double proton," Proc. Nat. Inst. Sci. Ind. **7**, 275 (1941).

P. M. S. Blackett, "On the analysis of α-ray photographs," Proc. Roy. Soc. **102**, 294 (1922).

P. M. S. Blackett, "The study of forked α-ray tracks," Proc. Roy. Soc. **103**, 62 (1923).

P. M. S. Blackett, "Ejection of protons from nitrogen nuclei," Proc. Roy. Soc. **107**, 349 (1925).

P. M. S. Blackett, "An automatic cloud chamber for the rapid production of α-ray photographs," J. Sci. Inst. **4**, 433 (1927).

P. M. S. Blackett, "On the automatic use of Wilson cloud chamber," J. Sci. Inst. **6**, 184 (1929)a.

P. M. S. Blackett, "Double camera for artificial disintegrations," Proc. Roy. Soc. **123**, 619 (1929)b.

P. M. S. Blackett, "On the collision loss of α-particles and *H*-particles," Proc. Roy. Soc. **135**, 132 (1932).

P. M. S. Blackett, "Technique of counter controlled Wilson chamber," Proc. Roy. Soc. **146**, 281 (1934).

P. M. S. Blackett, "The measurement of the energy of cosmic rays," Proc. Roy. Soc. **154**, 564 (1936).
P. M. S. Blackett, "Measurement of cosmic-ray energy spectrum," Proc. Roy. Soc. **159**, 1 (1937).
P. M. S. Blackett and R. Brode, "Curvature measurement and energy spectrum of cosmic rays," Proc. Roy. Soc. **154**, 573 (1936).
P. M. S. Blackett and D. S. Lees, "Range velocity relation of α-rays," Proc. Roy. Soc. **134**, 658 (1931).
P. M. S. Blackett and D. S. Lees, "The range velocity of recoil atoms," Proc. Roy. Soc. **134**, 658 (1932)a.
P. M. S. Blackett and D. S. Lees, "On the photography of artificial disintegration collision by α-rays," Proc. Roy. Soc. **136**, 325 (1932)b.
P. M. S. Blackett and G. P. S. Occhialini, "Some photographs of the tracks of penetrating radiations," Proc. Roy. Soc. **139**, 699 (1933).
P. M. S. Blackett and J. G. Wilson, "Energy loss of cosmic-ray particles in metal plates," Proc. Roy. Soc. **160**, 304 (1937).
P. M. S. Blackett and J. G. Wilson, "Scattering of cosmic-ray particles in matter," Proc. Roy. Soc. **165**, 290 (1938).
F. Bloch, "Stopping power of matter for swiftly moving charged particles," Ann. d. Physik **16**, 285 (1933)a.
F. Bloch, "Stopping power of atoms with several electrons," Zeits. f. Physik **81**, 363 (1933)b.
N. Bohr, "Successive transformations in nuclear fission," Phys. Rev. **58**, 864 (1940).
N. Bohr, J. K. Boggild, K. J. Brostrom, and T. Lauritsen, "Velocity range relation for fission fragments," Phys. Rev. **58**, 839 (1940).
N. Bohr, J. K. Boggild, K. J. Brostrom, and T. Lauritsen, "Velocity range relation for. fission fragments," Phys. Rev. **59**, 270 (1941).
T. W. Bonner, "Determination of the energy of neutrons," Phys. Rev. **59**, 237 (1941).
T. W. Bonner and W. M. Brubaker, "The disintegration of nitrogen by slow neutrons," Phys. Rev. **49**, 778 (1936)a.
T. W. Bonner and W. M. Brubaker, "Disintegration of Be, B, and carbon by deuterons," Phys. Rev. **50**, 308 (1936)b.
T. W. Bonner and L. M. Mott-Smith, "Energy spectrum of neutrons from the disintegration of F, B, and Be by α-particles," Phys. Rev. **46**, 258 (1934).
D. M. Bose, B. Chaudhuri, and M. Sinha, "Cosmic-ray meson spectra," Phys. Rev. **65**, 341 (1944).
W. H. Bostick, "Cloud-chamber photographs at 4300 meters altitude," Phys. Rev. **61**, 557 (1942).
H. Brinkman, "Continuously active cloud chamber," K. Akad. Amsterdam. Proc. **39**, 1185 (1939)a.
H. Brinkman, "Wilson chamber with several expansions per second," Physica **6**, 519 (1939)b.
R. B. Brode, "Specific ionization of high speed particles," Rev. Mod. Phys. **11**, 222 (1939).
R. B. Brode, H. G. Macpherson, and M. A. Starr, "The heavy particle component of cosmic radiation," Phys. Rev. **50**, 587 (1936).
K. J. Brostrom, J. K. Boggild, and T. Lauritsen, "Cloud-chamber studies of fission fragment track," Phys. Rev. **58**, 651 (1940).
K. J. Brostrom, J. K. Boggild, and T. Lauritsen, "Range and straggling of fission fragments," Phys. Rev. **59**, 275 (1941).
W. M. Brubaker and T. W. Bonner, "Automatic high pressure Wilson cloud chamber," Rev. Sci. Inst. **6**, 143 (1935).
J. Chadwick, N. Feather, and Davies, Proc. Camb. Phil. Soc. **30**, 357 (1934).
J. Chadwick, N. Feather, and E. Bretscher, "Range, angle, projection of protons from photo-disintegration of deuterium," Proc. Roy. Soc. **163**, 366 (1937).
F. C. Champion, "The distribution of energy in the β-ray spectrum of RaE," Proc. Roy. Soc. **134**, 672 (1932)a.
F. C. Champion, "On some close collisions of fast β-particles with electrons photographed by expansion method," Proc. Roy. Soc. **136**, 631 (1932)b.
F. C. Champion, "Scattering of fast β-particles by nitrogen nuclei," Proc. Roy. Soc. **153**, 353 (1936).
F. L. Code, "Scattering of mesotrons in tungsten," Phys. Rev. **59**, 229 (1941).
D. R. Corson and R. B. Brode, "The specific ionization and mass of cosmic-ray particles," Phys. Rev. **53**, 773 (1938).
D. R. Corson and R. L. Thornton, "Disintegration of uranium," Phys. Rev. **55**, 509 (1939).
Coulier, J. de Pharm. et de Chimie **22**, 165 (1875).
H. R. Crane, "Cloud chamber for nuclear disintegration studies," Rev. Sci. Inst. **8**, 440 (1937).
H. R. Crane, "New experimental evidence for a neutrino," Phys. Rev. **53**, 789 (1938).
H. R. Crane, E. R. Gaerttner, and J. J. Turin, "A cloud-chamber study of the Compton effect," Phys. Rev. **50**, 302 (1936).
H. R. Crane and O. H. Halpern, "Experiments on the recoil of nucleus in β-decay," Phys. Rev. **56**, 232 (1939).
M. Curie, "Distribution of α-ray ranges," J. de phys. et rad. **4**, 170 (1923).
I. Curie and F. Joliot, "Penetrating radiation," J. de phys. et rad. **4**, 494 (1933).
L. F. Curtiss, "A new method of analyzing α-ray photographs," Bur. Stand. J. Research **4**, 663 (1930).
L. F. Curtiss, "Simplified automatic cloud chamber," Bur. Stand. J. Research **8**, 579 (1932).
B. R. Curtiss and J. R. Richardson, "Radiations from radioactive In(116)," Phys. Rev. **57**, 1121 (1940).
O. Dahl, L. R. Hafstad, and M. A. Tuve, "Permanently sealed chamber with metallic sylphon bellows," Rev. Sci. Inst. **4**, 373 (1933).
P. I. Dee, "Disintegration of the diplon," Nature **133**, 564 (1934).
P. I. Dee, "Cloud track method for artificial transmutations," Proc. Roy. Soc. **148**, 623 (1935).
P. I. Dee and C. W. Gilbert, "The transmutation of heavy hydrogen investigated by the cloud track method," Proc. Roy. Soc. **149**, 200 (1935).
P. I. Dee and C. W. Gilbert, "The disintegration of boron into three α-particles," Proc. Roy. Soc. **154**, 294 (1936).
P. I. Dee and E. T. S. Walton, "Transmutations of Li and B," Proc. Roy. Soc. **141**, 733 (1933).

L. A. Delsasso, W. A. Fowler, and C. C. Lauritsen, "Protons from the disintegration of Li by deuterons," Phys. Rev. **48**, 848 (1935).

L. A. Delsasso, W. A. Fowler, and C. C. Lauritsen, "Energy and absorption of the γ-radiation from Li^7+H^1," Phys. Rev. **51**, 391 (1937)a.

L. A. Delsasso, W. A. Fowler, and C. C. Lauritsen, "Gamma-radiations from F bombarded with protons," Phys. Rev. **51**, 527 (1937)b.

A. J. Dempster, "Automatic Wilson cloud chamber of simple design," Rev. Sci. Inst. **5**, 158 (1934).

P. Duhem and M. Margules, "Observations on the vapor pressure of binary liquid mixtures," Zeits. f. physik. Chemie **35**, 483 (1900).

J. R. Dunning, "Emission and scattering of neutrons," Phys. Rev. **45**, 586 (1934).

H. Euler and W. Heisenberg, "Theoretical considerations for the interpretations of cosmic radiation," Ergeb. d. exakt. Naturwiss. **17**, 1 (1938).

L. Farkas, "Rate of formation of drops in supersaturated vapor," Zeits. f. physik. Chemie **125**, 236 (1927).

N. Feather, "Collisions of neutrons with nitrogen nuclei," Proc. Roy. Soc. **136**, 709 (1932).

N. Feather, "Collision of α-particles with F nuclei," Proc. Roy. Soc. **141**, 194 (1933)a.

N. Feather, "Collision of neutrons with light nuclei," Proc. Roy. Soc. **142**, 689 (1933)b.

N. Feather and F. Nimmo, "Distribution of ranges of α-particles," Proc. Camb. Phil. Soc. **25**, 198 (1929).

H. Flood, "Formation of drops in supersaturated ethyl alcohol water vapor mixture," Zeits. f. physik. Chemie **170**, 294 (1934).

W. A. Fowler, L. A. Delsasso, and C. C. Lauritsen, "Radioactive elements of low atomic numbers," Phys. Rev. **49**, 561 (1936).

W. A. Fowler and C. C. Lauritsen, "Radioactive α-particles from Li^7+H^2," Phys. Rev. **51**, 1103 (1937).

W. A. Fowler, E. R. Gaerttner, and C. C. Lauritsen, "γ-radiation from B bombarded with protons," Phys. Rev. **53**, 628 (1938).

J. A. Froemke, C. R. Bloomquist, and E. X. Anderson, "Formation of drops in methyl alcohol water vapor mixture," Zeits. f. physik. Chemie **166**, 305 (1933).

D. K. Froman and J. C. Stearns, "Cosmic-ray showers and bursts," Rev. Mod. Phys. **10**, 133 (1938).

L. Fussel, "Exhaust valve for pneumatic cloud chamber," Rev. Sci. Inst. **10**, 321 (1939).

E. R. Gaerttner and L. A. Pardue, "γ-radiations from N bombarded with deuterons," Phys. Rev. **57**, 386 (1940).

T. N. Gautier and A. E. Ruark, "Composition of mixed vapor in cloud chamber," Phys. Rev. **57**, 1040 (1940).

I. A. Getting, "A cloud-chamber control circuit," Rev. Sci. Inst. **10**, 332 (1939).

L. Grosev, N. Dobrotin, and J. Frank, "Stereocomparator for work with cloud chamber," Comptes rendus, U.S.S.R. **3–6**, 289 (1936).

O. Hahn and F. Strassman, "Fission tracks in Wilson chamber," Naturwiss. **27**, 11 (1939).

J. Halpern and H. R. Crane, "The internal conversion coefficient in the $F^{19}+H^1$ reaction and measurements on the γ-ray spectrum," Phys. Rev. **55**, 260 (1939).

J. Hamilton, W. Heitler, and H. W. Peng, "Cosmic-ray mesons," Phys. Rev. **64**, 78 (1943).

W. D. Harkins, D. M. Gans, and H. W. Newson, "The disintegration of the nuclei of light atoms by nitrogen," Phys. Rev. **47**, 52 (1935).

W. E. Hazen, "Some operating characteristics of the Wilson cloud chamber," Rev. Sci. Inst. **13**, 247 (1942).

W. E. Hazen, "Electrons in equilibrium with the penetrating component of cosmic rays in lead at 10,000 ft. and at sea level," Phys. Rev. **64**, 7 (1943).

W. E. Hazen, "Cascade showers and nuclear disintegrations," Phys. Rev. **65**, 67 (1944)a.

W. E. Hazen, "Average energy loss of mesotrons in air," Phys. Rev. **65**, 259 (1944)b.

G. Herzog, "A large cloud chamber," J. Sci. Inst. **12**, 153 (1935).

G. Herzog, "Wilson chamber for projection purpose," Helv. Phys. Acta **10**, 68 (1937).

G. Herzog, "Cloud track of cosmic rays in the substratosphere," Phys. Rev. **59**, 117 (1941).

G. Herzog and W. H. Bostick, "Cloud-chamber picture of cosmic rays at 29,000 ft. altitude," Phys. Rev. **59**, 122 (1941).

Hilsch, "Cloud chamber for lecture experiments," Physik. Zeits. **40**, 594 (1939).

R. Holm, "Cloud-chamber investigation of electric discharges through gases," Zeits. f. Physik **101**, 138 (1936).

D. J. Hughes, "Positive excess and electron component in the cosmic-ray spectrum," Phys. Rev. **57**, 592 (1940).

D. J. Hughes, "Cloud-chamber photographs of slow mesotron pair," Phys. Rev. **60**, 414 (1941).

L. Janossy, "Note on the production of cosmic-ray mesons," Phys. Rev. **64**, 345 (1943).

W. Jenstchke and F. Prankal, "Nuclear disintegration products of U," Physik. Zeits. **40**, 706 (1939).

T. H. Johnson, J. G. Barry, and R. P. Shutt, "Direct evidence of the proton component of cosmic radiation," Phys. Rev. **57**, 1047 (1940).

T. H. Johnson, S. D. Benedetti, and R. P. Shutt, "A hydrostatically supported cloud chamber of new design at high pressures," Rev. Sci. Inst. **14**, 265 (1943).

T. H. Johnson and R. P. Shutt, "Track of a decaying mesotron in cloud chamber," Phys. Rev. **61**, 380 (1942).

F. Jolliot, "Wilson apparatus for variable pressures," J. de phys. et rad. **5**, 216 (1934).

F. Jolliot, "Trajectories of products of uranium fission," Comptes rendus **208**, 647 (1939).

C. C. Jones, "Time delay circuit for Wilson cloud chamber," Rev. Sci. Inst. **8**, 319 (1937).

C. C. Jones and A. E. Ruark, "Apparatus for viewing and measurements on stereoscopic cloud-chamber photographs," Am. Phil. Soc. Proc. **82**, 353 (1940).

H. Jones, "Energy distribution and positive excess of mesotrons," Rev. Mod. Phys. **11**, 235 (1939).

H. Jones and D. J. Hughes, "Magnet and cloud chamber for cosmic-ray studies," Rev. Sci. Inst. **11**, 79 (1940).

Kiessling, Naturwiss. Verein d. Hamburg-Altona **8** (1884).
P. Kipfer, "A high pressure Wilson cloud chamber," Nature **135**, 431 (1935).
F. Kirchner and H. Neuert, "On the transformation of Be by slow protons," Physik. Zeits. **36**, 54 (1935).
P. Kunze, "Magnetic deflections of the cosmic radiations in the Wilson chamber," Zeits. f. Physik **80**, 559 (1933)a.
P. Kunze, "Investigations of cosmic rays in the Wilson chamber," Zeits. f. Physik **83**, 18 (1933)b.
P. Kunze, "A portable cloud chamber for demonstration purposes," Physik. Zeits. **42**, 405 (1941).
F. N. D. Kurie, "Use of Wilson chamber for measuring the range of α-particles from weak sources," Rev. Sci. Inst. **3**, 655 (1932).
F. N. D. Kurie, "New mode of disintegrations induced by neutrons," Phys. Rev. **45**, 904 (1934).
T. H. Laby, "The supersaturation and nuclear condensation of certain organic vapors," Phil. Trans. Roy. Soc. **208**, 445 (1908).
W. E. Lamb, "Passage of fission fragments through matter," Phys. Rev. **58**, 696 (1940).
W. E. Lamb, "Range of fission fragments," Phys. Rev. **59**, 687 (1941).
R. M. Langer, "Growth of droplets in Wilson chamber," Phys. Rev. **56**, 851 (1938).
A. Langsdorf, "A continuously sensitive diffusion cloud chamber," Rev. Sci. Inst. **10**, 91 (1939).
P. Leprince-Ringuet, and J. Crussard, "Study of high energy cosmic particles in the Bellevue electromagnet," J. de Phys. et rad. **8**, 207 (1937).
W. K. Lewis and E. Y. Murphee, "Relation between vapor pressure and vapor composition in binary mixtures of volatile liquids," J. Am. Chem. Soc. **46**, 1 (1924).
W. B. Lewis and C. E. Wynn-Williams, "The range of α-particles from radioactive emanations and A products," Proc. Roy. Soc. **136**, 349 (1932).
M. S. Livingston, "Projection cloud chambers," Am. Phys. Teach. **4**, 33 (1936).
M. S. Livingston and H. Bethe, "Nuclear dynamics," Rev. Mod. Phys. **9**, 285 (1937).
J. J. Livingood and G. T. Seaborg, "A table of induced radioactivities," Rev. Mod. Phys. **12**, 30 (1940).
G. L. Locher, "Cloud chamber photographs of cosmic-ray stosse," J. Frank. Inst. **216**, 673 (1933)a.
G. L. Locher, "Wilson cloud chamber for portable use," Rev. Sci. Inst. **7**, 471 (1933)b.
D. H. Loughridge and H. C. Trueblood, "Organic liquids suitable for cloud expansion works," Phys. Rev. **46**, 323 (1934).
A. C. B. Lovell, "Showers produced by penetrating cosmic rays," Proc. Roy. Soc. **172**, 568 (1939).
H. Maier-Leibnitz, "Investigations with slow Wilson chambers," Zeits. f. Physik **112**, 569 (1939).
L. Meitner, "Long range α's from Th C," Zeits. f. Physik **37**, 481 (1926).
L. Meitner and K. Philip, "Further measurements with neutrons," Zeits. f. Physik **87**, 484 (1934).
J. M. W. Miliatz and G. A. W. Rutgers, "Total and specific ionization of Po α-particles," Physica **7**, 13 (1940).
L. Mott-Smith, "A high pressure Wilson chamber," Rev. Sci. Inst. **5**, 346 (1934).
E. B. M. Murrel and C. L. Smith, "Transmutations of Na by deuterons," Proc. Roy. Soc. **173**, 410 (1939).
U. Nakaya and F. Yamasiki, "Applications of Wilson chamber to the study of spark discharge," Proc. Roy. Soc. **148**, 446 (1935).
S. H. Neddermeyer and C. D. Anderson, "Note on the nature of cosmic rays," Phys. Rev. **51**, 884 (1937).
H. Neurt, "Range measurements of fragments of a light element bombarded by fast protons," Physik. Zeits. **36**, 629 (1935).
H. Neurt, "Simple Wilson chamber," Physik. Zeits. **37**, 629 (1936).
C. E. Nielson and W. M. Powell, "Mesotron mass and heavy tracks on Mt. Evans," Phys. Rev. **63**, 384 (1943).
Y. Nishina, M. Takeuchi, and T. Ichimiya, "On the nature of the cosmic-ray particles," Phys. Rev. **52**, 1198 (1937).
R. Peierls, "The meson," Report Prog. Phys. **6**, 78 (1939).
C. F. Powell, "Condensation phenomenon at different temperatures," Proc. Roy. Soc. **119**, 553 (1928).
W. Powell, "Photon production of mesotrons," Phys. Rev. **58**, 474 (1940).
W. Powell, "Stars and protons at 14,125 ft.," Phys. Rev. **61**, 670 (1942).
H. Raether, "Gas discharge in a cloud chamber," Zeits. f. Physik **94**, 567 (1935).
H. Raether, "Electrical discharge in cloud chamber," Physik. Zeits. **37**, 560 (1936).
H. Raether, "Examination of electron surge in the expansion chamber," Physik. Zeits. **38**, 990 (1937).
H. Raether, "Ionizing radiation accompanying a spark discharge," Zeits. f. Physik **110**, 611 (1938).
G. Rathenau, "Simple Wilson chamber for demonstration purpose," Physica **5**, 427 (1938).
Lord J. W. S. Rayleigh, *Collected Scientific Papers* 1899–1920 (Cambridge University Press, Cambridge, England), Vol. 1, p. 415.
W. M. Rayton and T. R. Wilkins, "A Wilson cloud-chamber investigation of the alpha-particles from uranium," Phys. Rev. **51**, 818 (1937).
J. R. Richardson, "Radiations produced from artificially produced ratio elements," Phys. Rev. **53**, 124 (1938)a.
J. R. Richardson, "Valve control circuits for Wilson chamber," Rev. Sci. Inst. **9**, 152 (1938)b.
J. R. Richardson, "Radiations from radioactive substances, Au^{198}, Eu^{152}, Ag^{106}, Cu^{64}, N^{13}," Phys. Rev. **55**, 609 (1939).
J. R. Richardson and L. Emo, "Photo-disintegration of H^2 by γ-rays from Na^{24}," Phys. Rev. **53**, 234 (1938).
J. R. Richardson and F. N. D. Kurie, "The radiations emitted from artificially produced radioactive substances," Phys. Rev. **50**, 999 (1936).
H. O. W. Richardson and A. Leigh-Smith, "β-rays of Ra D," Proc. Roy. Soc. **162**, 391 (1937).
F. Richarz, "The value of the ratio of specific heats for a mixture of two gases," Ann. d. Physik **19**, 639 (1906).
D. Roaf, "Disintegration of B by α-particles," Proc. Roy. Soc. **153**, 568 (1936).

M. Rohr, *The formation of images in optical instruments* (Dept. of Scientific and Industrial Research, H. M. Stationary Office, London, 1920).
B. Rossi and K. Greisen, "Cosmic-ray theory," Rev. Mod. Phys. **13**, 240 (1941).
B. Rossi, L. Janossy, R. Rochester, and M. Bound, "Production of secondary ionizing particles by non-ionizing agents," Phys. Rev. **58**, 762 (1940).
Lord Rutherford, W. B. Lewis, and B. V. Bowden, "Analysis of long range α-particles from radium C′ by the magnetic focusing method," Proc. Roy. Soc. **142**, 347 (1933).
L. Scharrer, "Condensation of supersaturated vapor on ions," Ann. d. Physik **35**, 619 (1939).
G. T. Seaborg, "Table of isotopes," Rev. Mod. Phys. **16**, 1 (1944).
R. L. Sen Gupta, "Specific ionization of cosmic-ray particles," Proc. Nat. Inst. Sci. Ind. **9**, 295 (1943).
L. Seren, "Cloud-chamber study of collision electrons in equilibrium with mesons," Phys. Rev. **62**, 204 (1942).
T. Shimizu, "A reciprocating expansion apparatus for detecting ionizing rays," Proc. Roy. Soc. **99**, 425 (1921).
K. Shinohara and M. Hatoyama, "Pair production in the field of electrons," Phys. Rev. **59**, 461 (1941).
R. P. Shutt, S. D. Benedetti, and T. H. Johnson, "Cloud-chamber track of a decaying mesotron," Phys. Rev. **62**, 552 (1942).
G. C. Simpson, "On the formation of cloud and rain," Quat. J. Roy. Met. Soc. **67**, 99 (1941).
M. Sinha, "Cloud chamber study of shower production in lead," Trans. Bose Res. Inst. **15**, 191 (1943).
G. J. Sizoo and F. Barendregt, "Production of positrons by β-particles," Physica **6**, 1085 (1939).
D. Skobelzyn, "Intensity distribution in the spectrum of γ-rays from Ra C," Zeits. f. Physik **43**, 354 (1927).
D. Skobelzyn, "On a new type of fast β-rays," Zeits. f. Physik **54**, 686 (1929).
L. B. Snoddy and C. D. Bradley, "A method for investigating electrical breakdown process," Phys. Rev. **45**, 432 (1934).
J. C. Street and E. C. Stevenson, "Design and operation of counter-controlled Wilson chamber," Rev. Sci. Inst. **7**, 347 (1936).
J. C. Street and E. C. Stevenson, "New evidence for the existence of a particle of mass intermediate between the proton and electron," Phys. Rev. **52**, 1003 (1937).
J. E. Thomas and W. E. Ramsay, "Small cloud chamber for electron showers," J. Frank. Inst. **227**, 789 (1939).
G. Tohmfor and M. Volmer, "Production of condensation nuclei in the presence of electrical charges," Ann. d. Physik **33**, 109 (1938).
J. J. Thomson, "Charge carried by Röntgen ions," Phil. Mag. **46**, 528 (1898).
F. Trey, "A new radially expanding cloud chamber," Physik Zeits. **39**, 343 (1938).
F. Trey, "Production of clouds in gases saturated with water vapor by removal of heat from the vapor by conduction," Physik. Zeits. **41**, 415 (1940).
B. Trumpy, "Secondary processes of the soft and penetrating components of cosmic rays," Zeits. f. Physik **111**, 338 (1939).
J. J. Turin and H. R. Crane, "The absorption of high energy electrons, Part I," Phys. Rev. **52**, 63 (1937)a.
J. J. Turin and H. R. Crane, "The absorption of electrons, Part II," Phys. Rev. **52**, 610 (1937)b.
R. E. Vollrath, "Continuously active cloud chamber," Rev. Sci. Inst. **7**, 409 (1936).
M. Volmer and A. Weber, "Number of drops formed per cc per second in supersaturated space," Zeits. f. physik. Chemie **119**, 277 (1926).
M. Volmer and H. Flood, "Drop formation in saturated ethyl alcohol water vapor," Zeits. f. physik. Chemie **170**, 273 (1934).
H. Walke, E. J. Williams, and G. R. Evans, "K electron capture, nuclear isomerism and the long period activities of titanium and scandium," Proc. Roy. Soc. **171**, 360 (1939).
C. G. Webb, "On the scattering of light by water drops," Phil. Mag. **19**, 927 (1935).
J. A. Wheeler and R. Ladenburg, "Mass of meson by the method of momentum loss," Phys. Rev. **60**, 754 (1941).
E. J. Williams, "Sensitive time of a Wilson expansion chamber," Proc. Camb. Phil. Soc. **35**, 512 (1939)a.
E. J. Williams, "Some observations on cosmic ray using a large randomly operated cloud chamber," Proc. Roy. Soc. **172**, 194 (1939)b.
E. J. Williams and G. R. Evans, "Transformation of mesons into electrons," Nature **145**, 818 (1940).
E. J. Williams and E. Pickup, "Heavy electrons in cosmic rays," Nature **141**, 684 (1938).
E. J. Williams and G. E. Roberts, "Track of a decay electron," Nature **145**, 102 (1940).
E. J. Williams and F. R. Terroux, "Investigations on the passage of fast β-particles through gas, "Proc. Roy. Soc. **126**, 289 (1930).
C. T. R. Wilson, "Condensation of water vapor in the presence of dust free air and other gases," Phil. Trans. Roy. Soc. **189**, 265 (1897).
C. T. R. Wilson, "On the condensation nuclei produced in gases by the action of Röntgen rays, uranium rays, ultraviolet light and other agents," Phil. Trans. Roy. Soc. **192**, 403 (1899)a.
C. T. R. Wilson, "On the comparative efficiency as condensation nuclei of positively and negatively charged ions," Phil. Trans. Roy. Soc. **193**, 289 (1899)b.
C. T. R. Wilson, "Condensation method of demonstrating the ionization of air," Phil. Mag. **7**, 681 (1904).
C. T. R. Wilson, "Cloud-chamber technique," Proc. Roy Soc. **85**, 285 (1911).
C. T. R. Wilson, "Cloud-chamber technique," Proc. Roy. Soc. **87**, 277 (1912).
C. T. R. Wilson, "Investigation on x-rays and β-rays by the cloud method," Proc. Roy. Soc. **104**, 1, 192 (1923).
C. T. R. Wilson, "New type of expansion cloud chamber," Proc. Roy. Soc. **142**, 88 (1933).
C. T. R. Wilson and J. G. Wilson, "Falling cloud chamber and radially expanding cloud chamber," Proc. Roy. Soc. **148**, 523 (1935).

J. G. Wilson, "Production of secondary electrons by cosmic-ray particles," Nature **142**, 73 (1938).
J. G. Wilson, "Scattering of mesotrons in metal plates," Proc. Roy. Soc. **174**, 73 (1940).
K. Zuber, "Automatic Wilson cloud chamber," Helv. Phys. Acta **11**, 366 (1938).

General References

1. K. K. Darrow, *Introduction to Contemporary Physics* (D. Van Nostrand Company, Inc., New York, 1939).
2. H. Geiger, *Handbuch der Physik* (Verlagsbuchhandlung Julius Springer, Berlin, 1927), Vol. 22.
3. R. Glazebrooke, *Dictionary of Applied Physics* (Macmillan and Company, London 1927), Vol. 4.
4. W. Heitler, *Quantum Theory of Radiation* (The Clarendon Press, Oxford 1935).
5. Lord Rutherford, J. Chadwick, and C. D. Ellis, *Radiations From Radioactive Substances* (Cambridge University Press, Cambridge England, 1935).
6. M. N. Saha and B. N. Srivastava, *A Treatise on Heat* (Indian Press, Allahabad, India, 1935).
7. M. N. Saha and N. K. Saha, *A Treatise on Modern Physics* (Indian Press, Allahabad, India, 1934).
8. J. J. Thomson, *Application of Dynamics to Physics and Chemistry* (Macmillan and Company, London, 1888).
9. J. J. Thomson and G. P. Thomson, *Conduction of Electricity through Gases* (Cambridge University Press, Cambridge, England, 1928), Vol. 1.
10. F. A. B. Ward, *Atom Tracks* (London, 1937).

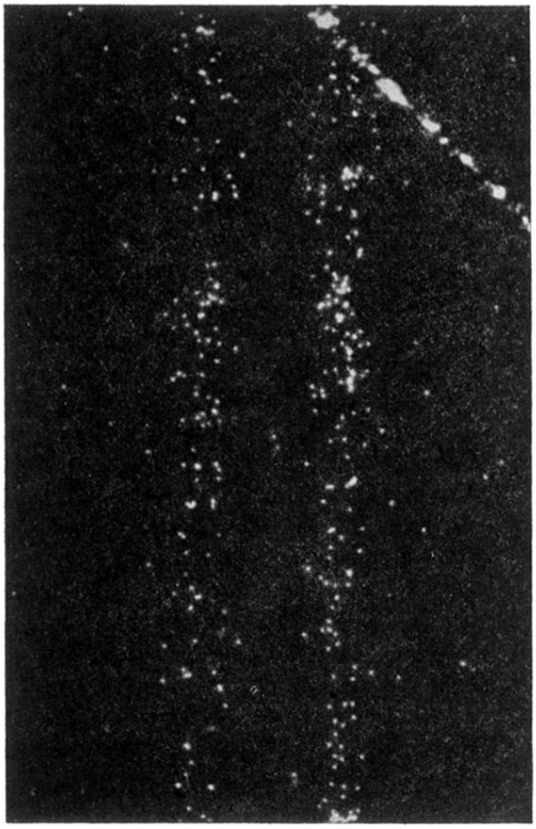

FIG. I-3. Difference in the action of positive and negative ions in producing condensation. The ions have diffused and formed into columns of positive and negative ions before the drops are formed. The denser column of drops is formed on positive ions. [From Hazen, Phys. Rev. **65**, 259 (1944).]

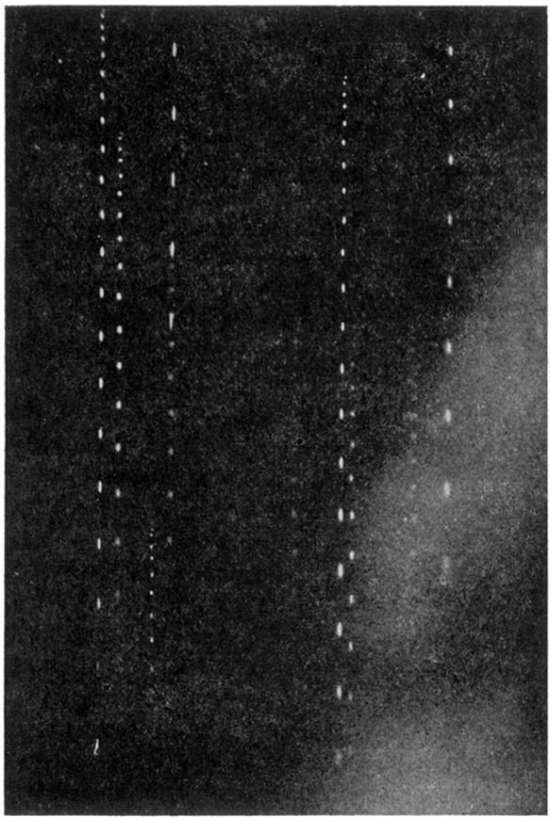

FIG. I-6. Growth of drops. Falling drops in helium and the vapor from 95 percent C_2H_5OH photographed with illumination which flashed 30 times per second. [Hazen, Rev. Sci. Inst. **13**, 247 (1942).]

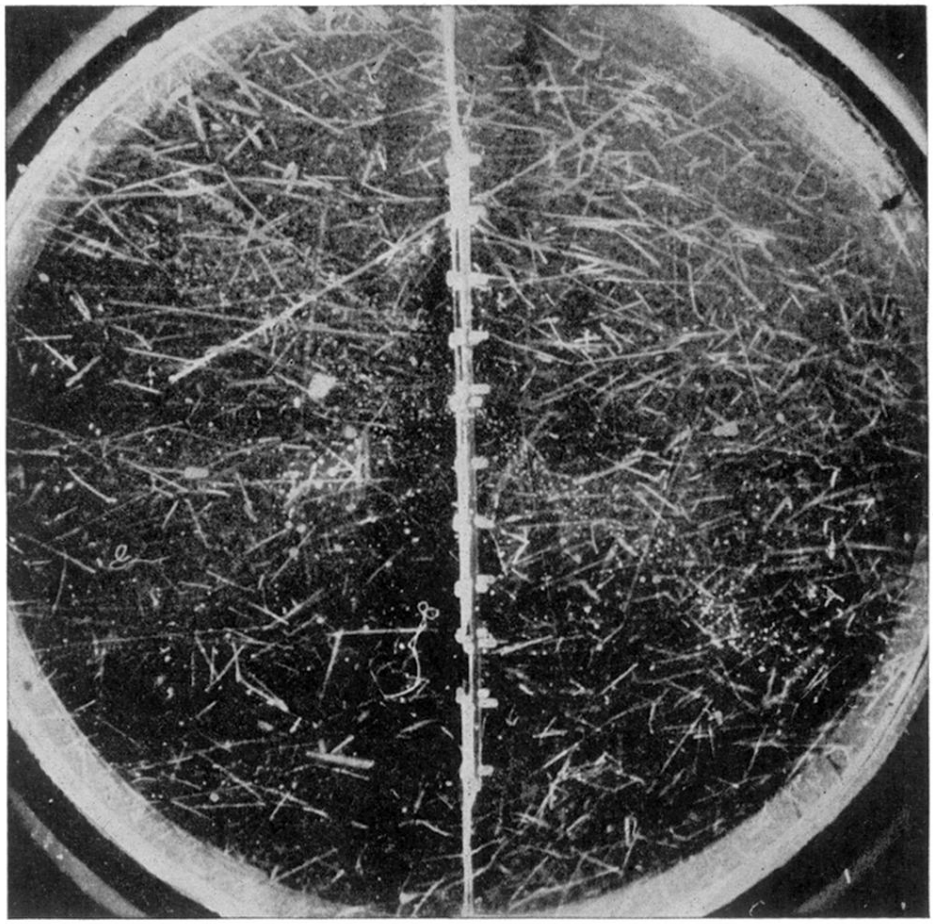

FIG. V-4. Typical pair fragments produced on fission.

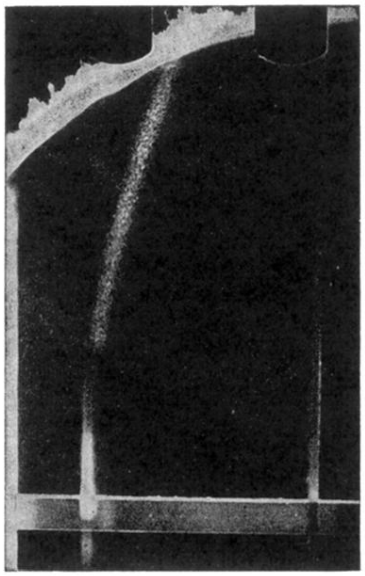

FIG. V-5. Track of particle of intermediate mass.